pennsylvania
DEPARTMENT OF TRANSPORTATION

Superpave In-Situ Stress/Strain Investigation – Phase II

FINAL REPORT
Vol. II: Materials Characterization

May 2009

By Mansour Solaimanian, Laxmikanth Premkumar, Hao Yin, Ghassan Chehab, and Shelley M. Stoffels

The Thomas D. Larson
Pennsylvania Transportation Institute

PENNSTATE
1855

COMMONWEALTH OF PENNSYLVANIA
DEPARTMENT OF TRANSPORTATION

CONTRACT No. 999012
PROJECT No. HA2006-02

Technical Report Documentation Page

1. Report No. FHWA-PA-2009-009-999012 HA 2006-02	**2. Government Accession No.**	**3. Recipient's Catalog No.**
4. Title and Subtitle SuperPave In-Situ Stress/Strain Investigation, Phase II Volume II: Characterization of Materials		**5. Report Date** May 2009 **6. Performing Organization Code**
7. Author(s) Mansour Solaimanian, Laxmikanth Premkumar, Hao Yin, Ghassan Chehab, and Shelley M. Stoffels		**8. Performing Organization Report No.** PTI 2009-17
9. Performing Organization Name and Address The Thomas D. Larson Pennsylvania Transportation Institute Transportation Research Building The Pennsylvania State University University Park, PA 16802-4710		**10. Work Unit No. (TRAIS)** **11. Contract or Grant No. 999012** Project HA2006-02
12. Sponsoring Agency Name and Address The Pennsylvania Department of Transportation Bureau of Planning and Research Commonwealth Keystone Building 400 North Street, 6th Floor Harrisburg, PA 17120-0064		**13. Type of Report and Period Covered** Final Report 6/23/2006 – 11/30/2008 **14. Sponsoring Agency Code**
15. Supplementary Notes COTR: Mr. Michael Long, johlong@state.pa.us		

16. Abstract

The characterization of materials is an integral part of the overall effort to validate the Superpave system and to calibrate the performance prediction models for the environmental conditions observed in the Commonwealth of Pennsylvania. Material properties are among the most important input parameters to the models of the *Mechanistic Empirical Pavement Design Guide* for flexible pavements. An extensive laboratory testing program was followed during Phases I and II of the Superpave In-situ Stress Strain Investigation (SISSI) project to determine binder properties, mix volumetric properties, and mix engineering properties. Testing of SISSI binders during Phase II with the bending beam rheometer at various temperatures and loading times showed that the equivalence principle of testing at low temperature is not satisfied. The indirect tensile creep and strength tests on wearing layers of SISSI provided a ranking of these mixtures based on their low-temperature material properties. Fracture analysis of SISSI mixtures indicated that the maximum tensile stress is independent of the type of asphalt concrete mixtures. Considerable deviations were observed between the calculated fracture energy from linear elastic and linear viscoelastic solutions. Results of repeated shear testing at maximum pavement temperature indicate performance of SISSI mixtures to be in the range of good to excellent since no excessive permanent deformation was observed from these laboratory tests. The present report is one of four volumes, Volume I: Summary Report; Volume II, Materials Characterization; Volume III: Field Data Collection and Summary; Volume IV: Mechanistic Analysis and Implementation.

17. Key Words Pavement materials, characterization, asphalt concrete, binder, modulus, creep compliance, shear deformation, mechanistic empirical pavement design guide models	**18. Distribution Statement** No restrictions. This document is available from the National Technical Information Service, Springfield, VA 22161

19. Security Classif. (of this report)	**20. Security Classif. (of this page)**	**21. No. of Pages**	**22. Price**
Unclassified	Unclassified	149	

Form DOT F 1700.7 (8-72) **Reproduction of completed page authorized**

This work was sponsored by the Pennsylvania Department of Transportation and the U.S. Department of Transportation, Federal Highway Administration. The contents of this report reflect the views of the authors, who are responsible for the facts and the accuracy of the data presented herein. The contents do not necessarily reflect the official views or policies of either the Federal Highway Administration, the U.S. Department of Transportation, or the Commonwealth of Pennsylvania at the time of publication. This report does not constitute a standard, specification, or regulation.

ACKNOWLEDGEMENTS

The work described in this report was the result of the foresight of the original Superpave In-Situ Stress-Strain Instrumentation (SISSI) Task Force, led by Mr. James Moretz and later by Mr. Dan Dawood and Mr. Mike Long. The other members of the task force are duly recognized, especially Ronald Cominsky, Carlos Rosenberger, and Zahur Siddiqui for their invaluable guidance. The kind counsel and perseverance of Mr. Michael Bonini and Ms. Michelle Tarquino is greatly appreciated.

The characterization of asphalt binders and mixtures reported in this document was possible because of the financial support of the Pennsylvania Department of Transportation (PennDOT). This financial support is greatly appreciated.

Thanks are also extended to Scott Milander of LTI for his assistance with laboratory testing.

TABLE OF CONTENTS

LIST OF FIGURES

LIST OF TABLES

EXECUTIVE SUMMARY

The Superpave mix design system was one of the major products of the Strategic Highway Research Program (SHRP). Implementation of this new technology began in the mid-1990s, soon after its introduction to state highway agencies and industry. After several years of using this new system, a major question that remained to be addressed in regard to the Superpave system was whether constructed Superpave pavements would meet design expectations. Furthermore, with the emergence of improved mechanistic-empirical performance prediction models, actual pavement response and performance data were needed to calibrate and validate such models.

To address these concerns, the Pennsylvania Department of Transportation (PennDOT) initiated a major five-year research program with Penn State that was titled "Superpave In-Situ Stress/Strain Investigation" (SISSI). The project began in May 2001 and was completed in May 2006. The project was then extended under Phase II for an additional two and a half years and ended in November 2008. The main objectives achieved under the SISSI project included instrumentation of several pavements through the Commonwealth of Pennsylvania, direct measurement of the response of Superpave asphalt pavement sections to vehicle loading and environmental effects, direct evaluation of distresses developed in pavements using Superpave mixes, and collection of the data for validation of the mechanistic-empirical pavement design guide (MEPDG) and validation of the integrated climatic models for pavement design. The major objective achieved during Phase II of the program included utilization of SISSI data with MEPDG and comparing predicted performance versus observed field measurements.

Considering the project objectives, the work included an extensive effort toward instrumentation of eight pavement sites throughout the Commonwealth of Pennsylvania. Instrumentation took place during pavement construction to minimize interference to common and normal paving operations. Four of the selected sites were full-depth new construction or reconstruction. These included sites in Tioga, Mercer, Somerset, and Blair counties. The remaining sites included structural overlay and were located in Mercer, Warren, Perry, and Delaware counties. Both Mercer sites were constructed on the West bound but the full depth construction site and the overlay site are, respectively, referred to as Mercer East and Mercer West site, terms that are used to indicate their relative position with respect to each other. Instrumentation included dynamic (load-associated) sensors and environmental (non-load) sensors. Upon completion of the instrumentation, a vast amount of effort was applied to testing, measurements, and data collection. In general, these efforts fell into two major categories: field activities and laboratory activities.

An extensive testing program was conducted in the laboratory to characterize the materials used at the sites of the SISSI project. Characterization of materials is an integral part of the overall effort to validate the Superpave system and to calibrate the performance prediction models for the environmental conditions observed in the Commonwealth of Pennsylvania. Phase I of the project concentrated on specific testing

to characterize both the binder and hot-mix asphalt, which were procured from the sites at the time of construction. The major laboratory tests conducted on the procured binders during Phase I included the Superpave grading tests: short- and long-term aging, rotational viscometer, dynamic shear rheometer (DSR), and bending beam rheometer (BBR). The mixture testing included the tests required for verification of mix design, as well as dynamic modulus testing at a range of temperatures and frequencies to capture properties required for input to performance prediction models. The results of Phase I laboratory testing and the significance of those results were provided in a SISSI Phase I Materials Characterization report.

Laboratory testing during Phase II included indirect tensile creep and strength tests at three temperatures to capture low temperature properties of SISSI mixtures, constant-height repeated tests at maximum pavement temperature to capture rutting resistance properties, and constant-height strain-controlled frequency sweep tests to characterize the variation of shear modulus of SISSI mixtures with temperature and loading time. The testing also included characterizing the behavior of SISSI binders at low temperatures under extended loading times to validate the Superpave low temperature binder specification.

The validity of the Superpave binder specification in regard to the equivalence principle for the binder flexural creep stiffness was evaluated during Phase II. Based on this principle, the binder creep stiffness at a specified temperature under two hours of loading [S(7200)] was found to be approximately equal to its creep stiffness at a temperature 10ºC warmer under 60 seconds of loading [S(60)]. This principle assumes that all asphalt binders can be characterized by similar shift factors. Our testing and analysis indicated that the S(60) at T_1+10 is significantly higher than the S(7200) values, and the differences range between 40 and 52 percent. Through this work, alternate testing times and temperatures were developed and introduced to satisfy the equivalence principle for the SISSI binders.

The SISSI sites were ranked based on their low temperature material properties obtained from indirect tensile creep and strength tests. Based on measured properties, it seems that the SISSI mixture used at the wearing course of the Delaware site is the most susceptible to thermal cracking. Field observations at this site have shown a significant number of transverse cracks even though it cannot be concluded with certainty that observed cracks are thermally induced.

Results of repeated shear testing at maximum pavement temperature indicates performance of SISSI mixtures in the range of good to excellent since no excessive permanent deformation was observed from these laboratory tests. For the wearing layer, the permanent shear strain ranged from 0.3 to 1.7 percent, indicating an excellent to good rutting resistance. For the binder layer, the range was between 0.4 and 1.7 percent, indicating good to excellent rutting resistance. The exception was the binder layer of the Perry site, for which a permanent strain of 2.4 percent was obtained, indicating fair rutting resistance even though no excessive rutting was observed in the field for this site.

Overall, the field-measured rutting, after 5 to 8 years of service, ranged from 2.5 to 8.5 millimeters, indicating good to excellent rut resistance of SISSI mixtures at all the sites. This is in general consistent with laboratory-measured shear strains as discussed above.

CHAPTER 1
INTRODUCTION

Background

Development of performance prediction models for hot-mix asphalt concrete pavements has been pursued aggressively since the beginning of the Strategic Highway Research Program (SHRP). This comprehensive project, conducted from 1987 through 1993, resulted in the Superpave System. The models of the system were developed to predict fatigue cracking, thermal cracking, and rutting over time using results from accelerated laboratory tests. Visco-elasto-plastic properties of the materials are determined from these tests. The models rely on detailed material properties, pavement structure, traffic, and detailed environmental data as input. While Superpave models underwent some validation during the 5-year research program of SHRP, modifications, improvements, and validations continued beyond 1993 with the goal of obtaining a thoroughly reliable model. In 1997, the project moved into a new phase with NCHRP project 1-37: "Development of the 2002 Guide for the Design of New and Rehabilitated Pavement Structures." This project was extended as Phase II under NCHRP 1-37A and was completed in 2004. Parallel to NCHRP 1-37, in 1999, NCHRP project 9-19 was initiated under the title of "Superpave Support and Performance Models Management." This project was targeted toward developing and validating an advanced material characterization model and the associated calibration and testing. The final product is what is today known as the mechanistic empirical pavement design guide. Recent NCHRP projects 9-30A (Calibration of Rutting Models for HMA Structural and Mix Design) and 1-40B (User Manual and Local Calibration Guide for the Mechanistic-Empirical Pavement Design Guide and Software) are aimed at providing guidance for calibrating and validating these models at the local level.

The accuracy of performance prediction models depends on an effective process of calibration and subsequent validation with independent data sets. Pavement engineers need to see an acceptable correlation between field-observed levels of permanent deformation, fatigue cracking, and low-temperature cracking and levels predicted with the hot-mix asphalt (HMA) performance models selected for use in structural and mix design. Such accuracy is also important if the results of these models are to be used in the development of performance-related specifications. Models developed under MEPDG NCHRP projects must be refined and validated for use at the state level. To this end, the PENNDOT research project on "Superpave In-Situ Stress/Strain Investigation" (SISSI) includes both field measurements of pavement performance and behavior as well as laboratory testing and material characterization. Engineering properties of SISSI materials from laboratory tests are among the most important input parameters to the performance prediction models. These laboratory-produced properties are also very important in regard to direct comparison with observed field performance.

Role of Material Characterization

There are important reasons that the engineering properties of the materials used in pavement construction must be determined as accurately as possible. There are four important roles for these properties because they can be used:

- as part of the hot-mix asphalt design process.
- as input for performance prediction models to determine the long-term performance of the pavement as a function of traffic and years of service. In this regard, the properties can be divided into two major categories: those as input for pavement response models and those related to pavement distress models.
- to validate and calibrate performance prediction models. For this purpose, measured parameters along with pavement response data are used.
- for comparison of the performance of different mixes.

The material parameters for pavement response modeling include the modulus, creep compliance, Poisson's ratio, and phase angle of the bound material (i.e., hot-mix asphalt) and stress-dependent behavior of unbound material (i.e., granular material and fine-grained soil).

Instrumentation Sites

Materials used in laboratory testing were procured from the SISSI instrumented sites, as outlined in Table 1.

Table 1. Location of sites selected for instrumentation

Site	Highway	County	Year of Construction	Structure
1	SR 0015	Tioga	2000	Full Depth
2	I-80	Mercer	2000	Full Depth
3	I-80	Mercer	2000	Structural Overlay
4	SR 0006	Warren	2001	Structural Overlay
5	SR 0022	Perry	2001	Structural Overlay
6	SR 0202	Delaware	2002	Structural Overlay
7	PA Turnpike	Somerset	2002	Full Depth
8	SR 1001	Blair	2003	Full Depth

Procurement of Materials

Details of material procurement are covered in a Phase I report on material characterization. Sampling included asphalt binder, hot-mix asphalt/aggregate mixture, aggregates, and subgrade material.

Procured binder was used both for characterization testing and preparation of asphalt/aggregate mixtures. Samples of the loose hot-mix asphalt were obtained from the screed behind the paver. The samples were obtained for all hot-mix layers. Sampling took place at the time of production. Aggregate samples were obtained for each course from the stockpiles in the hot-mix plant facility.

Laboratory Characterization of Materials

During Phase I of the SISSI project, significant effort was made to characterize the binders and mixtures used at all of the instrumented sites. The major mechanical test conducted on SISSI mixtures during Phase I was the dynamic modulus test. Dynamic modulus is the major engineering property used as input to MEPDG software. Results of Phase I testing are presented and discussed elsewhere.

This report presents the results of laboratory testing from Phase II of the study. Major laboratory testing conducted during Phase II included indirect tensile creep and strength test to characterize low temperature cracking resistance, stress-controlled repeated shear and strain-controlled frequency sweep tests to characterize permanent deformation resistance, and extended bending beam rheometer test for validating low temperature Superpave binder specification.

Report Organization

Chapter 2 of this report covers the experimental program carried under Phase II. It includes the test equipment, material and specimen preparation, and the laboratory test protocols. Theoretical background on low temperature cracking and deformation is covered in Chapter 3. The results of testing and the corresponding analysis are presented in Chapter 4. Finally, Chapter 5 presents the summary and conclusions from characterization of SISSI materials.

CHAPTER 2
EXPERIMENTAL PROGRAM

Laboratory testing during Phase I of the SISSI project included tests to characterize both binders and mixtures. The primary tests conducted for the binder characterization included rotational viscometer (RV), dynamic shear rheometer (DSR), and bending beam rheometer (BBR). Short-term and long-term aging of the binders were accomplished using the Rolling Thin Film Oven (RTFOT) and Pressure Aging Vessel (PAV), respectively.

The tests on HMA during Phase I included tests on the loose mixture and tests on the compacted specimens. The tests on the loose mixture included determination of the maximum theoretical specific gravity and determination of binder content and aggregate gradation. AASHTO procedures were followed for this purpose. The tests on the compacted specimens included determination of the bulk specific gravity and the dynamic modulus tests. Details of the binder and mixture testing during Phase I was provided in a separate report on material characterization (Solaimanian et al., 2006).

Phase II testing concentrated on evaluating resistance of SISSI mixtures to low temperature cracking and permanent deformation. Testing included the indirect tensile (IDT) creep and strength test, constant height repeated shear test, and strain-controlled frequency sweep test. Testing also included characterizing SISSI binders at low temperatures for validation of the Superpave binder specification and for comparing the results from those tests with the low temperature mixture tests. In summary, the following testing program was included in Phase II of the SISSI project:

- Indirect Tensile Creep and Strength Test (on mixture).
- Bending Beam Test (on binder).
- Stress-Controlled Constant Height Repeated Shear Test (on mixture).
- Strain-Controlled Constant Height Frequency Sweep Test (on mixture).

Materials

Asphalt mixtures and binders were obtained from all SISSI sites, as discussed in Phase I Materials Characterization Report. The characteristic of SISSI sites from which materials were obtained are summarized in Table 2 and Table 3.

Table 2. Characteristics of SISSI sites in terms of traffic, thickness of layers, and aggregate size

Site 1. Tioga County, SR-0015, Full Depth, < 30 million ESALs 11.5" CSSB[a], 37.5 mm AC[b] @ 9", 19 mm AC @ 2", 12.5 mm AC wearing @ 1.5",
Site 2. Mercer County, I-80, Full Depth, > 30 million ESALs 8" CSSB, 37.5 mm AC @ 15", 25 mm AC @ 3", 12.5 mm AC wearing @ 1.5",
Site 3. Mercer County, I-80, Structural Overlay, > 30 million ESALs 12" Cracked PCC, 37.5 mm AC @ 9", 25 mm AC @ 3", 12.5 mm AC wearing @ 1.5"
Site 4. Warren County, SR -0006, Structural Overlay, < 30 million ESALs 25 mm AC @ 4", 37.5 mm AC @ 5.5", 25 mm AC @ 2", 9.5 mm AC @ 1.5"
Site 5. Perry County, SR-0022, Structural Overlay, < 30 million ESALs 19 mm AC @ 2", 12.5 mm AC @ 1.5"
Site 6. Delaware County, SR-0202, Structural Overlay, < 30 million ESALs 19 mm AC @ 2.5", 12.5 mm AC @ 2.0"
Site 7. Somerset County, I-76, Full Depth, > 30 million ESALs 300 mm Lime Stabilization, 150 mm CSSB, 100 mm ATPM[c], 37.5 mm AC @ 7", 25 mm AC @ 3.0", 19 mm AC @ 2.0"
Site 8. Blair County, SR 1001, Full Depth, < 30 million ESALs 180 mm CSSB, 25 mm AC @ 8", 19 mm AC @ 2.0", 12.5 mm AC @ 1.5"

[a]CSSB indicates crushed stone subbase.

[b]AC indicates asphalt concrete designed according to Superpave system. Value in mm indicates mix designation, value in inches indicates layer thickness.

[c] ATPM indicates Asphalt Treated Permeable base.

Table 3. Sites from which materials were available for laboratory testing

County	Highway	Layer	Date of Construction	Grade
Tioga	SR 0015	Wearing	9/20/2000	PG64-28
Tioga	SR 0015	Binder	8/3/2000	PG64-22
Tioga	SR 0015	BCBC	6/24/2000	PG64-22
Mercer E.	I-80	Wearing	9/28/2000	PG76-22
Mercer E.	I-80	Binder	9/19/2000	PG76-22
Mercer E.	I-80	BCBC	8/22/2000	PG64-22
Mercer W.	I-80	wearing	10/13/2000	PG76-22
Mercer W.	I-80	Binder	9/7/2000	PG76-22
Mercer W.	I-80	BCBC	8/24/2000	PG64-22
Perry	SR 0022	Wearing	9/18/2001	PG76-22
Perry	SR 0022	Binder	8/29/2001	PG64-22
Warren	SR 0006	Wearing	9/12/2001	PG64-22
Warren	SR 0006	Binder	9/10/2001	PG64-22
Warren	SR 0006	BCBC	8/29/2001	PG64-22
Delaware	SR 0202	Wearing	6/16/2002	PG76-22
Delaware	SR 0202	Binder	5/29/2002	PG76-22
Somerset	Turnpike	Wearing	10/29/2002	PG64-22
Somerset	Turnpike	Binder	10/15/2002	PG64-22
Somerset	Turnpike	BCBC	9/13/2002	PG64-22
Blair	SR 1001	Wearing	10/25/2003	PG64-22
Blair	SR 1001	Binder	9/30/2003	PG64-22
Blair	SR 1001	BCBC	9/11/2003	PG64-22

Test Equipment and Instrumentation

Various pieces of equipment were used during Phase II. The major units included Indirect Tensile Tester, Superpave Shear Tester (SST), and Bending Beam Rheometer (BBR).

Indirect Tensile Tester (IDT)

The IDT tests were conducted using a closed loop hydraulic universal testing machine manufactured by Material Test Systems (MTS). The MTS consists of a 100-kN (22-kip) load cell and actuator that is interfaced with an MTS® 458.20 Microconsole. The loading waveform is programmed using an MTS® 458.91 Microprofiler that is part of the Microconsole. Different types of waveforms, including haversine, sine, square, triangle, and trapezoidal, can be programmed using the Microprofiler. The waveforms can be programmed as blocks or segments, and a program can consist of several blocks or segments depending on the waveform required.

An MTS® 409.80 temperature controller along with an MIC 2000 Partlow controller was interfaced with an environmental chamber fitted with an electric heater. Low temperature was obtained by using liquid nitrogen gas for cooling the environmental chamber. A dummy specimen embedded with a K-type thermocouple and with properties similar to the actual test specimen was used to monitor the specimen temperature. The test was conducted only after the specimen stabilized at the required test temperature. Data acquisition was performed using a separate computer fitted with a National Instruments® 6329 DAQ card, and data acquisition programs in LabView were used for data collection. The complete setup is shown in Figure 1.

The deformation values are measured by means of Linear Variable Differential Transformers (LVDTs). For the IDT test, four XS-B LVDTs with a range of ± 0.25mm are used for measuring the vertical and horizontal deformations. The deformation values are measured along a gauge length of 25.4 mm for a specimen diameter of 100 mm and height of 38.1 mm.

It should be noted that a 150-mm jig, as shown in Figure 2, was used for all the IDT tests instead of a 100-mm jig. Because the deformations were measured close to the center, the effect of jig geometry on the creep compliance values was minimal (Lytton et al., 1993); however, there could be slight errors associated with the strength values. In the analysis presented in this report, corrections for change in jig were not applied considering the insignificant impact of such correction.

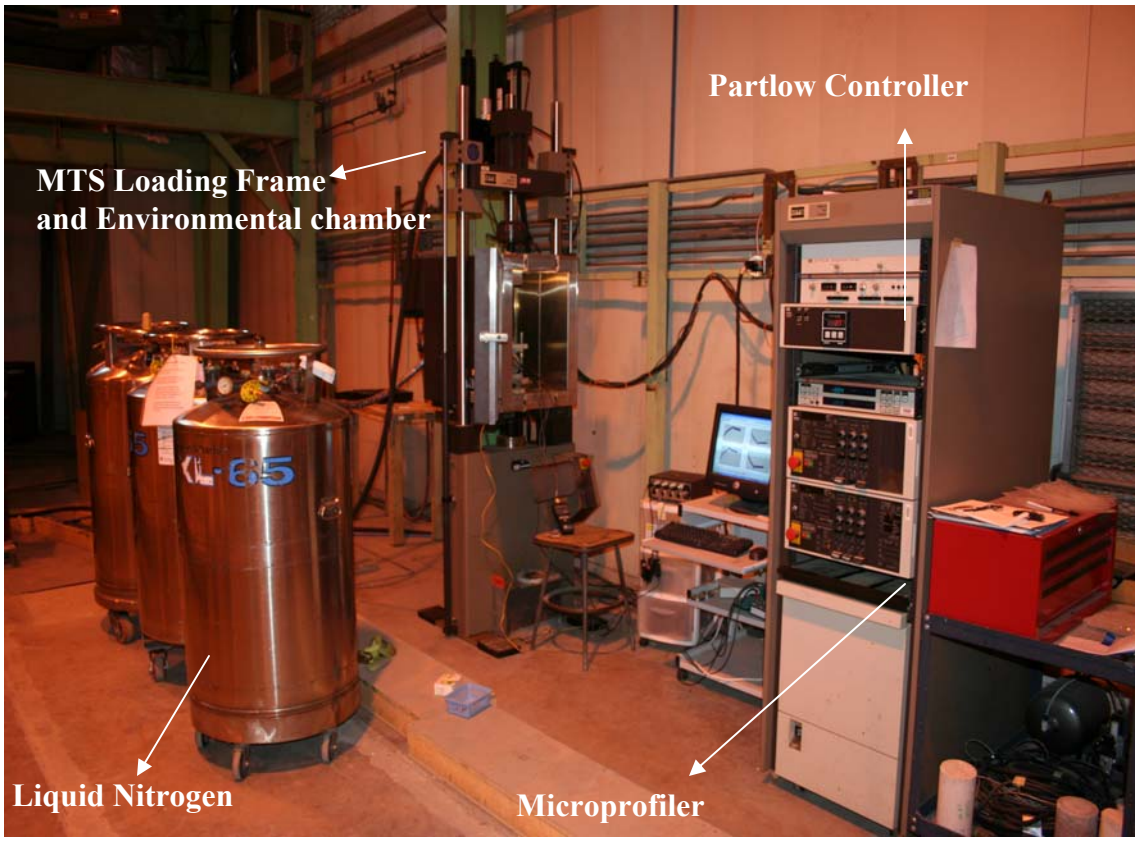

Figure 1. Complete setup of the MTS and Partlow controller

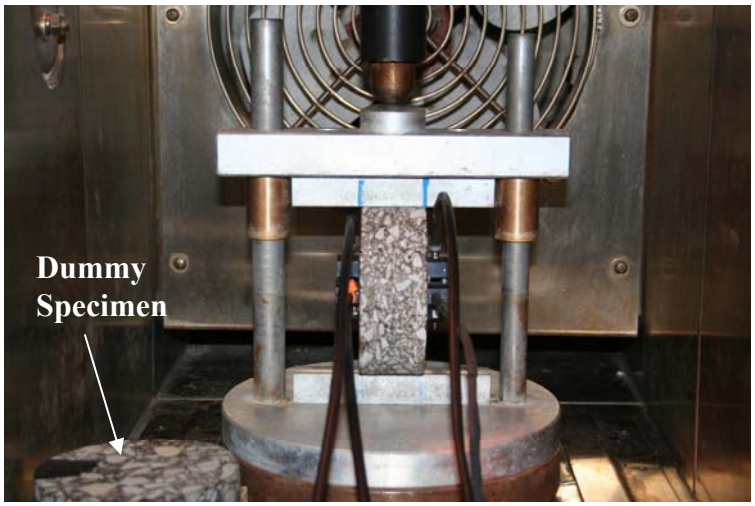

Figure 2. IDT test setup

Bending Beam Rheometer (BBR)

Bending Beam Rheometer (BBR) is an instrument used to measure the flexural creep stiffness of asphalt binder over a temperature range of -5˚C to -40˚C in a three-point bending arrangement. The BBR test apparatus consists of three major components: the control unit, the load unit, and the refrigeration unit. The load and the control units are supplied by Cannon Instruments, Inc., and the refrigeration unit is manufactured by Julabo USA, Inc. The Julabo refrigerated circulators employ a circular head and a cooling machine with capabilities of heating and cooling liquids in bath tanks.

The control unit contains the electronic components required to condition the signals from the LVDT, to provide loading, and to communicate with the host computer via the serial port. Also included in this unit are gauges and switches required for operation and adjustment of the pneumatic system. The load unit consists of a vertical shaft, the movement of which is measured precisely by an LVDT with a range of 10 mm. An air chamber below the air bearing provides a force that counterbalances the load applied to the specimen from the entire weight of the load cell. The load applied to the specimen can be controlled by adjusting the switches on the control unit.

According to test specifications, the fluid in the BBR bath must have low viscosity, high heat capacity, and low vapor pressure over a wide range of temperatures (AASHTO T313). Ethyl alcohol (Ethanol) that matches the specifications closely was used for this study. The original data collection software, BBR version 1.23, developed by Cannon Instruments, Inc., was not capable of capturing data after 240 seconds. Since testing SISSI binders under Phase II required extended testing time, a special software BBR version 3.21 (also known as BBR-Long) developed by the same company was used. This new software was capable of capturing data for a maximum period of two weeks. For this study, data were collected at a sampling rate of one data point per 2 seconds for the 2-hour duration of the test. Higher sampling frequency was discouraged to avoid large data files. The complete setup of BBR is shown in Figures 3 and 4.

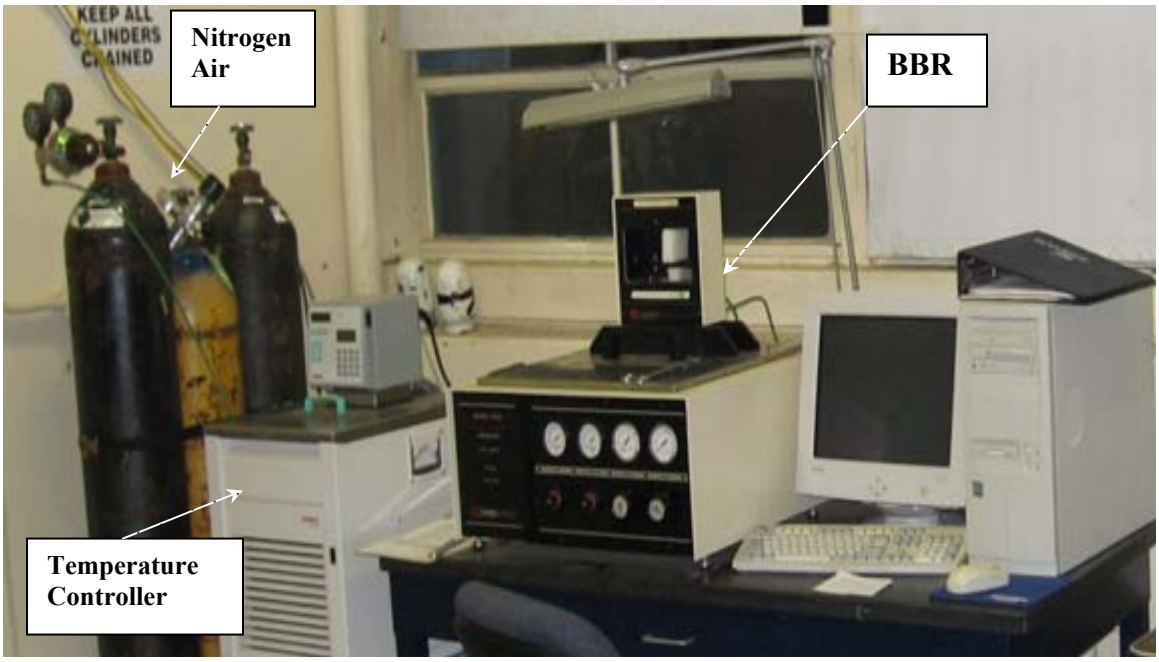

Figure 3. Complete setup of the BBR

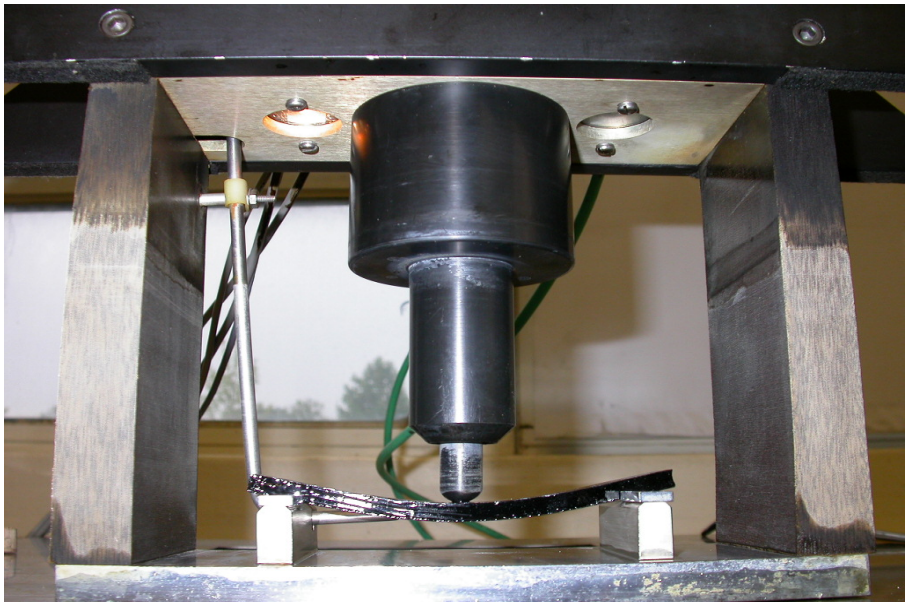

Figure 4. BBR test specimen between supports

Superpave Shear Tester

An Interlaken Superpave Shear Tester (SST) was used to capture properties of SISSI mixtures for evaluation of permanent deformation. This is a closed-loop feedback, servo-hydraulic system that can induce various stress paths in the specimen through application of axial loads, shear loads, and confinement pressures at controlled temperatures. There are six major components to this testing equipment: testing chamber, control and data acquisition system, environmental control chamber, air pressurizing system, load and deformation measuring transducers (load cells and LVDTs, respectively), and hydraulic system. Typical dimensions for test specimens are a diameter of 150 mm and a height of 50 mm. The environmental chamber can control the temperature in the range of 0ºC to 70ºC. The Interlaken Series 3410 hydraulic motors power two actuators, each with a capacity of approximately 32 KN (7 kips). The vertical actuator applies the axial load while the horizontal actuator induces the shear load through moving the shear table. Testing chamber and specimen assembly are presented in Figure 5.

Figure 5. Superpave shear tester and specimen assembly

The vertical and horizontal shear deformations are measured by means of LVDTs. For the strained-controlled frequency sweep test at constant height, LVDTs with ± 1-mm travel range were used for measuring the vertical and horizontal shear deformations. For the stress-controlled constant-height repeated shear test, both ± 1-mm and ± 2.5-mm LVDTs were used for the vertical and horizontal deformation measurements, respectively. Longer travel range LVDT in the latter test was due to greater shear deformation induced compared to the small strain frequency sweep test. Programs developed under the LabView software were used for control and data collection for these tests.

Specimen Preparation for Different Tests

Indirect Tensile Test Specimens

All specimens for IDT testing were obtained from SISSI field mixtures. Because thermal cracking is more prominent in the wearing layer (OECD, 2005), IDT specimens were only prepared from the wearing layer of each site.

The materials, available in 20-litre buckets, were heated at 130°C to become sufficiently loose for sampling. The loose mixture was then conditioned in the oven at 5°C to 10°C above the compaction temperature. This procedure was followed to minimize the heat lost during the compaction process. Temperature probes were positioned in the mixture to monitor the actual temperature of the mixture. The compaction temperature and maximum theoretical specific gravity (G_{mm}) for the mixtures are shown in Table 4. All specimens were compacted to a height of 115 mm and were later cored and cut to obtain two 100-mm by 38-mm (diameter by height) specimens for IDT testing. The mass of mixture used for compaction varied for each site based on the G_{mm} of the mixture. All specimens were compacted to achieve a target air void content of 7 ± 0.5 percent.

Table 4. Compaction temperature (°C) and G_{mm} for wearing layers of SISSI sites

Mixture ID	Layer	County	Compaction Temperature (ºC)	G_{mm}
M0264	wearing	Tioga	153	2.502
M0272	wearing	Mercer E.	153	2.468
M0287	wearing	Mercer W.	153	2.486
M1255	wearing	Warren	153	2.349
M1261	wearing	Perry	169	2.498
M2167	wearing	Delaware	168	2.457
M2302	wearing	Somerset	153	2.500
M3298	wearing	Blair	156	2.535

Specimens compacted using the gyratory compactor tend to have non-uniform air void distribution along the diameter and height. From previous studies conducted by Chehab et al. (2000), it was observed that the top and bottom parts of the specimen have significantly higher air voids, and for variation along the diameter, the ring has more air voids than the core. Hence, to obtain uniform air void content, the specimen had to be cored from a larger specimen with top and bottom portions removed through sawing. From the study conducted by Chehab et al., it was also observed that the 100-mm by 150-mm specimens had the least variation of air voids along their height, as shown in Figure 6.

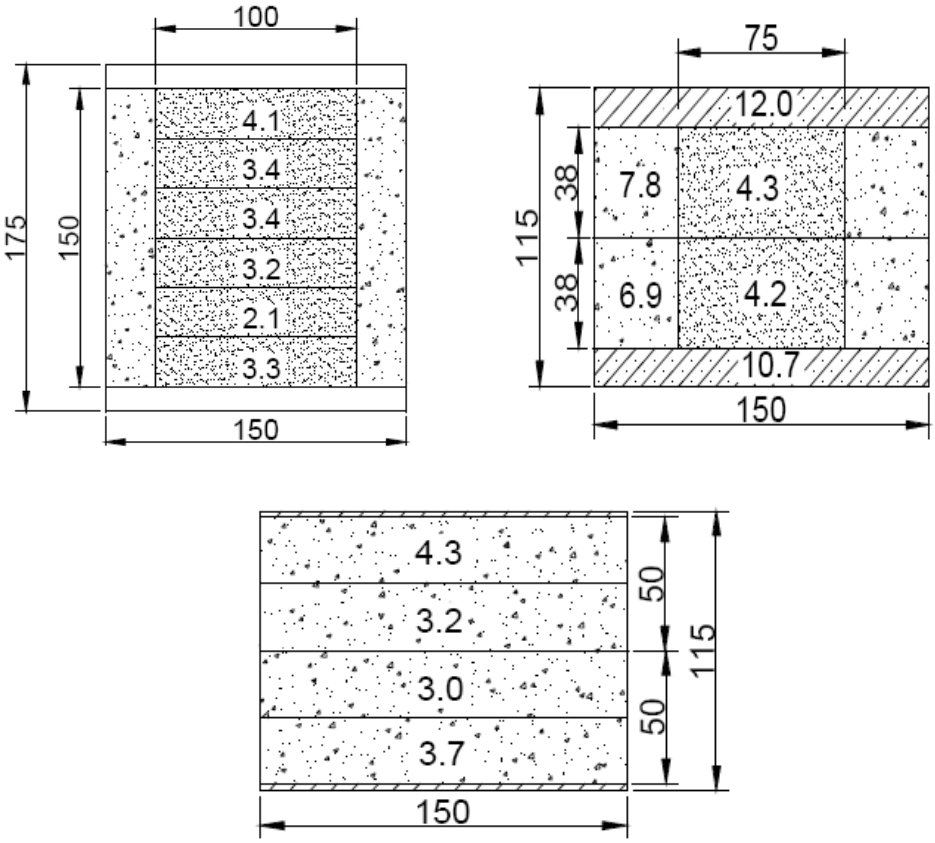

Figure 6. Distribution of air void content (%) in gyratory compacted specimens (Chehab et al., 2000)

Although the 100-mm by 150-mm (cored from 150-mm by 175-mm) specimen had the least amount of air voids, specimen geometry of 115 mm by 150 mm was selected for compaction, keeping in mind the limited material available for specimen fabrication. Test specimens were cored from compacted specimens. Even though AASHTO 322 specifies specimen geometry of 150 mm by 38 mm for IDT testing, all the IDT tests in this study were conducted on 100-mm by 38-mm specimens. This specimen geometry was adopted after considering that the 150-mm diameter specimens have a greater variation of air void content along the diameter in comparison to the 100-mm-diameter specimens (Wen, 2000).

Superpave™ mix design procedures require the design air void content to be 4 percent for laboratory-prepared specimens (Asphalt Institute, 1996), while compaction in the field takes place at 2 percent to 4 percent above the design air void content (i.e., 6 percent to 8 percent). One of the objectives of the SISSI project involves predicting pavement performance using the MEPDG, with material characterization test data as input. In order to get a meaningful comparison between pavement performance predicted from MEPDG and field observation, it is ideal that material properties, including air void

contents, in the field and laboratory match. Level 1 input for the thermal cracking model in the MEPDG requires tensile strength, creep compliance, and air voids content as input (Applied Research Associates, 2003). The as-constructed air void content is used to calculate the coefficient of thermal contraction used as input for the thermal cracking model. Hence, to obtain good correlation between field- and laboratory-compacted specimens, as-constructed air void content of 7 ± 0.5 percent was chosen for testing purposes. Details on the MEPDG software and the thermal cracking model are available in a separate report (Applied Research Associates, 2003).

BBR Test Specimens

For the BBR tests, pressure aging vessel (PAV)-aged binders from the wearing layers of seven sites, excluding Tioga, were used for preparing specimens. There was not sufficient binder available from the Tioga site to be included in this part of the study. Typically, asphalt binder undergoes aging, i.e., it becomes brittle because of volatilization of light oils and exposure to oxygen. After the asphalt pavement is constructed, oxidation dominates the aging process, and this in-service aging is simulated by the Superpave™ PAV test. The detailed procedure for preparing BBR specimens is discussed in AASHTO T313. The steps involved in preparing the specimen are shown in Figure 7.

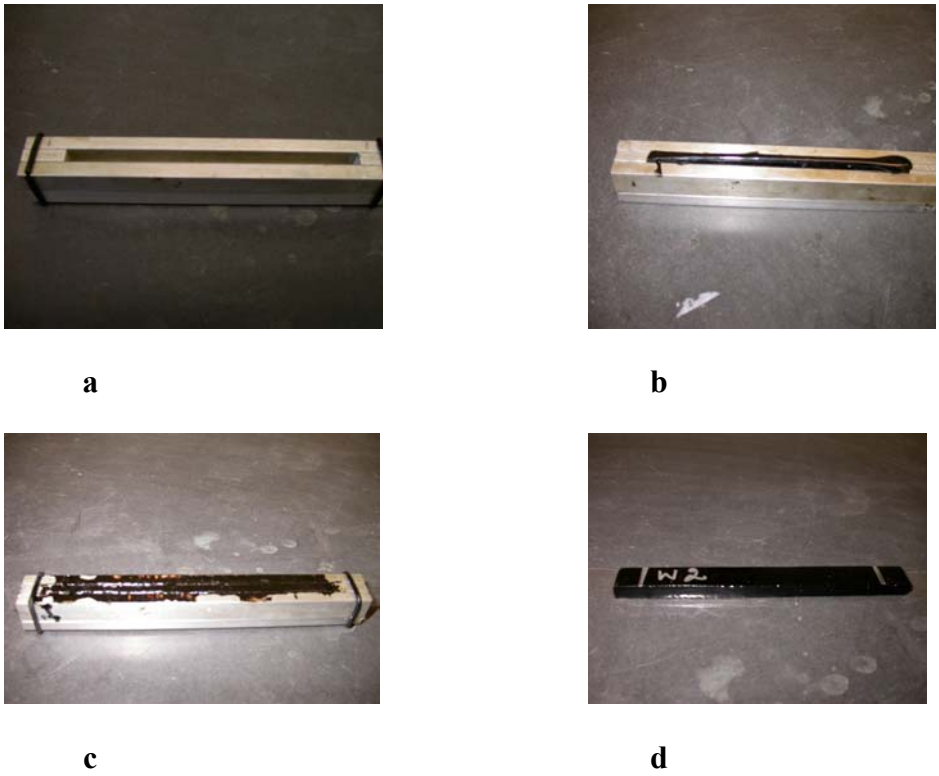

Figure 7. Steps involved in preparing a BBR specimen: (a) mold preparation, (b) pouring the asphalt binder, (c) trimming the surface, (d) sample specimen

SST Test Specimens

The first step in specimen preparation for testing with the Superpave Shear Tester was to compact specimens with diameters of 150 mm using the Superpave Gyratory Compactor. The specimens were then trimmed to a thickness of 50 mm and glued between two platens.

A gluing device, seen in Figure 8, was used to squeeze the specimen between the platens while the glue cured. An epoxy-type of glue, such as Devcon Plastic Steel, was employed for this purpose. The gluing device rigidly holds the platens and specimen to ensure that the platen faces are parallel.

After the glue cured, brackets were affixed to the sides of the platens. These brackets hold the horizontal LVDT as well as vertical LVDTs, shown in Figure 9.

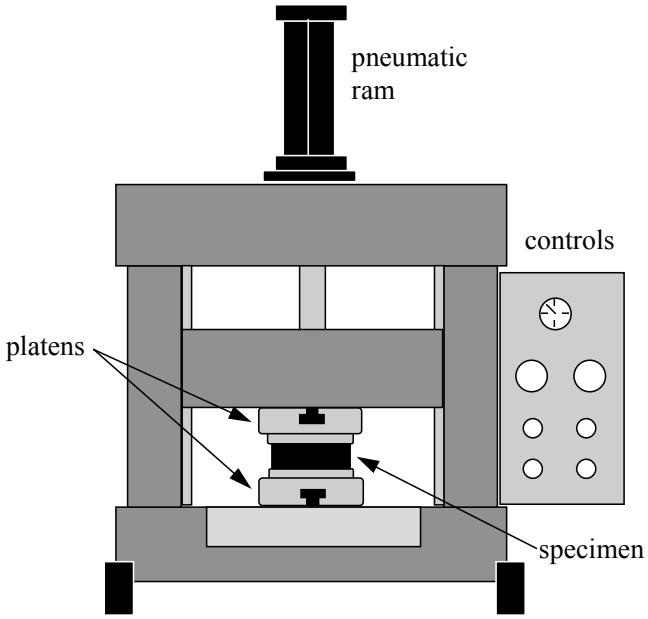

Figure 8. SST gluing device

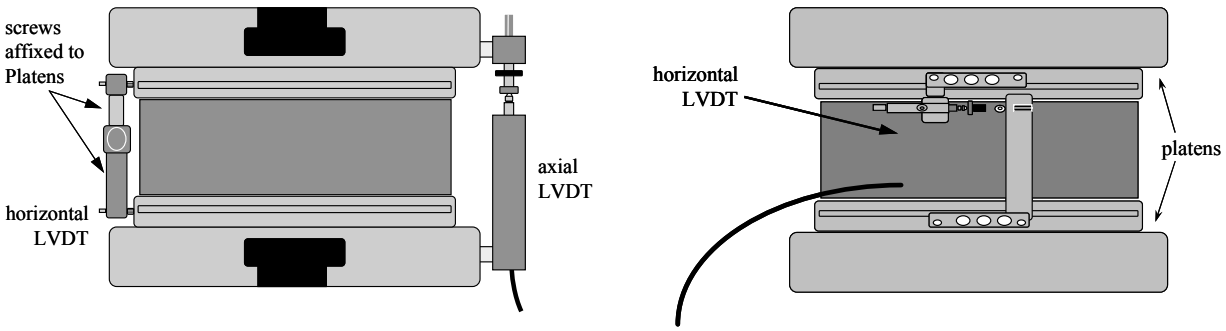

Figure 9. Schematics of specimen and transducer assembly for SST tests

Testing Protocols

Indirect Tensile Test Protocol

The IDT tests for creep compliance D(t) and tensile strength were conducted in accordance with AASHTO T322; Four X-SB LVDTs, two for measuring vertical deformation and two for measuring horizontal deformation, were fitted onto the specimen by means of LVDT mounts. Eight brass gauge points having a diameter of 8 mm and a thickness of 3.2 mm were glued to the specimen, four on each face, using a Devcon 5-minute epoxy. These points served for mounting LVDTs. A special template was used to facilitate this process. After securing the screws on the mounts, the LVDT signals were checked to ensure that each LVDT was measuring near the middle of its range and was repositioned if required.

A gauge length of one inch (25.4 mm) was used for mounting the LVDTs as specified by AASHTO 322. Use of larger LVDT gauge lengths minimizes the effects due to large aggregate particles between the gauge points. However, considering that the viscoelastic solutions developed by Wen (2001) used in this study to calculate the D(t) of the mixtures did not accommodate the 38.1-mm gauge length, and to minimize the effects due to stress concentrations near the loading strips, a gauge length of 25.4 mm was used. In this regard, it should be noted that the nominal maximum aggregate size for the wearing layers of all SISSI sites is 12.5 mm or 9.5 mm. The horizontal and vertical LVDT setup is shown in Figure 10.

D(t) tests were conducted for a 100-second loading time at -20^{o}C, -10^{o}C, and 0^{o}C by loading the specimens along the diametric axis to produce vertical and horizontal deformations. Specimens were tested at the lowest temperature first and progressively at higher temperatures. At low temperatures, the X-SB LVDT coils tended to freeze and stall during testing. In such cases, the environmental chamber was left open to defreeze the LVDTs before testing at the test temperature. Prior to testing, to check the positioning of the specimen, a small creep load for a period of 20 seconds was applied. The position of the specimen on the jig was later adjusted, if required, to obtain similar deformations on the horizontal and vertical LVDTs on both sides. The AASHTO specifications stipulate that the asphalt concrete specimen remain in linear viscoelastic range (i.e., no damage) throughout the creep test. This can be achieved by maintaining the horizontal strains below 0.05 percent (AASHTO T322) for 150-mm-diameter specimens. In testing for SISSI Phase II, loads were applied to maintain the horizontal strains below 0.01 percent since 100-mm-diamter specimens were used. If this limit was reached, the test was stopped immediately, and the specimens were allowed to relax for a minimum of 5 minutes before resuming with appropriate load levels.

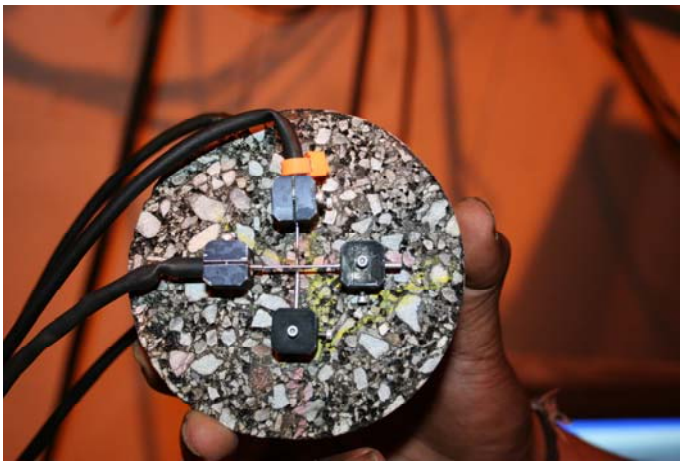

Figure 10. LVDT setup on the IDT specimen

Once all D(t) testing was completed, the specimens were cooled to -10°C to conduct the tensile strength test by loading the specimens at a constant crosshead movement rate of 12.5 mm/sec until failure. In this study, the LVDTs were removed prior to strength tests to avoid any damage caused due to possible sudden specimen failure (Christensen et al., 2005).

BBR Testing Protocol

The BBR is used to obtain the flexural creep stiffness S(t) of PAV-aged SISSI binders by loading beam specimens in a three-point bending arrangement. The test specimens are in the shape of rectangular beams with dimension of 125 mm by 12.5 mm by 6.2 mm. The asphalt beam is loaded at mid-point with the load applied using a pneumatic actuator and a piston guided by air bearing. Creep load is then applied and held constant for the required test duration. The loads are varied according to the temperature and asphalt stiffness to maintain the strain level within the linear viscoelastic range, i.e., within 0.5 percent (Bahia, 1991).

Superpave™ specifications require the testing to be conducted for a period of 240 seconds at a test temperature of 10°C higher than the lower temperature grade of the asphalt binder (AASHTO T313). This specification was developed with the assumption that the flexural creep stiffness of the asphalt binder at 2 hours [S(*7200*)] at the temperature of the lower temperature grade is equivalent to its flexural creep stiffness at 60s [S(*60*)] at a temperature 10°C higher. This was concluded through comprehensive studies conducted by Anderson et al. (1992), proving that the shift factor curve for all asphalt binders are similar and have a slope approximately between 0.173 log(s)/°C and 0.199 log(s)/°C. Details of the study can be found in the SHRP reports (Anderson et al., 1994). Because the main goal of this study was to revisit and build on the research conducted previously, the S(t) of the asphalt binders was obtained at three temperature levels: 1) at the lowest binder grade temperature, 2) at a temperature 10°C higher than the

lower temperature grade of the binder, and 3) at a temperature of -5°C for the purpose of constructing a stiffness master curve. Initially, a temperature of 0°C was used for testing, but because of problems with applying low loads to maintain linear viscoelastic response, a temperature of -5°C was chosen (Bahia, 1991). Because the low temperature grade for all the asphalt binders tested in this study was the same (XX-22), the lower temperature grade will be referred to as T_1.

In order to satisfy both objectives of this study, i.e. to verify whether S(7,200) at T_1 is equal to S(60) at T_1 +10 and to check whether all asphalt binders have similar shift factor curves, BBR tests had to be conducted for both 240 seconds and 2 hours at all three temperatures. Master curves were developed individually for the 2-hour and 240-second data for comparison and verification. At each temperature, the 240-second test was conducted prior to the 2-hour test, and the stiffness values were compared to make sure the specimen was in the linear viscoelastic range. Marasteanu and Anderson (2000) specified that in order for the asphalt binder to be linear viscoelastic (LVE), the conditions for homogeneity and superposition must be satisfied. The check for homogeneity is considered satisfied if the asphalt binder stiffness remains within 5 percent after testing at various loads at a given temperature. In this study, the condition for LVE was checked by conducting 240-second tests immediately after the 2-hour test with the same or increased load levels. It was observed that the stiffness values at 60 seconds for the final 240-second tests were higher than those of the 2-hour tests at all three testing temperatures, proving the specimen was in the LVE range, as shown in Figure 11.

The specimens were marked to make sure they remained in the same position for all temperatures during the test. During initial testing, the displacement values at the beginning and end of each test and at every temperature were recorded to check whether the specimen relaxed to its original position. Alternative methods to check the specimen relaxation, such as recording the relaxation data (Marasteanu and Anderson, 2000), could prove to be more effective. Because of time constraints, it was decided that a relaxation time of 20 minutes after the 240-second test and a relaxation time of 2 hours after the 2-hour test should be sufficient. The relaxation times were chosen considering the total time of testing and the fact that it was possible for the specimen not to relax to its original position with the relaxation times provided. The relaxation times were primarily provided to ensure that the specimen remained in LVE range throughout the course of the test. However, for all BBR tests, the LVE condition was satisfied by means of the homogeneity principle, which overrides any insufficient relaxation time.

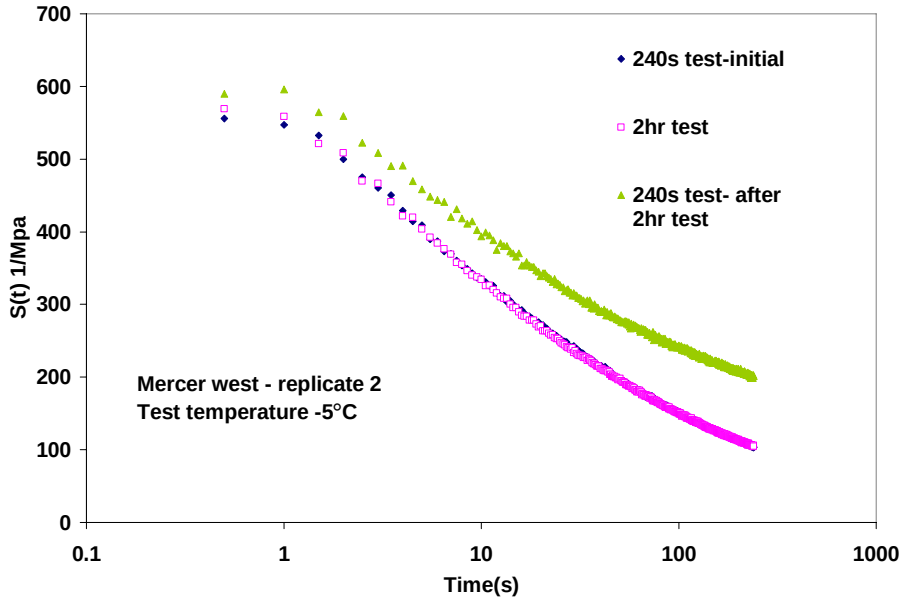

Figure 11. Check for LVE conditions

Initially, a dummy specimen was placed inside the control unit water bath to monitor the exact temperature of the test specimen; however, it was observed that it took less than 10 minutes for the dummy specimen to reach the testing temperature. AASHTO specifications require the specimen to be conditioned at the test temperature for one hour before testing. In this study, because of the introduction of a 2-hour relaxation time between temperatures, the conditioning time was considered more than sufficient. Hence, the dummy specimen was not used to monitor temperatures for subsequent tests. It should be noted that after the completion of a 2-hour test at a particular temperature, the temperature of the bath was changed to the subsequent test temperature. Ideally, the specimen must be allowed to relax for 2 hours at the current test temperature to avoid any possible effects associated with the coefficient of thermal expansion of the asphalt binder specimen; however, because of time constraints, the time taken for change in temperature was also included in the relaxation time.

Before each test, the standard calibration procedures were followed, as explained in detail in AASHTO T313. While placing the test specimen between the supports, it was observed that the specimen slid away from the supports because of the forces exerted by ethanol circulating in the liquid bath. To circumvent this problem, the vertical shaft had to be brought down to apply a small load and hold the specimen in position. Later, a valve was fitted to control the flow of ethanol circulating in the bath, which eliminated this problem. Between testing temperatures, the test specimen was removed from its supports and placed inside the bath to eliminate any creep from self load.

During initial periods of testing, creeping of the load with time was observed both during the 240-second and 2-hour tests, as shown in Figure 12. The load increased by up to 50 percent during certain tests, especially at higher temperatures. Similar problems were also noticed during the SHRP projects (Bahia, 1991), but no concrete solution was available to solve this problem. The front panel of the BBR was replaced and a needle valve installed (to assist the ramp in a square wave) to reduce the increase in load during the creep tests. The problem was solved by placing the thick steel specimen (used for calibration) in load mode for an hour before testing.

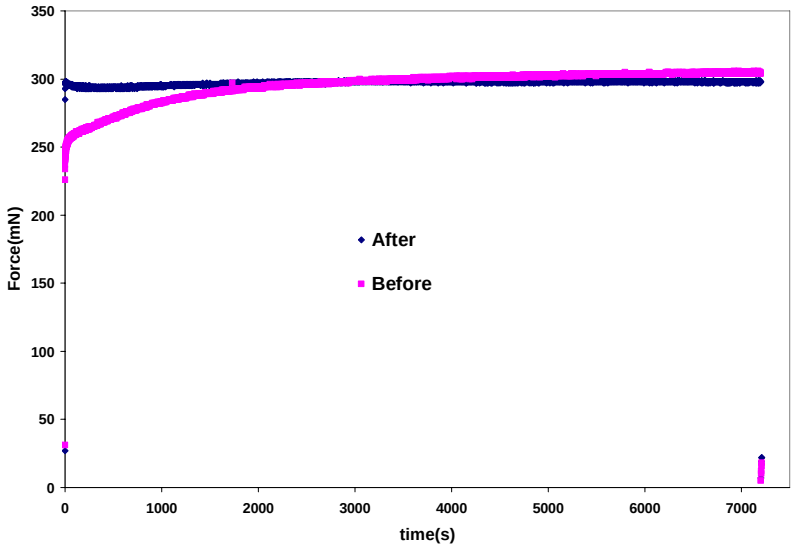

Figure 12. Loading curve before and after installation of needle valve

The sequence of loading time under the bending beam rheometer at each test temperature is best presented by schematics in Figure 13. The figure shows that short loading is followed by a rest period before long loading. Afterward, short loading and recovery period is repeated before moving to the next test temperature.

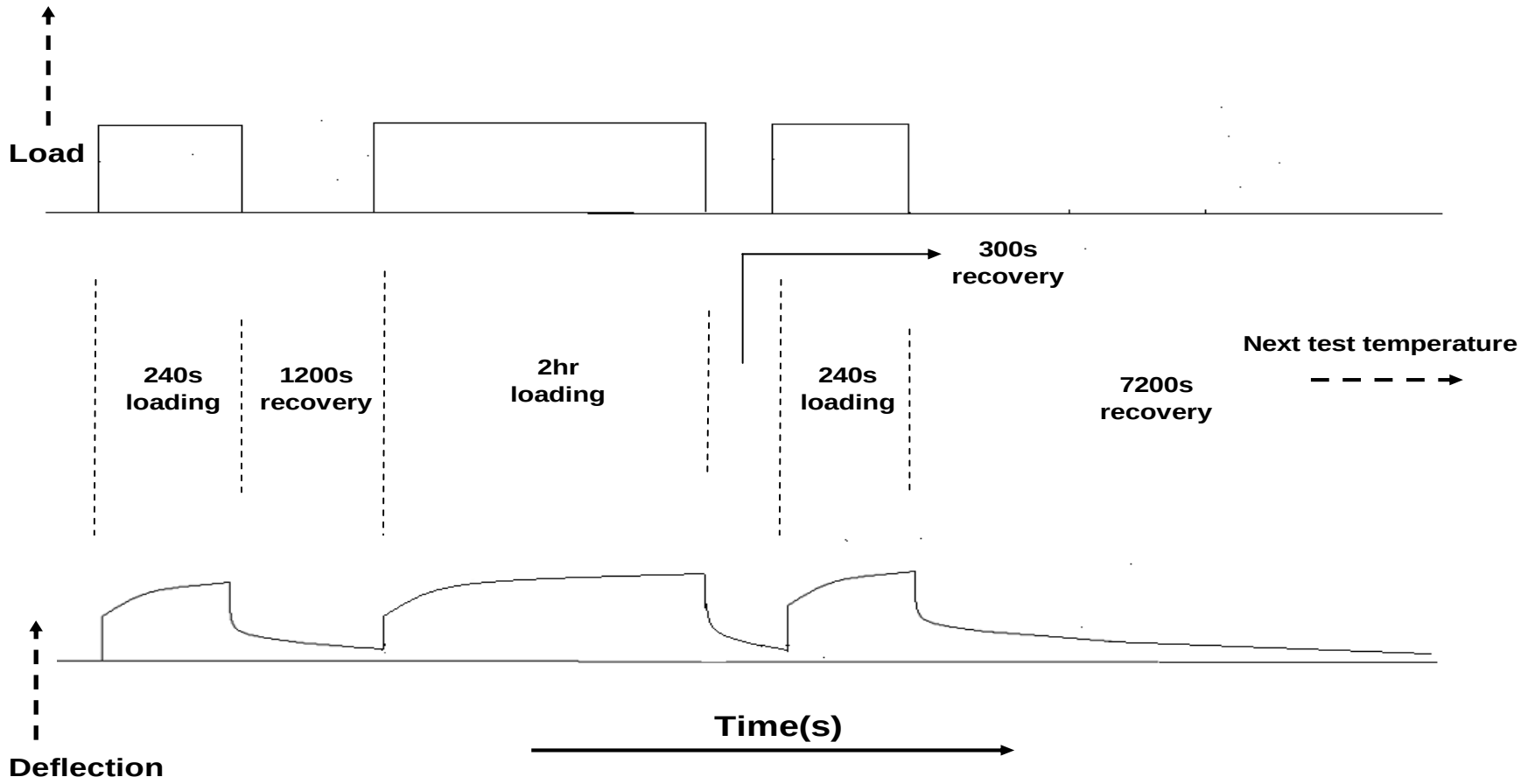

Figure 13. BBR testing protocol for one test temperature

Constant Height Repeated Shear (RSCH) Test Protocol

The RSCH test was conducted in accordance with AASHTO T320. In this test, a haversine shear load is applied to achieve a controlled shear stress level of 68 KPa (approximately 10 psi). When the repeated shear load is applied, the test specimen seeks to dilate. The signal from the axial LVDT is used as feedback by the vertical actuator to apply sufficient axial load to keep the specimen from dilating. In this test, the height is maintained within a range of ±0.013 mm by controlling the vertical actuator using the closed-loop feedback from the vertical LVDT.

A load cycle consists of 0.7 seconds, which is composed of a 0.1-second shear load application followed by 0.6-second rest period. Test specimens are subjected to 5000 load cycles or until the permanent shear strain reaches 5 percent.

The test temperature used was T_{max}, which is the 7-day maximum pavement temperature at a 50-mm depth. For SISSI mixtures, the RSCH tests were conducted at 52ºC. During the test, axial and shear loads and deformations were measured and recorded. Figure 14 shows typical stress pulses in the test.

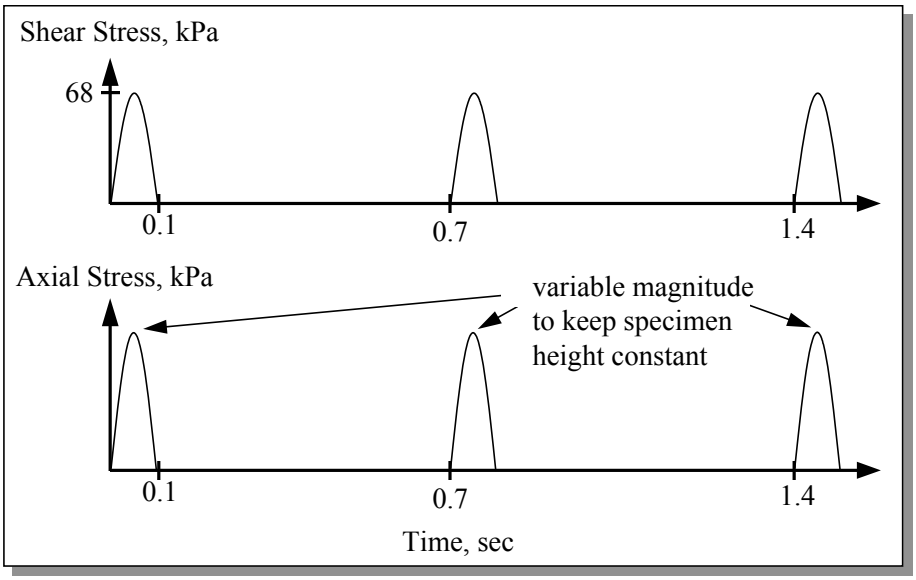

Figure 14. Stress pulses in repeated shear test at constant height

Strain-Controlled Frequency Sweep Test Protocol

This test is performed at a series of temperatures and frequencies to evaluate mix properties in regard to resistance against permanent deformation and fatigue cracking. From the test results, modulus is defined as a function of temperature and loading rate, and a corresponding master curve is developed. A repeated sinusoidal shearing load is applied to the specimen to achieve a controlled shearing strain of ±0.005 percent. A limited number of loading cycles are used at each of these frequencies: 10, 5, 2, 1, 0.5,

0.2, 0.1, and 0.01 Hz. The number of induced cycles is reduced as load frequency is decreased.

As the test specimen is sheared, it seeks to dilate, which increases its height. The vertical actuator uses the signal from the axial LVDT to apply sufficient axial stress to keep the specimen height constant. For SISSI mixtures, the test was performed at three different temperatures (4ºC or 5ºC, 20ºC, and 40ºC).

During the test, axial and shear loads and deformations were measured and recorded. Figure 15 illustrates the application of shearing strains and axial stresses during the test.

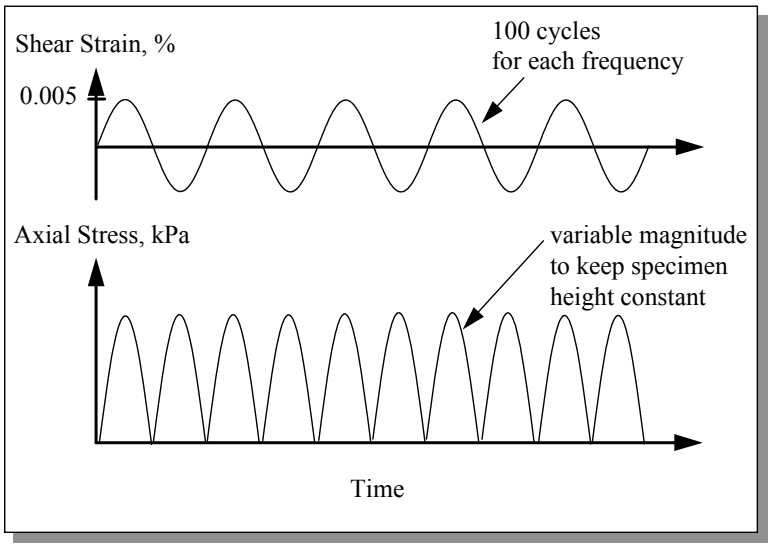

Figure 15. Shear strain and axial stress applications in frequency sweep test at constant height

CHAPTER 3
THEORETICAL BACKGROUND ON LOW TEMPERATURE CRACKING AND DEFORMATION

Thermal Cracking in Asphalt Pavements

Low temperature cracking or thermal cracking occurs in asphalt pavements when the induced tensile stresses in the pavement exceed its tensile strength. This results in cracks transverse or perpendicular to the direction of the traffic, as seen in Figure 16. The cracks are usually equally spaced (Jung et al., 1992). Thermal cracking primarily occurs because of temperature variations and is augmented by traffic loading. Thus, the top layer or the wearing layer of the pavement structure, which is exposed to greater temperature variations than the underlying layers, is usually more susceptible to thermal cracking (OECD, 2005).

Thermal cracks permit the migration of water and fines into the pavement structure, causing local settlement of the pavement. The water entering through these cracks forms ice lenses that can lead to the formation of cavities that eventually collapse under heavy vehicular loads. Thus, control of thermal cracking is essential for the design of good-quality flexible pavements (Buttlar, 1996).

Several factors influence thermal cracking in asphalt pavements, including material type, pavement structure, rate of cooling of the pavement structure, and temperature (Jung et al., 1992). To control thermal cracking, the low temperature properties of the asphalt mixture and binder need to be considered and modified, if necessary, by the designer.

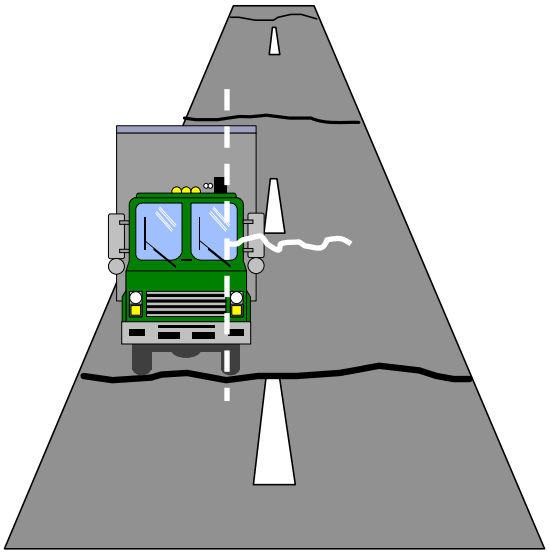

Figure 16. Thermal cracking in flexible pavements

Creep and Tensile Strength from Indirect Tensile Test (IDT)

Thermal stresses developed in the pavements are the primary causes of thermal cracking in asphalt pavements. In addition, the fracture property of the mixture is important because it determines the amount of cracking that will develop when subjected to thermal stresses (Lytton et al., 1993). It is, therefore, important to measure developed thermal stresses and fracture properties of the asphalt mixture to understand its low temperature behavior. Thermal stresses can be derived from the relaxation modulus of a mixture. Determination of the relaxation modulus requires conducting a test in which a constant level of strain is maintained throughout the test. Such test is more difficult to conduct than a test in which stress is maintained constant during the test. Hence, it is more common to conduct stress controlled creep tests from which creep compliance is determined. Specifically, when tensile creep compliance and strength are needed, indirect tension test (IDT) is selected because of the simplicity in test set-up.

The vertical and horizontal stress distribution for a 100-mm by 38-mm (diameter by height) asphalt concrete specimen used in IDT tests is shown in Figure 17. The stress distribution, near the center of the specimen, is uniform. The stresses in this zone are also unaffected by the end effects near the loading strips; thus, deformation measurements near the center of the face of the specimen are not significantly influenced by stress concentrations near the loading strips (Lytton et al., 1993).

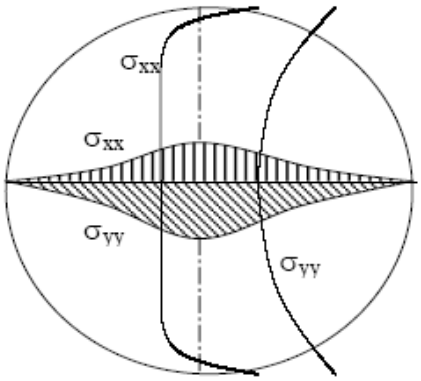

Figure 17. Elastic stress distributions in an IDT specimen (Wen, 2001)

Typically, cracking due to loading in asphalt pavements starts at the bottom of the asphalt layer, under the wheel load, with horizontal tensile stresses occurring at the bottom and compressive stresses at the top, as shown in Figure 18. It should also be noted that the stress state in the center of an IDT specimen is very similar to that occurring in the bottom of asphalt pavements. Additionally, as shown in Figure 19, in the IDT mode, cracking occurs in the direction perpendicular to loading, unlike uniaxial tests, thereby depicting field conditions.

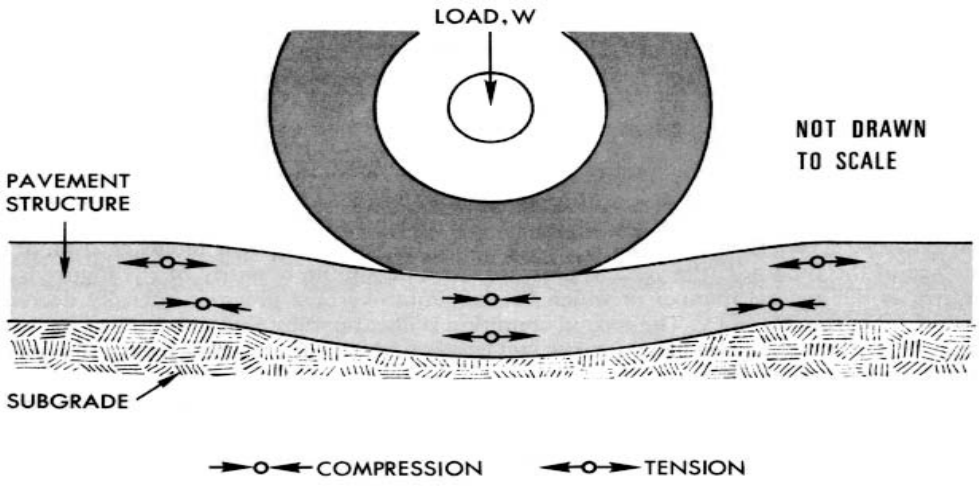

Figure 18. Typical stress states in asphalt concrete layers with loading (Santucci, 1998)

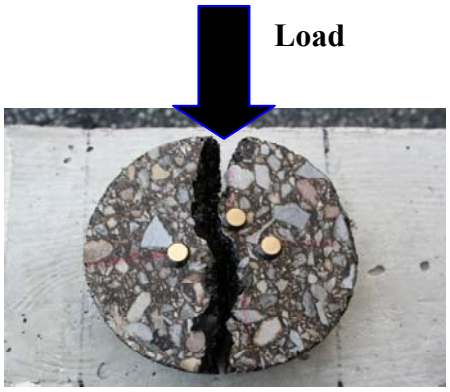

Figure 19. Direction of crack in an IDT specimen

A measurement and analysis system for determining the creep compliance and tensile strength in the IDT mode was developed by Roque and Butler (1992) and is incorporated in ASSHTO T322, *Standard Test Method for Determining the Creep Compliance and Strength of Hot Mix Asphalt (HMA) Using the Indirect Tensile Test Device.* A new gauge-point measurement system was developed, and the measured vertical and horizontal deformations were used to calculate Poisson's ratio rather than assuming a constant value of 0.35. The aggregate size effect, stress distribution in the specimen area, and bulging effects were considered in the design of the mounting system used and positioning of LVDTs on the specimen surface. Based on finite element analysis, gauge lengths of 25 mm and 38 mm for 100-mm and 150-mm specimens were recommended, respectively. The elastic solutions for determining the creep compliance

and Poisson's ratio of asphalt mixtures tested in the IDT mode is shown in Equations 1 and 2:

$$D(t) = \frac{X \times D \times b}{P \times GL} \times C \tag{1}$$

where

D(t) = creep compliance
X = average, normalized horizontal deformation at 50 seconds
D = diameter of specimen
b = thickness of specimen
P = load applied
GL = gauge length
C = correction factor for bulging

$$\nu = -0.1 + 1.48\left(\frac{X}{Y}\right)^2 - 0.778\left(\frac{b}{D}\right)^2\left(\frac{X}{Y}\right)^2 \tag{2}$$

where

υ = Poisson's ratio
X = the horizontal deformation
Y = the vertical deformation

Wen (2001) proposed viscoelastic solutions for determining the creep compliance and Poisson's ratio, as shown in Equation 3.

$$\begin{aligned} D(t) &= -\frac{d}{P}\{aU(t) + bV(t)\} \\ \upsilon &= -\frac{cU(t) + dV(t)}{eU(t) + fV(t)} \end{aligned} \tag{3}$$

where

d = specimen thickness
P = load applied to specimen in indirect tension mode
$U(t)$ = horizontal deformation of specimen
$V(t)$ = vertical deformation of specimen
υ = Poisson's ratio

a, b, c, d,e and f = coefficients

For a 100-mm-diameter specimen and gauge length of 25.4 mm, the coefficients developed by Wen (2001) are shown in Table 5.

Table 5. Coefficients to calculate the creep compliance and Poisson's ratio (after Wen, 2001)

Coefficient	*Value*
a	0.7874
b	2.2783
c	3.385
d	1.081
e	1.000
f	3.122

The tensile strength of the mixture is important in determining its fracture properties and is also included in the theory of crack growth of non-linear viscoelastic materials developed by Schapery (1984). The tensile strength test is conducted at -10°C, where the specimen is failed under a constant crosshead rate. It is observed that micro-cracks tend to form even before the specimen fails. For obtaining the fracture parameters, it is more important to know the true load for failure than the maximum. The true point of failure is defined as occurring when the difference between the vertical and horizontal deformations reaches a maximum that can be determined by using LVDT measurements. It was found, however, that using LVDTs for strength tests resulted in damage or destruction of the transducers (Christensen et al., 2005). Hence, it was recommended by those researchers that LVDTs not be used during the strength test and that the uncorrected strength be adjusted using the empirical relationship shown in Equation 4.

$$Tensile\ Strength = 0.25 + (0.78 * IDT\ strength)\ MPa \quad (4)$$

The precision evaluation of the IDT tests was conducted as part of Phase III of NCHRP Project 9-29, which assessed the AASHTO T322 method. IDT test data from six laboratories were used in this evaluation. The d2s precision or the maximum allowable difference between two samples for 95 percent of the time was calculated, and it was observed that the variability in D(t) was as high as 10 to 30 percent. For single operator

precision, the average d2s for all laboratories was 22, 28, and 32 percent at the lowest, intermediate, and high temperatures of testing, respectively. Figures 20 and 21 represent the d2s precision values for D(t) and Poisson's ratio.

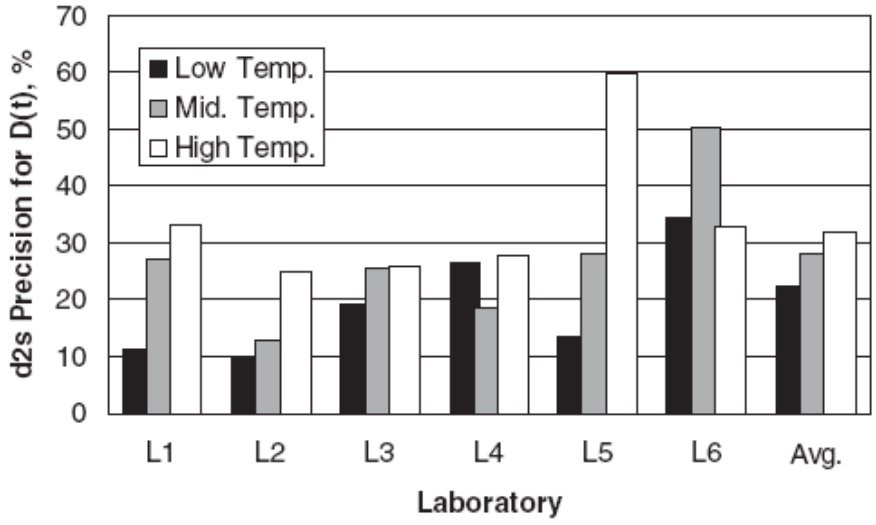

Figure 20. D2S Precision for compliance for six laboratories (Christensen et al., 2005)

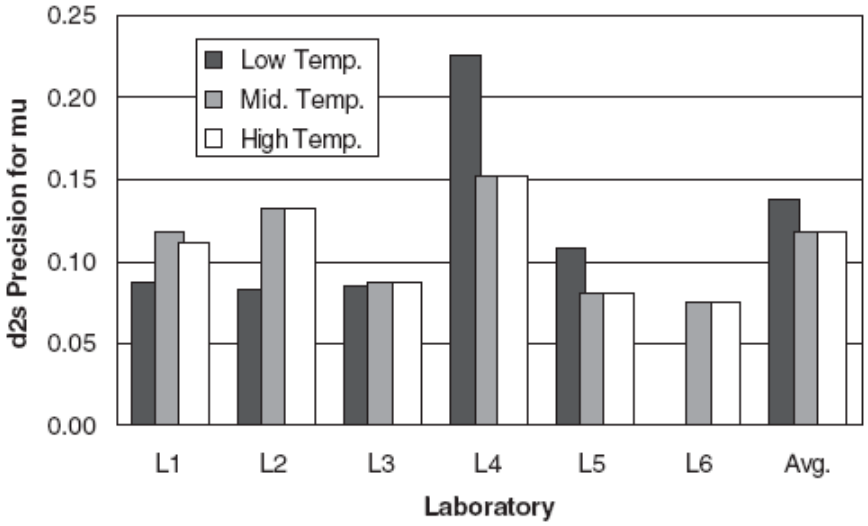

Figure 21. D2s Precision for Poisson's ratio for six laboratories (Christensen et al., 2005)

Limiting Stiffness for Low Temperature Cracking

The relationship between asphalt binder properties and thermal cracking has been investigated by many researchers in the past. It has been established that thermal cracking

occurs in asphalt pavements when the thermal stress exceeds its strength. Specifying the right asphalt binder that can absorb thermal strains is important for reducing thermal cracking; therefore, a limiting stiffness value for asphalt binders has been proposed by several researchers.

Van der Poel (1954) formulated a nomograph for estimating the stiffness values from empirical measurements. McLeod (1968) introduced the Penetration Viscosity Number (PVN) and a modified nomograph to estimate the stiffness values. From his research involving field observations, it was concluded that the critical stiffness of bitumen is 2.4 x 10^8 N/m^2 (240 MPa) for 30 minutes loading time and that cracking would not occur if this value was not reached at the service temperature encountered (Readshaw, 1972). The most reported loading times range from 3000 seconds to 20,000 seconds, with 7,200 seconds being the most common in literature (Bahia and Anderson, 1993). Typical values for the limiting stiffness of asphalt binders vary between 140Mpa and 1Gpa at loading times of 2.8 hours and 30 minutes, respectively (Anderson et al., 1994). However, a limiting stiffness value of 200 Mpa at a loading time of 7,200 seconds is used widely based on the correlation between cracking and S(t), as estimated from nomographs {(McLeod (1968) and Readshaw (1972), Bahia and Anderson, 1993)}.

Several attempts have been made to introduce a device to measure the rheological properties of asphalt, such as the Schweyer forced capillary rheometer and the sliding plate rheometer (Anderson et al., 1990). However, these instruments have analytical problems with the loading mode or specimen geometry (Bahia and Anderson, 1993). Other instruments developed to measure the properties of asphalt are detailed in a separate report (Anderson et al., 1990). The BBR was developed at The Thomas D. Larson Pennsylvania Transportation Institute (LTI) as part of the Strategic Highway Research Program (SHRP) A002A project. This instrument is currently part of the Superpave™ Binder Specifications.

With a testing span of 102 mm (4 inches), the specimen dimension chosen for the BBR tests were 127 mm (5 inches) in length, 12.7 mm (0.5 inches) in width, and 6.3 mm (0.25 inches) in depth (Figure 22). The specimen geometry was chosen to meet two criteria: the criterion for applying elementary bending theory of beams and ASTM recommended criterion for dimension of specimens for testing flexural properties of plastics.

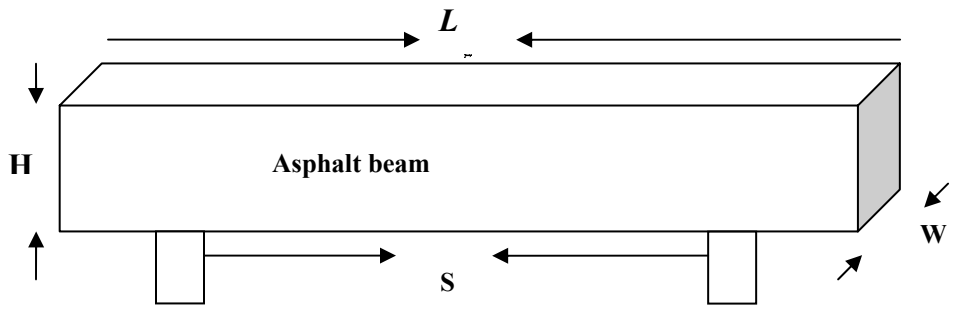

l: Length; H: Height; W: Width and S: Span

Figure 22. Specimen geometry for BBR test

As part of the SHRP A-002A project, an experiment was conducted to evaluate important test parameters for the BBR test and the rheometer, itself. The experiment involved testing of eight different asphalts, also known as the eight-core asphalts, at various temperatures and loading times. For simplicity, the eight-core asphalts will be denoted as SHRP asphalt binders henceforth.

Though several researchers correlated thermal cracking of asphalt pavements with long loading times ranging from 3,600 to 20,000 seconds (Anderson et al., 1990), it was not considered practical for laboratory testing. Therefore, it was decided to shorten the loading time using the time-temperature superposition principle, which is explained later in Chapter 4. After several preliminary tests, a test period of 240 seconds was considered appropriate. This test time was found as a compromise between decreasing the time for testing and collecting sufficient data to perform the analysis.

Studies conducted to evaluate the BBR indicated that shift factor functions for a wide variety of asphalt binders were similar regardless of their loading time within the lower range of pavement temperatures. The slope of the shift factor curve was also found to be linear with a slope between 0.173 log(s)/°C and 0.199 log(s)/°C. Figure 23 and Table 6 show the shift factor values for the SHRP asphalts. It was concluded that an offset of 10°C above the lowest pavement design temperature was sufficient for equating S(t) at 60 seconds to 7,200 seconds at the lowest design temperature; however, the actual 2-hour tests were not performed to check the experimental validity of the equivalence principle (Anderson et al., 1994).

Table 6. Temperature shift factors for SHRP asphalt binders at reference temperature of -15ºC (Bahia, 1991)

SHRP Asphalt	Temperature (° C)					
	-35	-25	-10	-5	Slope^2	R^2
AAA-1	4.026	2.036	-0.924		-0.199	0.9997
AAB-1	3.996	1.951	-0.833		-0.194	0.9984
AAC-1	3.547	1.793	-0.883	-1.82	-0.179	0.9999
AAD-1	3.659	1.855	-0.819		-0.18	0.9996
AAF-1	3.461	1.799	-0.795	-1.736	-0.173	0.9995
AAG-1	3.637	1.770	-0.892	-1.948	-0.184	0.9992
AAK-1	3.735	1.905	-0.764	-1.611	-0.179	0.9986
AAM-1	3.554	1.902	-0.755	-1.763	-0.177	0.9986

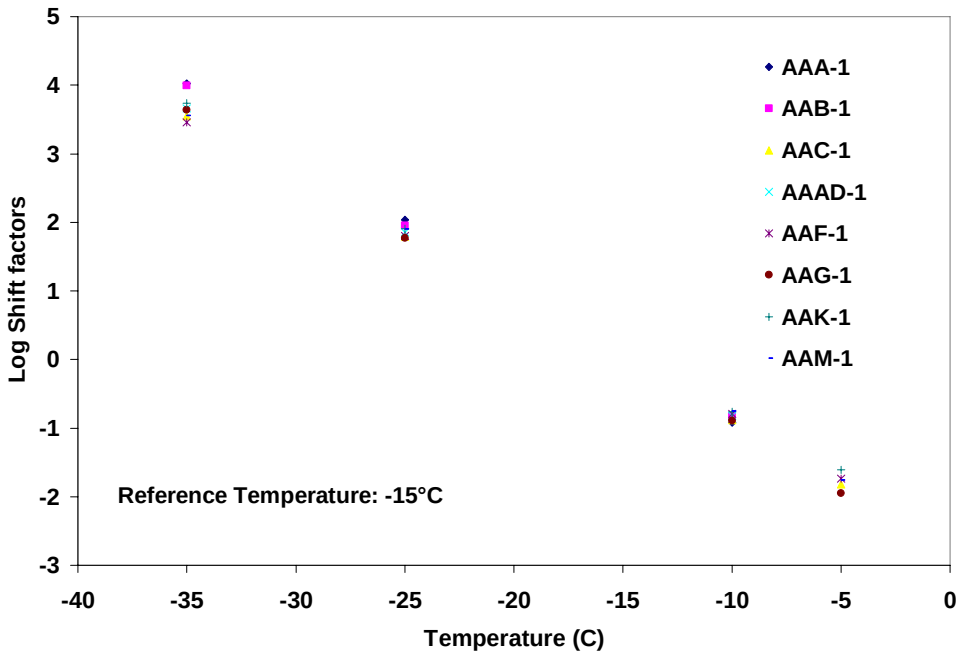

Figure 23. Time-temperature shift factors for SHRP asphalt binders (Bahia, 1991)

The specification for thermal cracking included a maximum S(t) of 300 Mpa at 60 seconds loading time and a minimum m-value of 0.3 at the same loading time. The m-value, which is the slope of the stiffness curve, is an indicator of the stress relaxation capabilities of the asphalt binder. A typical stiffness value of 200 Mpa was used in the majority of the studies, which was estimated from nomographs (McLeod, 1968 and Readshaw, 1972); however, evaluation of the data obtained from the BBR showed that the nomographs under-predicted the creep stiffness by almost 50 percent (Bahia and Anderson, 1992). To eliminate the difference between measured and estimated values, the stiffness value was increased by 50 percent (Bahia and Anderson, 1993). The schematic of the BBR is shown in Figure 24.

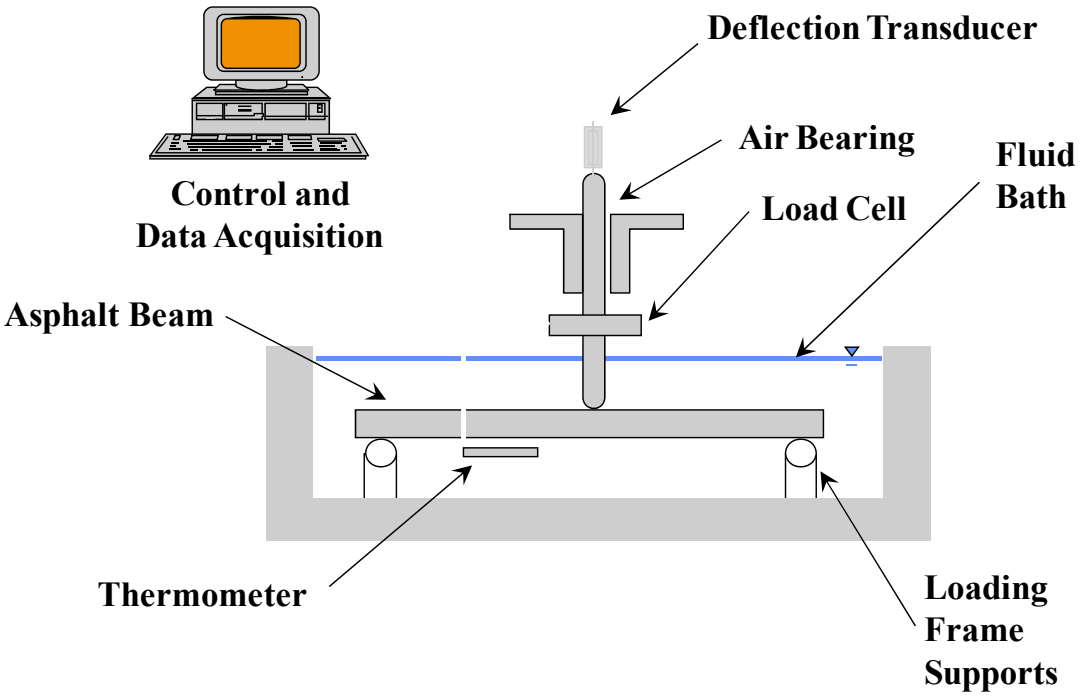

Figure 24. Schematic of the BBR

Arindam et al. evaluated the equivalence principle of the current BBR specifications. BBR tests were conducted at two different temperatures, at the PG low temperature and at 10°C higher, on nine different asphalt binders. Tests were conducted on two replicates and two isothermal conditioning times of 1 hour and 3 days, and the Christensen-Anderson-Marasteanu (CAM) model was used to develop the stiffness master curves. The CAM model for asphalt binders is shown in Equation 5.

$$S(\xi) = S_{glassy}\left[1+(\xi/\lambda)^{\beta}\right]^{\frac{-\kappa}{\beta}} \quad (5)$$

where

$S(\xi)$ = stiffness at a reduced time ξ (s)
S_{glassy} = 3 GPa (assumed constant)
λ, β, and k = parameters in the model, considered unknown in the nonlinear regression

From their study, it was concluded that the binder stiffness values at 60 seconds and 7,200 seconds showed differences ranging from 32 percent to 66 percent. Significant differences were also observed for the m-values. Increasing the isothermal age was found to reduce the difference between stiffness values but showed no such effect for the m-values. The authors also recommended that more testing be conducted on different types of asphalts to reach a comprehensive consensus.

Viscoelastic Material Characterization

Elastic materials exhibit an instantaneous and recoverable response to stress applied and are not dependent on the time of loading. On the other hand, the response of a viscous material to static loading or stress is highly time dependent, wherein the strain increases at a decreasing rate. Viscoelastic materials such as asphalt concrete combine the properties of both elastic and viscous materials (William et al., 1989). In viscoelastic materials, the current response is dependent not only on time but on the current and past input (stress) history (Schapery, 1999). Thus, by applying a static stress to a viscoelastic material, there is an instantaneous elastic response followed by a gradual time-dependent deformation (Anderson et al., 1994). When the stress is removed, a continuous decreasing strain follows elastic recovery. This phenomenon is shown in Figure 25. It should be noted that in asphalt concrete, the response to static loading depends on the time and temperature of loading, loading history, and the age of the material (Roque and Buttlar, 1992).

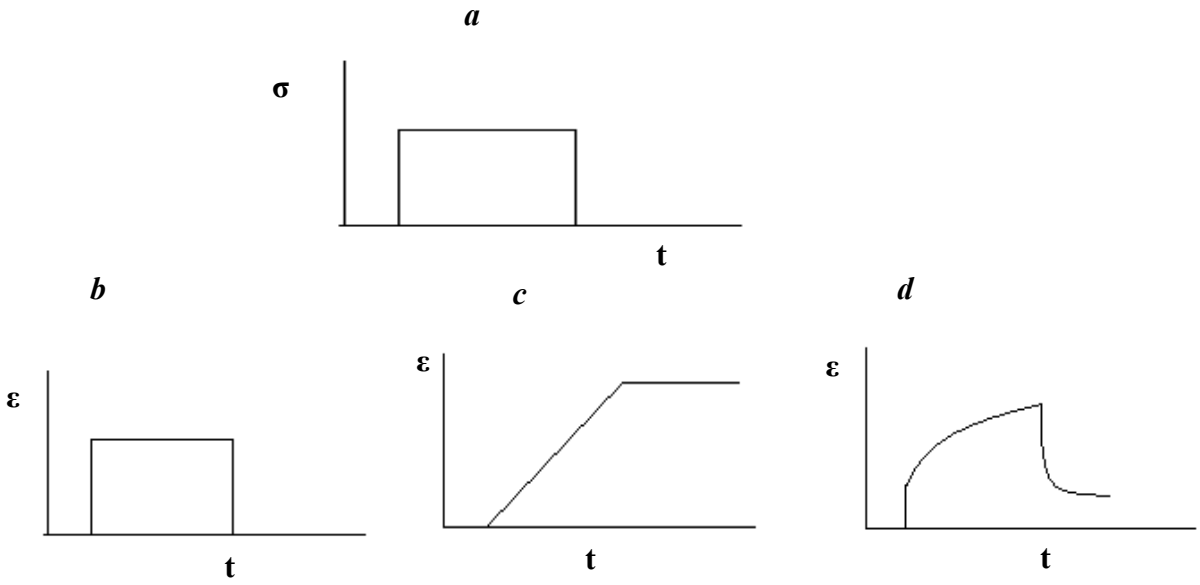

Figure 25. Strain responses to a static load input: (a) stress input, (b) elastic, (c) viscous, (d) viscoelastic

Typically, the input and response functions of asphalt concrete can be related directly to each other through the convolution integral for a linearly viscoelastic (LVE) material, i.e., if the material is not considered damaged. The material is said to be linearly viscoelastic if the principles of homogeneity and linear superposition hold. These linear requirements can be stated mathematically in two equations:

$$R(A.I) = A.R(I) \tag{6}$$

where $R(I)$ is the response to input I, and A is a constant.

$$R(I_1 + I_2) = R(I_1) + R(I_2) \tag{7}$$

where I_1 and I_2 are independent inputs.

Equation 6 states the principle of homogeneity, according to which the output is directly proportional to the input. At a particular temperature and frequency/time for asphalt concrete mixtures in the undamaged state, doubling the stress produces double the

strain to maintain the modulus constant. Thus, the principle of homogeneity applies to asphalt concrete mixtures that are linear viscoelastic.

Equation 7 depicts the principle of superposition, which states that the response to the sum of individual inputs is equivalent to the sum of the response of individual inputs. For example, consider two input creep loads of magnitude I_1 and I_2 applied to an asphalt concrete specimen. The response (i.e. deformation) as a result of the sum of the loads I_1 and I_2 will be equal to the sum of the individual responses (i.e. sum of deformations from each load).

The input-response relationship of linear viscoelastic materials can be mathematically expressed by the convolution integral shown in Equation 8:

$$\boldsymbol{R(t)} = \int_{-\infty}^{t} \boldsymbol{R_H(t-\tau)} \frac{\boldsymbol{dI(\tau)}}{\boldsymbol{d\tau}} \boldsymbol{d\tau} \tag{8}$$

where

R(t) = response at time t due to input ***I(t)***
$\boldsymbol{R_H(t)}$ = the unit response function, i.e., response of the material to an input of unit magnitude
$\boldsymbol{\tau}$ = an integration variable

Linear Viscoelastic Unit Response Functions

Unit response functions denote the response of a linear viscoelastic material to a unit input. Four unit response functions are used to characterize a linear viscoelastic material, namely, complex modulus (E*), complex compliance (D*), relaxation modulus [E(t)], and creep compliance [D(t)]. In this chapter, only the unit response functions complex modulus and creep compliance are discussed.

Creep Compliance D(t)

Creep compliance is the LVE unit response function that characterizes the strain response to a unit step load input. Mathematically, D(t) is defined by the ratio of the strain response at time(t) to the constant stress input as shown in Equation 9.

$$\boldsymbol{D(t)} = \frac{\boldsymbol{\varepsilon(t)}}{\boldsymbol{\sigma_0}} \tag{9}$$

where

D(t) = creep compliance as a function of time
ε(t) = strain
σ_0 = unit stress applied

A typical plot of applied load and deformation response during the IDT test is shown in Figure 26.

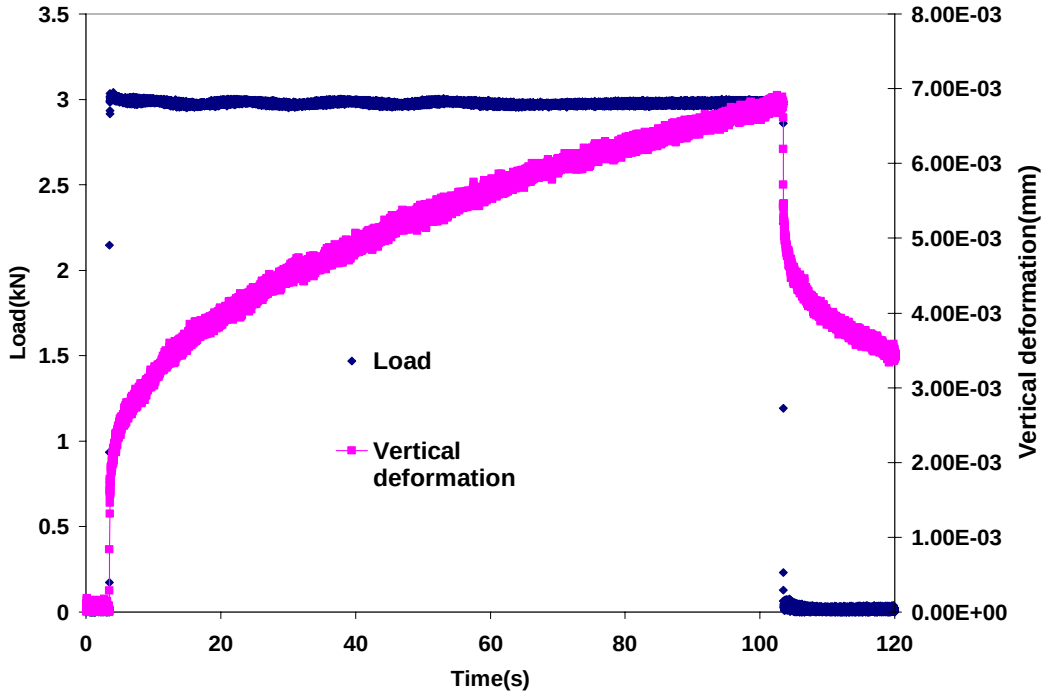

Figure 26. Typical load vs. vertical deformation plot for an IDT test

Linear Viscoelasticity Fundamentals

For accurate material characterization, it is crucial that experimental data, e.g., *E(t)* and *D(t)*, are fitted with appropriate mathematical representations regardless of how these functions are obtained. Various forms of power-law expressions, Pure Power Law (PPL), General Power Law (GPL), and Modified Power Law (MPL, Williams 1964), have been used to represent the viscoelastic response. A study by Park et al. (1996) showed that the MPL (Equation 10) fits the *D(t)* data much better than the PPL and GPL by generating a characteristic, broad-band, S-shaped curve. In particular, the MPL is capable of describing the glassy and rubbery behavior at short and long times, respectively.

$$D(t) = D_g + \frac{D_e - D_g}{(1 + \frac{\tau}{t})^n} \tag{10}$$

where D_g is glassy compliance, D_e is long-time rubbery compliance, and τ and n are regression coefficients. The exponent n gives the slope of the creep curve through the transition region between the glassy and rubbery behavior, and τ fixes a characteristic retardation time.

The Prony series is another type of mathematical representation of viscoelastic response. The Prony series representation contains a physical basis in the theory of mechanical models dealing with springs and dashpots. The popularity of the Prony series representation is attributed mainly to its ability of describing a wide range of viscoelastic response and to the relatively simple and rugged computational efficiency associated with its exponential basis functions (Tschoegl 1989). For the relaxation modulus, the Prony series expression is given in Equation 11:

$$E(t) = E_\infty + \sum_{m=1}^{M} E_m e^{-t/\rho_m} \tag{11}$$

where E_∞, ρ_m, and E_m are long-time equilibrium modulus, relaxation time, and Prony regression coefficients, respectively. Although Equation 11 is for *E(t)*, it can similarly apply to *D(t)*.

To fit Equations 10 and 11 to experimental data, nonlinear regression is usually needed. In this study, the Levenberg-Marquardt method (Marquardt 1963) was used because it has been proven to be an effective computational way to solve nonlinear least squares problems (Davis 1993).

Fracture Mechanics

Fracture mechanics considers the principles governing crack initiation and propagation in materials. Sharp internal or surface flaws that exist in various materials intensify local stress distribution. In this study, Mode I was considered as the fracture mode for the stress field at the crack tip.

The predominant application of fracture mechanics on AC materials is Linear Elastic Fracture Mechanics (LEFM). The basis of LEFM is that the stress and strain field in the small zone ahead of the crack tip, called the fracture process zone, in which fracture occurrence is controlled by a single parameter (for example, stress intensity factor), depending on the size scale of the yielding in the material.

To understand the fracture of AC, however, one must accept that the material is viscoelastic (Lytton 2000). The energy dissipation in the bulk makes the energy flow to the crack tip a less well-defined quantity because the material does not possess a unique modulus (Baney and Hui 1999). The application of fracture mechanics to viscoelastic materials goes back to the middle 1960s. Extending Griffith's work (1921) to LVE materials, Williams (1965) found that the crack initiation criterion depends on the loading history. Vincent and Gotham (1966) and Retting and Kolloid (1966) were among the first to note that the work of fracture in polymers was a function of the crack growth rate. Kostrov and Nikitin (1970), following the lead of Dugdale (1960) and Barenblatt (1962) for time independent materials, were the first to note that a process (failure) zone needs to be introduced ahead of the crack if the time dependence of the fracture process is to be properly modeled. Williams and Marshall (1975) generated an idea that fracture mechanics for viscoelastic materials could be treated with an approach that is similar to the traditional LEFM by simply replacing the time-independent values for modulus and flow stress with equivalent viscoelastic relaxation moduli and flow stresses.

In a sequence of papers, Schapery (1975) demonstrated that viscoelastic crack growth could be described using the approach developed for metals by Barenblatt (1962) by applying elastic-viscoelastic correspondence principle. Schapery's theory assumes that the material outside the process zone behaves as linearly viscoelastic before and during the fracture process, while no restriction is placed on the behavior of the damaged material contained in the process zone. Assuming a power law dependence for the viscoelastic constitutive relationship, taking an appropriate transformation of the governing field and boundary conditions with respect to time and reducing them mathematically to those for elasticity materials with the substitution of elastic moduli, Schapery obtained a simple analytical relationship between the steady state crack growth rate (G) and the applied stress intensity (K_I) for Mode I.

To apply Schapery's theory of crack growth in AC, it suffices to know the viscoelastic compliance (relaxation modulus), the tensile strength, and the fracture energy to characterize the resistance to crack growth. In principle, all these parameters can be obtained from the indirect tensile (IDT) test.

Finite Element Modeling to Evaluate Asphalt Fracture

Many FE programs have been developed specifically for pavement analysis. For example, a two-dimensional (2-D) FE program, CRACKTIP, has been successfully employed to calculate K_I and predict thermal cracking in AC pavements (Chang et al. 1976). Limitations in 2-D FE analysis, however, such as plain stress/strain conditions usually over-predict pavement materials' responses to loads; therefore, ABAQUS, commercially available FEM software (ABAQUS 2006), was used in this study to develop a 3-D FE model for numerical analyses.

Asphalt Binder Flexural Creep Stiffness S(t) and M-value

When an asphalt beam is centrally loaded, the flexural creep stiffness S(t) is defined by the ratio of the bending strain over the unit load applied. According to the elastic-viscoelastic correspondence principle, it can be assumed that if a linear viscoelastic beam is subjected to a constant load applied at t = 0 and held constant, the stress distribution in the beam is the same as that in a linear elastic beam under the same load. Further, the strains and displacements depend on time and are derived from those of the elastic case by replacing E with 1/D(t) (ASTM D 6648-08).

Hence, the flexural creep stiffness is simply defined as the inverse of its creep compliance and is calculated using Equation 12. The m-value is an indicator of the material ability to relax stresses and is simply the slope of the stiffness master curve.

$$S(t) = \frac{PL^3}{4bh^3\delta(t)} \tag{12}$$

where

t = time
S*(t)* = time-dependent flexural creep stiffness, MPa
P = constant load, N
L = span length, mm
b = width of beam, mm
h = depth of beam, mm
δ *(t)* = deflection of beam, at time t, mm

Construction of Master Curve Using Time-Temperature Superposition

Asphalt concrete is a thermorheologically simple material; i.e., it exhibits both time and temperature dependence. Therefore, the time- and temperature-related properties can be related with each other through a single joint parameter. For example, the same magnitude of a specific property of a material can be obtained at a higher loading time if a lower temperature is used and vice versa. This joint parameter that is used to relate time and temperature is known as the 'shift factor' and is related to frequency and time, as shown in Equation 13 and Equation 14, respectively.

$$f_R = fa_T \tag{13}$$

$$t_R = \frac{t}{a_T} \tag{14}$$

where

f_R = the reduced frequency, and f is the frequency
t_R = the reduced time, and t is the time
a_T = the shift factor

The translation from temperature to either frequency or time is possible through the reduced frequency at a desired reference temperature; thus, for creep compliance at a particular time and temperature:

$$D(t,T) = D(t_R, T_0) \tag{15}$$

where T and T_0 represent the testing temperature and reference temperature, respectively, with other symbols retaining their usual meanings.

To develop a master curve, then, the modulus values of the specimen at various temperatures and times/frequencies are obtained and transformed into one characteristic curve at a reference temperature by means of shift factors. The primary reason for developing the master curve is to predict the modulus/stiffness values of the material at various temperatures and frequencies other than those tested.

To illustrate, the time-temperature principle is applied to the stiffness results obtained from the BBR test of the asphalt binder at a duration of 2 hours at three different temperatures, as shown in Figure 27. In order to represent the modulus values at three different temperatures to one reference temperature (-12°C in this case), the modulus values at -5°C are shifted to the right and -22°C to the left along the horizontal time axis to obtain a single continuous master curve at -12°C. The final master curve after shifting is shown in Figure 28. The shift factors obtained during this process are shown in Figure 29. It should be noted that the value of the logarithmic shift factor at the reference temperature is always zero.

The stiffness master curves obtained from the same 2-hour BBR tests at reference temperatures of -12°C and -22°C are shown in Figure 30. From this figure, it can be observed that, using time-temperature superposition, the same stiffness values can be obtained at higher times and lower temperatures or vice versa.

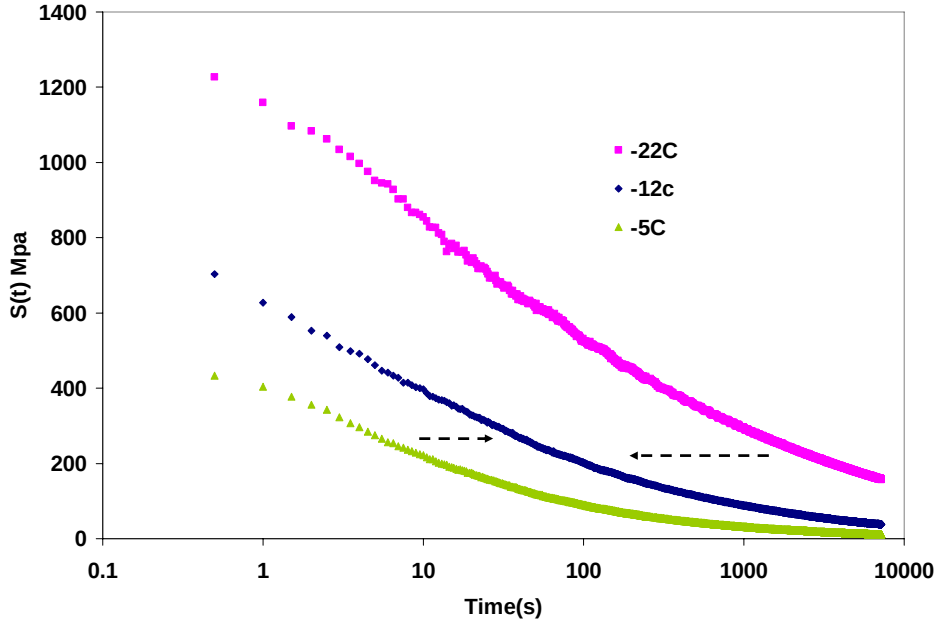

Figure 27. Flexural creep stiffness vs. time curves for a typical BBR test

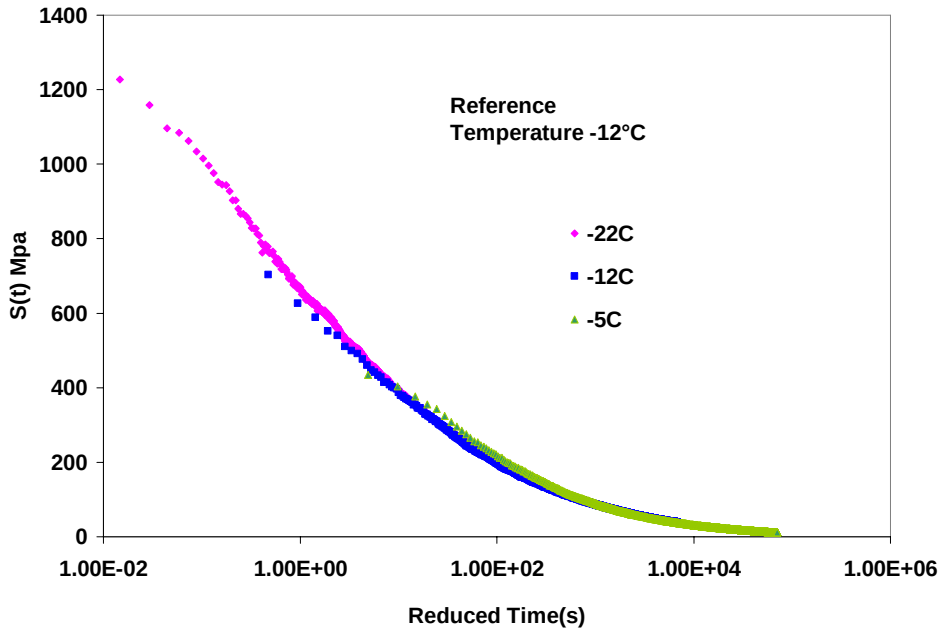

Figure 28. Flexural creep stiffness master curve at reference temperature of -12°C on a semi-log scale

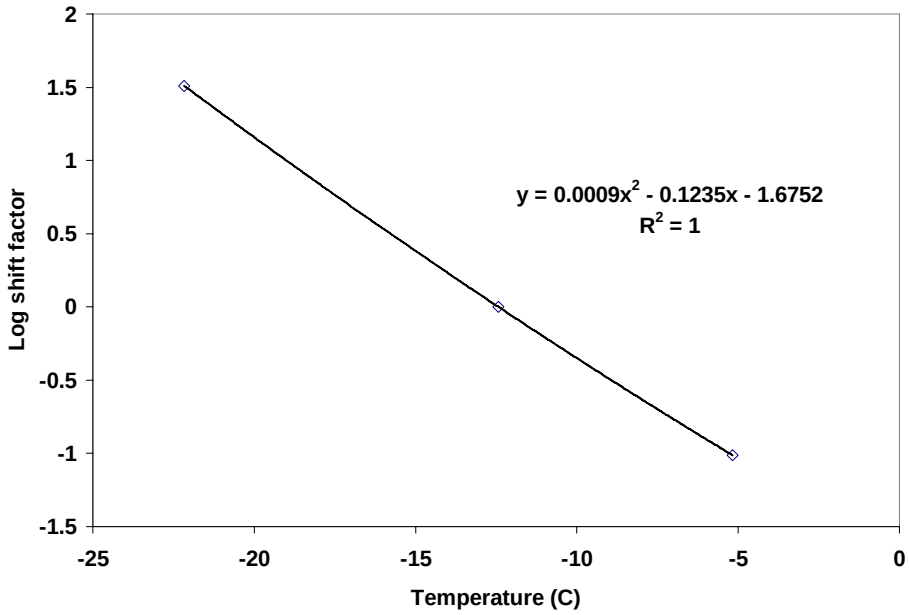

Figure 29. Log shift factor vs. temperature for the BBR test

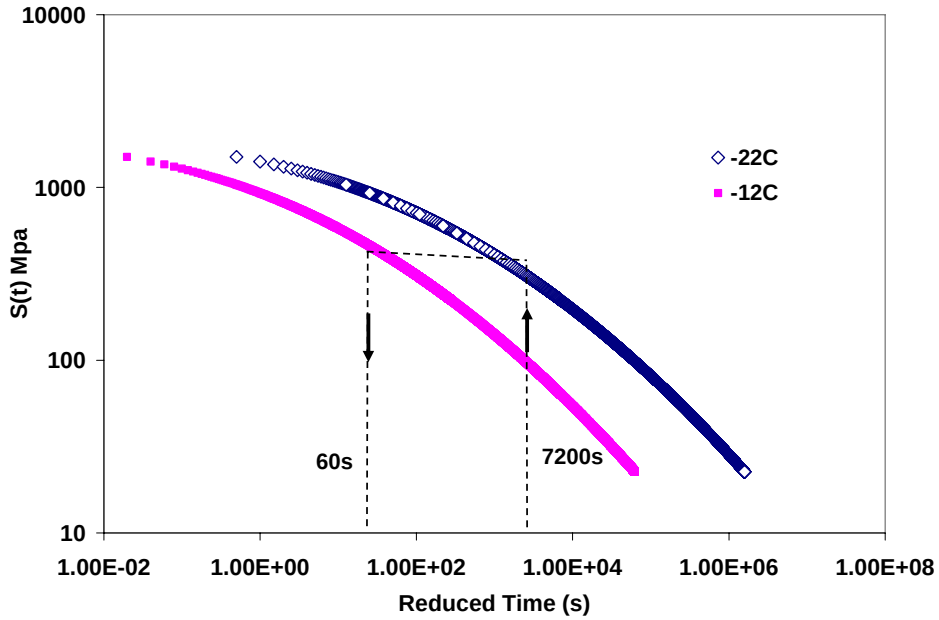

Figure 30. Flexural creep stiffness master curve at reference temperatures of -12°C and -22°C on log-log scale

Though the samples are tested at specific temperatures, the resultant master curve can be developed at a reference temperature of choice. This can simply be done by forcing the shift factors of the desired reference temperature to zero and making appropriate changes to shift factors at other temperatures. Figure 31 illustrates this process of shifting the reference temperature from -22°C to -12°C. It is also possible to develop a master curve by shifting to a reference temperature outside the range of testing temperatures.

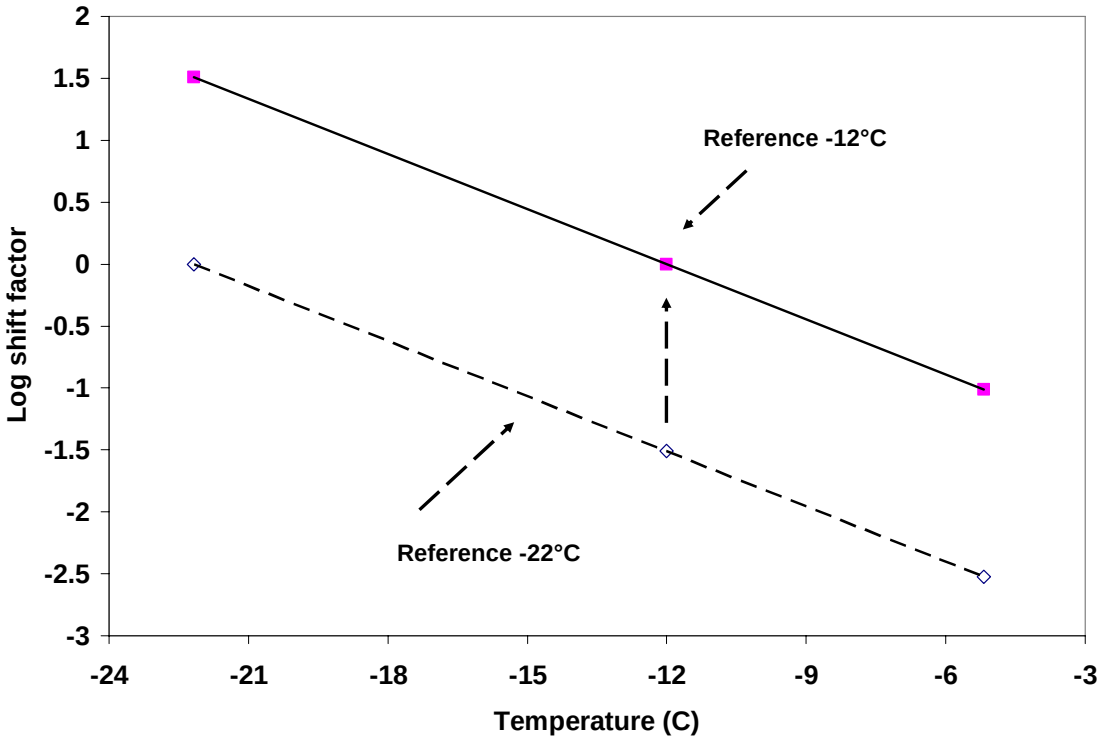

Figure 31. Method for shifting the reference temperature

The D(t) and S(t) master curves are fitted by means of the sigmoidal and hyperbolic fits as shown in Equation 16 and Equation 17, respectively.

$$\log[D(t)] = a_1 + \frac{a_2}{\left\{a_3 + \frac{a_4}{\exp[a_5 + a_6 \log(t_R)]}\right\}} \tag{16}$$

where

D(t) = the creep compliance (1/MPa)

a_1 through a_6 = regression coefficients
t_R = the reduced time(s)

$$\log(S_t) = (\beta_3 - \beta_2) \times \left[0.5 \left\{ t_n - \sqrt{t_n^{\,2} + 4\lambda^2} \right\} \right] + \beta_3 \tag{17}$$

where

$$t_n = \frac{(t_o - \log t + a_T)}{(\beta_3 - \beta_2)},$$

$$\lambda = \frac{2}{[\exp(x) + \exp(-x)]},$$

$X = 0.339 * t_n + 0.00637 * t_n^{\,3}$
t = loading time(s)
S(t) = flexural creep stiffness (MPa)
a_T = temperature shift factor [log(sec)]
β_1, β_2, and β_3 = regression coefficients

Complex Modulus (E*)

Complex modulus (E*) is the unit response function of a sinusoidal input function. The dynamic modulus ($|E^*|$), which is the magnitude of the complex modulus, is equivalent to the amplitude of the sinusoidal stress load yielding a unit strain response. The dynamic modulus is calculated by dividing the steady state sinusoidal stress amplitude (σ_1) by the steady state sinusoidal strain amplitude (ε_2). The steady state stress and strain responses are shown in Figure 32 and are expressed by Equations 18 and 19.

$$\sigma = \sigma_0 + \sigma_1 \cos(2\pi f t) \tag{18}$$

$$\varepsilon = \varepsilon_0 + \varepsilon_1 t + \varepsilon_2 \cos(2\pi f t + \phi) \tag{19}$$

$$|E^*| = \frac{\sigma_1}{\varepsilon_2} \tag{20}$$

The phase angle (ϕ) represents the time lag, Δt, between the stress input and strain response according to Equation 21, as follows.

$$\phi = 2\pi f \Delta t \tag{21}$$

where

σ and ε = stress and strain, respectively
t and f = time and frequency, respectively
σ_0, σ_1, ε_0, ε_1, ε_2, = regression constants

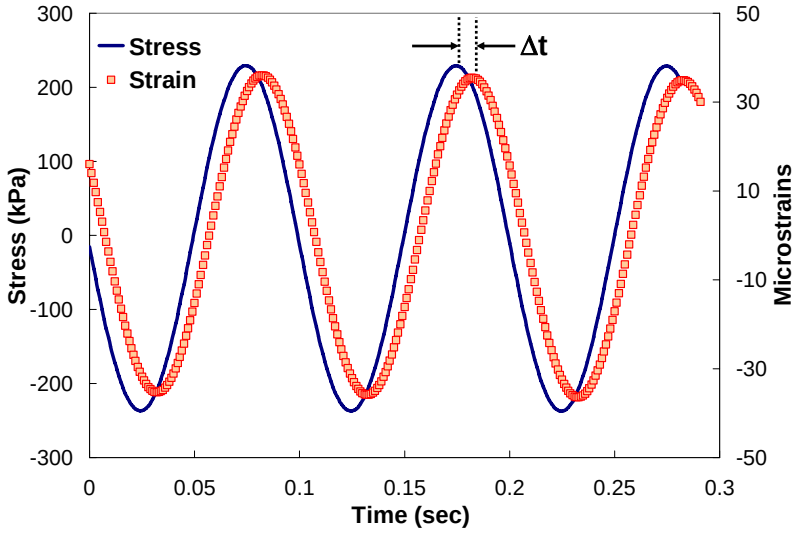

Figure 32. Sinusoidal stress and strain response

Complex modulus is deconstructed into two major components, the storage modulus and loss modulus, as represented in Equation 22 and Figure 33.

$$E^* = E' + iE'' \tag{22}$$

where

E' = storage modulus (represents elastic response)
E'' = loss modulus (represents viscous response)
$i = (-1)^{1/2}$

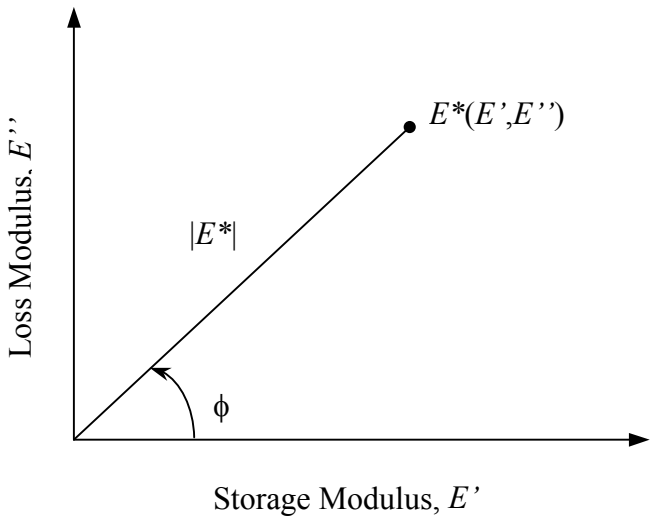

Figure 33. Complex modulus broken into real and imaginary components

The dynamic modulus is the amplitude of the complex modulus and is defined as follows:

$$\left|E^*\right| = \sqrt{(E')^2 + (E'')^2} \tag{23}$$

The values of the storage and loss moduli are related to the dynamic modulus and phase angle, as shown in Equations 24 and 25:

$$E' = \left|E^*\right| \cos\phi \text{ and} \tag{24}$$

$$E'' = \left|E^*\right| \sin\phi \tag{25}$$

From Figure 33, it can be observed that the value of phase angle can vary between 0 and 90 degrees. If the phase angle is 0, then the material is deemed as completely elastic, and the material is viscous if the phase angle is 90 degrees.

CHAPTER 4
RESULTS, INTERPRETATION, AND ANALYSIS

This chapter deals with characterization of asphalt binders and asphalt concrete mixtures obtained from the SISSI sites. As part of material characterization under SISSI Phase II, indirect tensile test (IDT) and repeated shear at constant height (RSCH) tests were conducted on specimens from SISSI mixtures. Furthermore, the SISSI binders underwent a bending test at low temperature using the Bending Beam Rheometer. Details of testing procedures and protocols were explained in Chapter 2. Theoretical background for this testing was covered in Chapter 3. This chapter includes the results and the analysis and the conclusions based on those results.

Creep Compliance D(t) and Tensile Strength of SISSI Mixtures

The IDT tests were conducted on specimens from all eight SISSI sites as described in Chapter 2. The number of replicates tested for each site along with the air void content is shown in Table 7. Though the target air void is 7 ± 0.5 percent, some of the replicate specimens from the SISSI sites are off target and could not be reproduced because of material quantity constraints.

Table 7. Air void content (%) and number of replicates for SISSI - IDT specimens

Site	Replicate #	Air Void (%)
Blair	1	6.5
	2	6.9
Delaware	1	6.3
	2	6.8
Mercer East	1	7.2
	2	7.6*
Mercer West	1	6.3*
	2	6.6
Perry	1	6.5
	2	6.7
Somerset	1	6.6
	2	6.8
Tioga	1	8.9*
	2	9*
Warren	1	6.6
	2	6.7
	3	7.2
	4	7.5

* specimen's air void is outside acceptable tolerance.

Figure 34 represents the D(t) vs. time chart for both replicates of the Mercer East site. The D(t) vs. reduced time and extended sigmoidal fitted at reference temperature of -10°C are shown in Figure 35 and Figure 36, respectively. The shift factor curve and sigmoidal coefficients for both the replicates are shown in Figure 37 and Table 8, respectively. IDT test data for the other SISSI sites are documented in Appendix A.

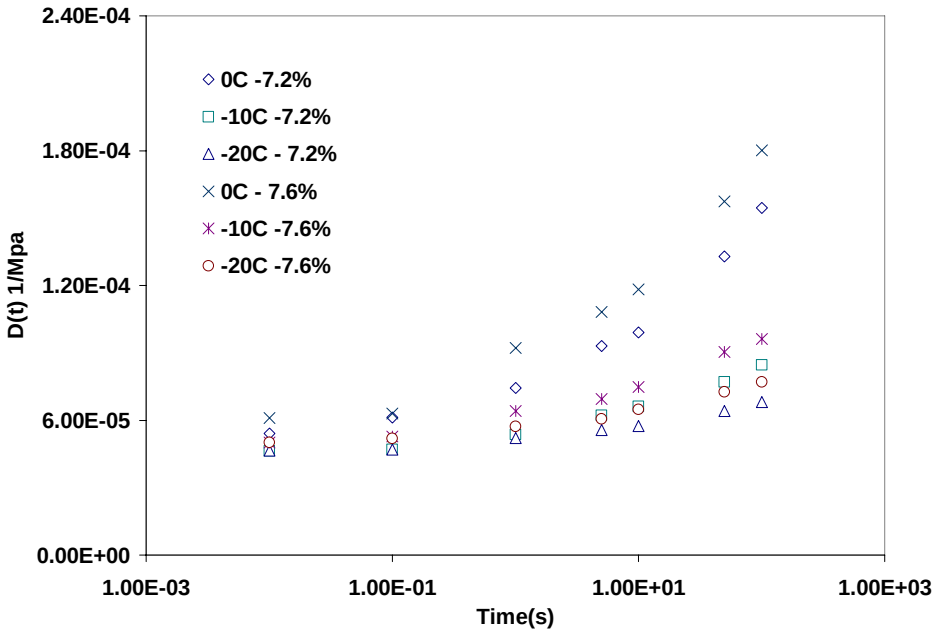

Figure 34. Creep compliance vs. time for replicates of Mercer East in semi-log domain

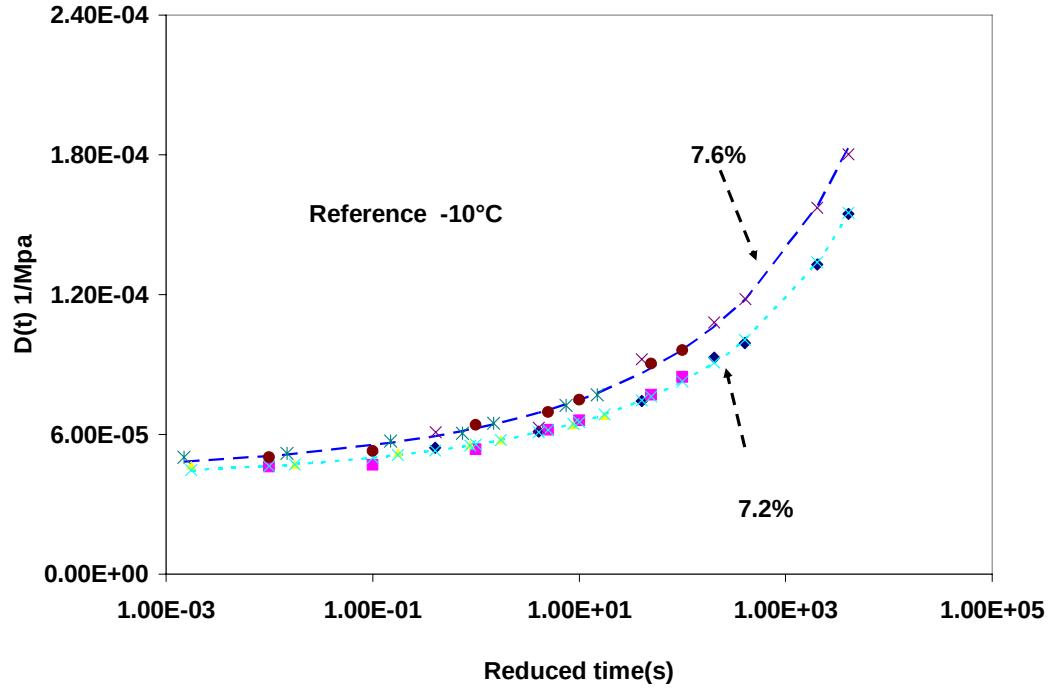

Figure 35. Creep compliance vs. reduced time for replicates of Mercer East in semi-log domain

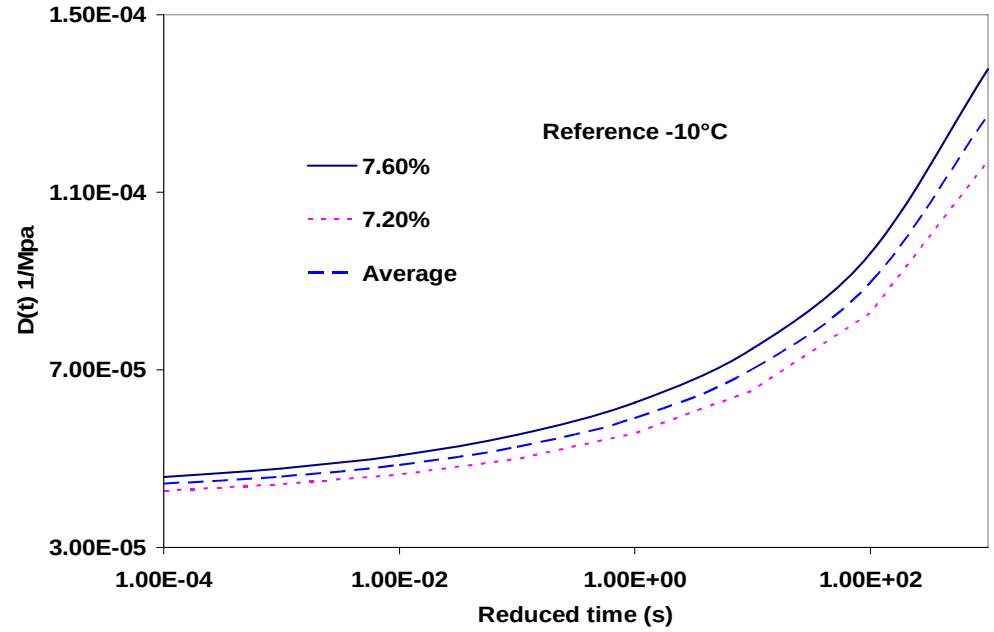

Figure 36. Extended sigmoidal fit for replicates of Mercer East in semi-log domain

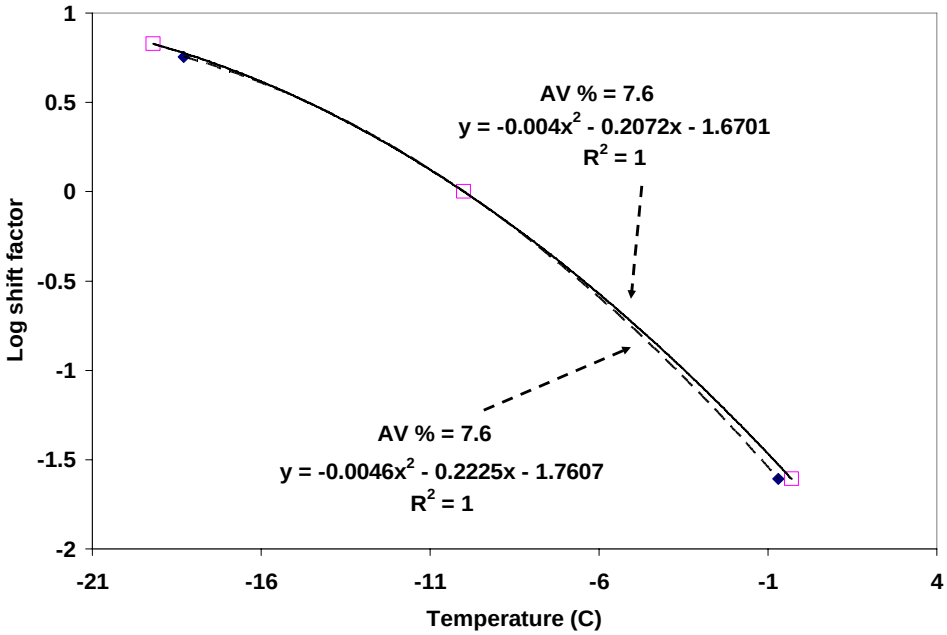

Figure 37. Shift factor curve for replicates of Mercer East

Table 8. Sigmoidal coefficients for Mercer East mixture

	7.20 (% AV)	7.60 (% AV)
A1	7.88576693	7.917016431
A2	-29.07045919	-29.06715893
A3	2.36672053	2.363894395
A4	2.87353936	2.932640128
A5	4.635804919	4.446491814
A6	-0.402479796	-0.369121547

The difference in creep compliance between replicates for all SISSI sites was observed to be within 30 percent, which follows the values reported by Christensen et al. (2005). It should be noted that the differences stated are based on the results from direct testing and not for data extrapolated using the sigmoidal function. The average creep compliance data shifted to the reference temperature of -10°C, and tensile strength data for all the SISSI sites are shown in Figures 38 and 39, respectively. The ranking of specimens based on the creep compliance and tensile strength of the mixtures is discussed later in this chapter.

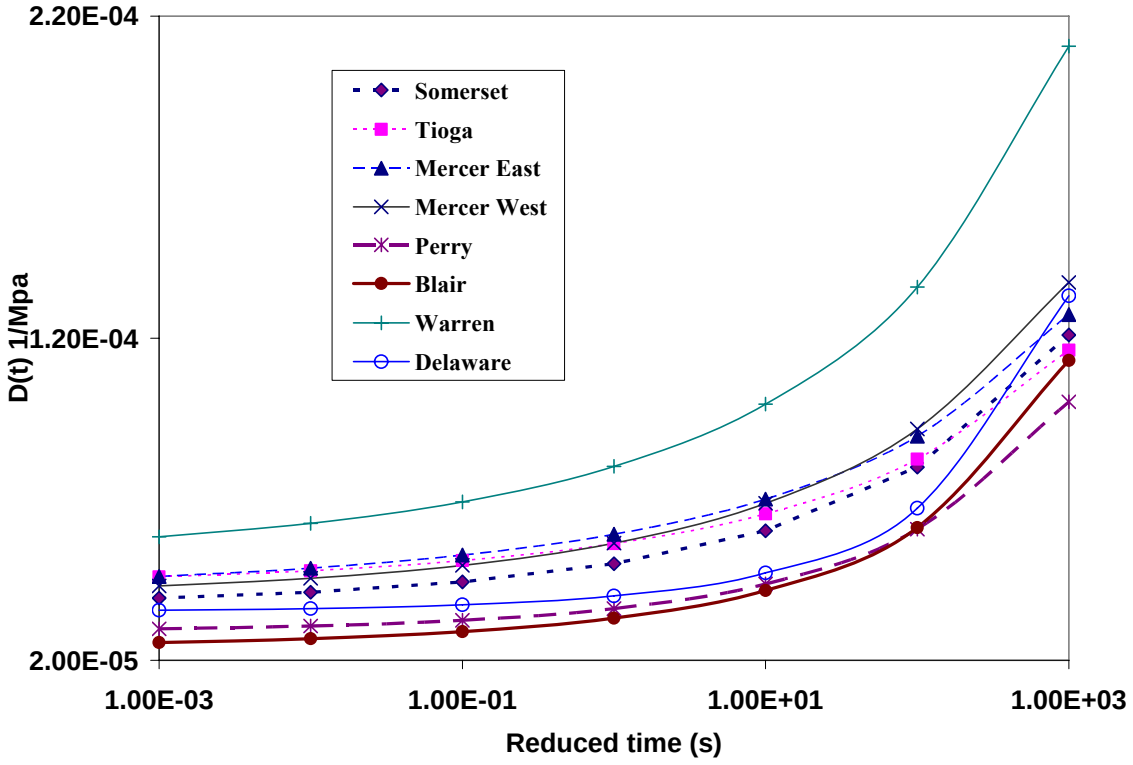

Figure 38. Compliance master curves for all SISSI sites at reference temperature of -10°C

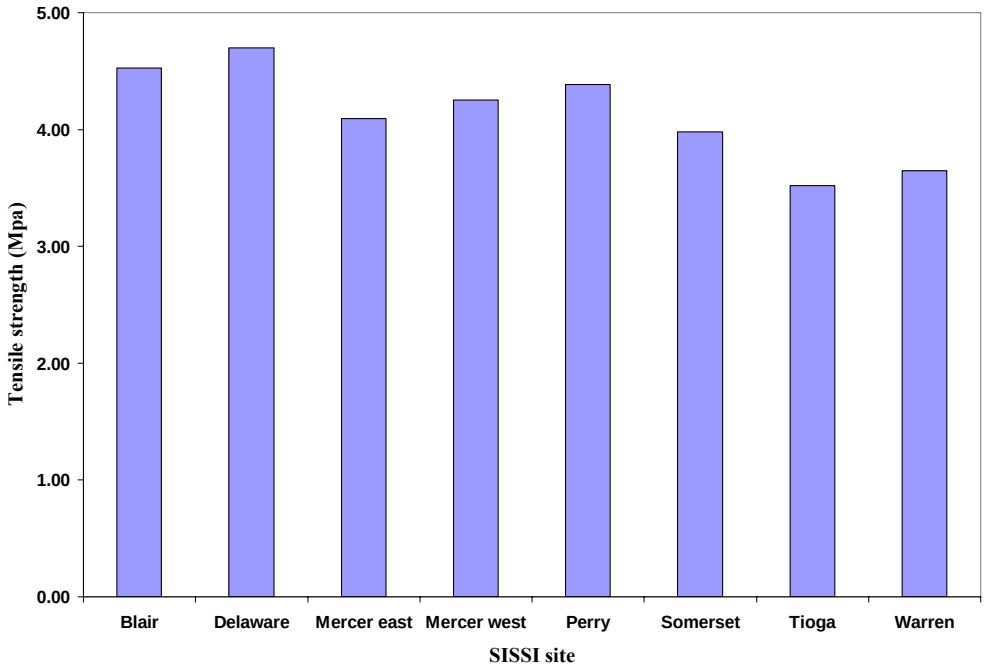

Figure 39. Average tensile strength values for all SISSI sites

Alternate Approach in Analysis of Creep Compliance

Unlike the uniaxial test, the stress and strain fields in the IDT specimen are biaxial. This biaxial state of stress and strain requires that appropriate analysis be conducted to obtain reliable material properties. Additionally, correction factors addressing non-uniform strain distribution, localization, and bulging effects also need to be included, as was done in deriving a linear elastic solution for *D(t)* by Roque and Buttlar (1992). As discussed in Chapter 3, for more accurate material characterization, an LVE solution for *D(t)* in IDT mode has been recently developed for AC mixtures (Wen, 2001 and Kim and Wen 2002). In their study, *D(t)* is calculated through the following equation which was previously discussed in Chapter 3.

$$D(t) = -\frac{d}{p}\left[a * U(t) + b * V(t)\right] \tag{26}$$

where d is the thickness of the specimen, p is applied load, c and e are specimen diameter and gauge length specific coefficients, and $U(t)$ and $V(t)$ are horizontal and vertical displacement, respectively. The displacements are obtained by integrating the strain over the entire gauge length (l) of the horizontal and vertical LVDTs mounted on the specimen. For the study presented in this paper, 100-mm-diameter specimens were tested with a gauge length of 25 mm, yielding values of 0.7874 and 2.2783 for a and b, respectively. Creep compliance master curves were regenerated using Equation 26 and time-temperature superposition, as shown in Figure 40.

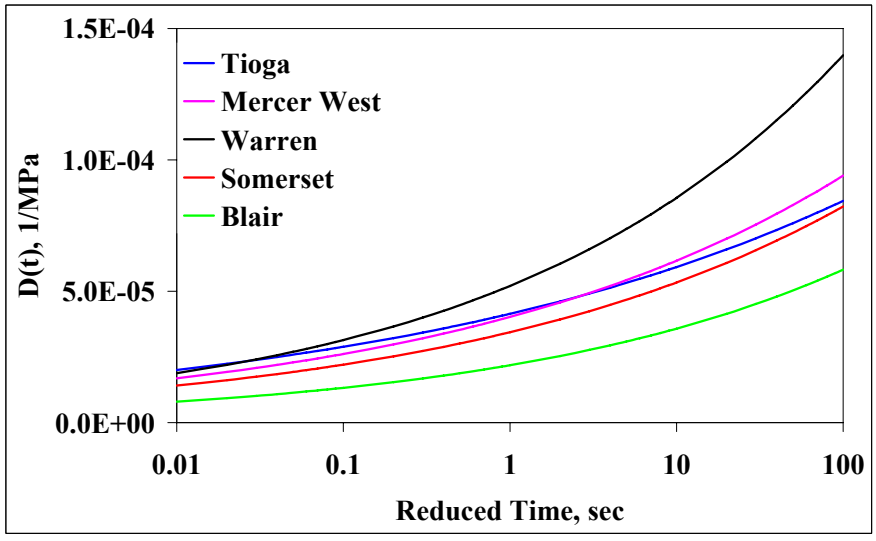

Figure 40. Creep compliance master curves at -10°C

Poisson's Ratio

For a perfectly incompressible material deformed elastically at small strains, Poisson's ratio would be exactly 0.5. Most materials have υ between 0.0 and 0.5. For viscoelastic materials, such as AC, Poisson's ratio is in general a time-dependent or a frequency-dependent quantity. It has been suggested (Tschoegl et al. 2002) that the time-dependent Poisson's ratio $\upsilon(t)$ must be monotonically non-decreasing in all cases and that experimental results that indicate otherwise must be erroneous by virtue of the theory of viscoelasticity. As for the IDT test, Poisson's ratio can be directly obtained from measured vertical and horizontal deformations, assuming AC specimens are isotropic. As discussed in Chapter 3, from linear viscoelasticity, Kim and Wen (2002) developed the following equation (previously discussed in Chapter 3) to calculate time dependent Poisson's ratio, $\upsilon(t)$:

$$\upsilon(t) = -\frac{c * U(t) + d * V(t)}{e * U(t) + f * V(t)} \tag{27}$$

For the specimens and LVDTs used in this study, values of 3.358, 1.081, 1.000, and 3.122 were obtained for *c*, *d*, *e*, and *f*, respectively. Similar to the creep compliance, master curves of Poisson's ratio were generated using Equation 27, as shown in Figure 41. Since time-dependent $\upsilon(t)$ is needed to infer shear and bulk relaxation moduli, as discussed later in this paper, $\upsilon(t)$ values are reported to four significant digits (Lu et al. 1997).

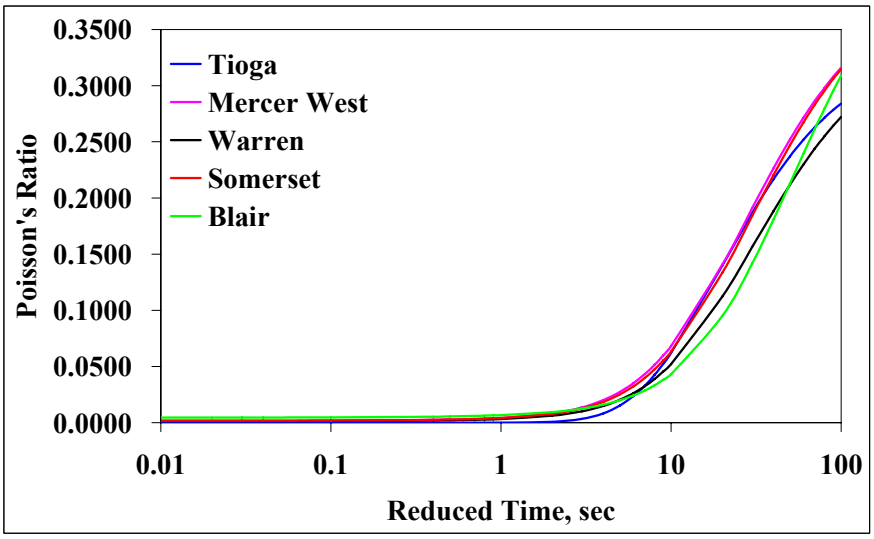

Figure 41. Poisson's ratio master curves at -10°C

Fracture Analysis of Asphalt Concrete at Low Temperatures

Specific assumptions were made in conducting fracture analysis of the SISSI asphalt mixtures at low temperatures. The asphalt mix was assumed to be homogeneous, linear viscoelastic, and isotropic. Both experiment and numerical analyses were employed to study the fracture of AC mixtures at low temperatures. Viscoelastic material properties, obtained from the creep tests at -20°C, -10°C, and 0°C, were fed into a three-dimensional (3-D) finite element model. Simulated horizontal strains at the center of the specimen were then compared with an analytical solution. At the end, finite element analysis (FEA) was performed to simulate the fracture of SISSI mixtures during the strength test at -10°C. A far field solution by means of energy release rate (*J*-integral) was used to study the crack initiation. The *J*-integral allows an approximate treatment without the need of a precise modeling of the nonlinear behavior at the crack tip (Schapery 1984, 1988). The crack opening displacement (COD) during the crack propagation was also investigated through FE simulations.

Development of Finite Element Model

The developed 3-D FE model represents the actual dimensions of the specimen and loading strips used in the IDT test. While the top loading strip is only allowed to move downward, the bottom strip is constrained in all directions. A perfect bonding condition is assumed for the interface between the specimen and loading strips.

To obtain accurate results when analyzing the stress field around a crack tip, a refined mesh must be used to capture the strong gradients near the tip. The required mesh refinement can make fracture mechanics models large since a crack is normally a very small feature compared with the model dimensions. An alternative technique that reduces computational resources is the use of the Global-Local FEM approach to obtain accurate results by running a local model sequentially instead of performing a single global analysis with a refined mesh around the crack (Bradford et al. 1984, Whitcomb and Woo 1993, Bakuckas 1999, Diamantoudis and Labeas 2005, Allen and Searcy 2006). The first step is to solve a less refined global model (Figure 42a) to obtain a displacement solution that is accurate away from the crack tip but is not sufficiently refined to capture strong gradients near the region of interest. A refined local model of the crack-tip region is then used to obtain a more accurate solution and, hence, more accurate contour integrals (Figure 42a).

In ABAQUS, the energy release rate is calculated using a domain integration method. This method predicts accurate values that are obtained even with quite coarse meshes because the integral is taken over a domain of elements so that errors in local solution parameters have less effect. Each contour corresponds to a successive ring of elements progressing outward radially from the crack tip. A refined mesh at the crack tip is required to obtain contour-independent results; i.e., there is no significant variation in the integral values calculated for successive rings of elements around the crack tip. In the circular region surrounding the crack tip where the contour integrals are calculated, the

mesh was biased moderately toward the crack tip. A swept mesh used in the inner ring creates wedge elements to introduce a singularity at the crack tip. The outer ring is meshed with 20-node linear hexahedral elements using the structured meshing technique. Results from the first contour are generally not used when dealing with fracture problems because the first contour is influenced by the singularity associated with the crack tip (ABAQUS 2006).To obtain an accurate value of the integral, 10 contours were evaluated until the value of the integral values remained approximately constant from one contour to the next (Figure 42b).

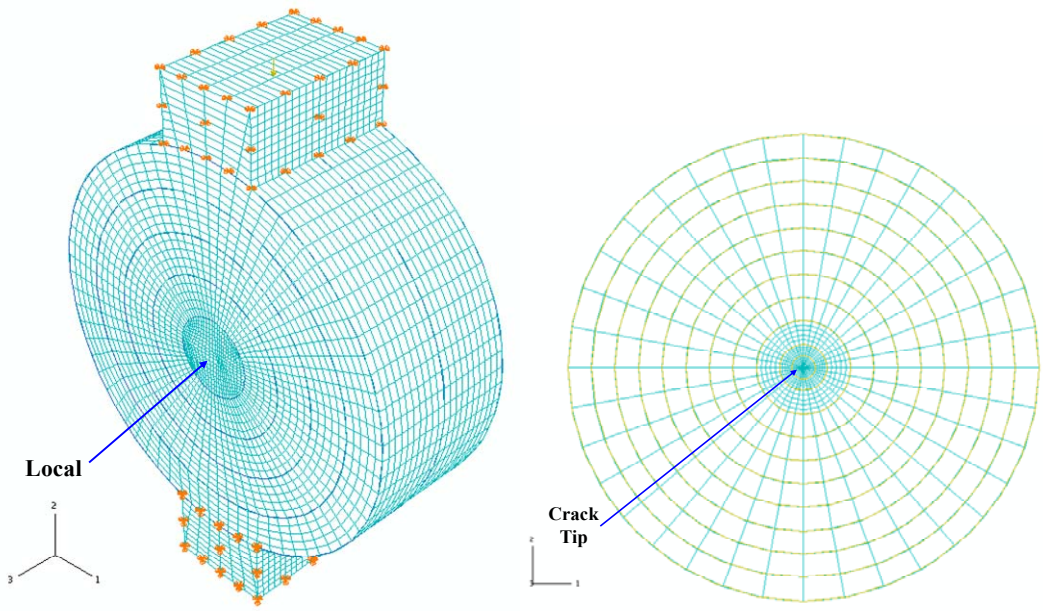

Figure 42. (a) Global-local approach (b) Detailed mesh design

In ABAQUS, key material properties required for the viscoelastic model is the relaxation modulus. It is desirable to use the Prony series representation of linear viscoelastic response because of its amenability to mathematical operations as long as the local waviness of the fit and negative values of some coefficients that might result is resolved. Park and Kim (2001) proposed using the MPL to pre-smooth the *D(t)* data to which a Prony series is subsequently fit. They found that the resulting Prony series fitted to the pre-smoothed experimental data yields a smoother reconstructed curve that is free of local waviness and that is analytically simple for mathematical operations. They also suggested that a five-term MPL (Equation 10) would result in an acceptable accuracy. In the study, the *D(t)* data were first fitted using Park and Kim's algorithm. The *E(t)* data were then calculated from fitted *D(t)* data using Equation 4. Relaxation master curves are shown in Figure 43.

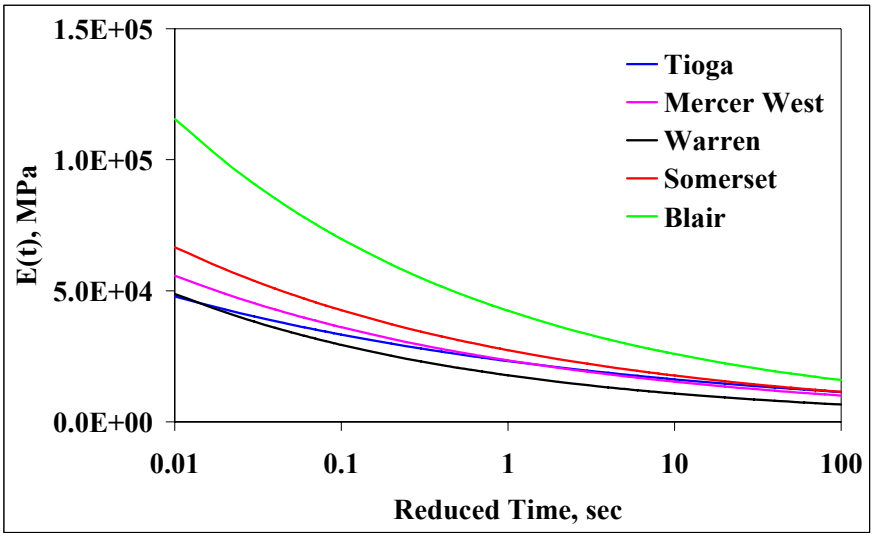

Figure 43. Relaxation modulus master curves at -10°C

Model Validation

Although an effort was made to approach real laboratory testing conditions in the developed FE models based on the available material properties and modeling techniques, some approximations were inevitable. Therefore, model validation was considered as an essential step for mechanistic analysis using FE simulations.

To evaluate the effectiveness of the developed FE model in simulating the materials' responses, the center tensile strains of the specimen predicted from FE models were compared with the values calculated from the analytical solution derived by (Kim and Wen 2002):

$$\varepsilon(t) = U(t) * \frac{g + h * \upsilon(t)}{i + j * \upsilon(t)} \tag{28}$$

For the specimens and LVDTs used in this study, values of 12.4, 37.7, 0.291, and 0.908 were obtained for g, h, i, and j, respectively. Overall, the FE solution predicts comparable center tensile strains to the analytical solution. Two sets of center tensile strains are given in Figure 44.

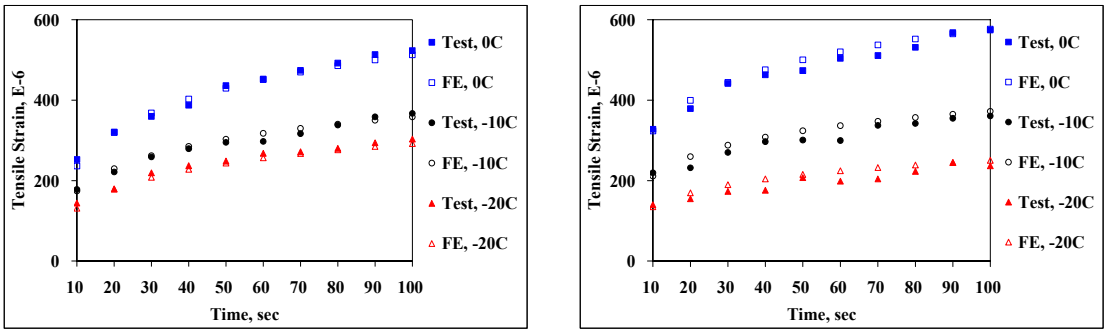

(a) Mercer West **(b) Blair**

Figure 44. Comparison of center tensile strains from analytical and FE solutions

Finite Element Analysis

The finite element analysis (FEA) was carried out in two stages, seen in Figure 45. The first stage simulates the creep test, seen in Figure 45a. In the IDT test, a crack initiates and propagates toward the loading strips along the vertical direction due to the tensile stress. Therefore, the location of crack initiation under IDT mode is of interest. No crack growth is specified during this analysis stage. In the second stage, the crack is allowed to propagate from the location of crack initiation identified in the first stage while the top loading strip moves downward at a constant rate of 12.5 mm/min. The second stage simulates the tensile strength test. To simulate the crack propagation, a single crack is allowed to propagate from a single crack tip where two surfaces were initially partially bonded, shown in Figure 45b. After debonding, the traction between two surfaces is initially carried as equal and opposite forces at the node on one surface and the corresponding point on the other. This force is then slowly and linearly reduced to zero after debonding starts at a particular node on the bonded surface to improve convergence. This process continues at each element node along the direction of crack propagation, shown in Figure 45b. Finally, the crack stops propagating at the edges of specimen that are in contact with the load strips.

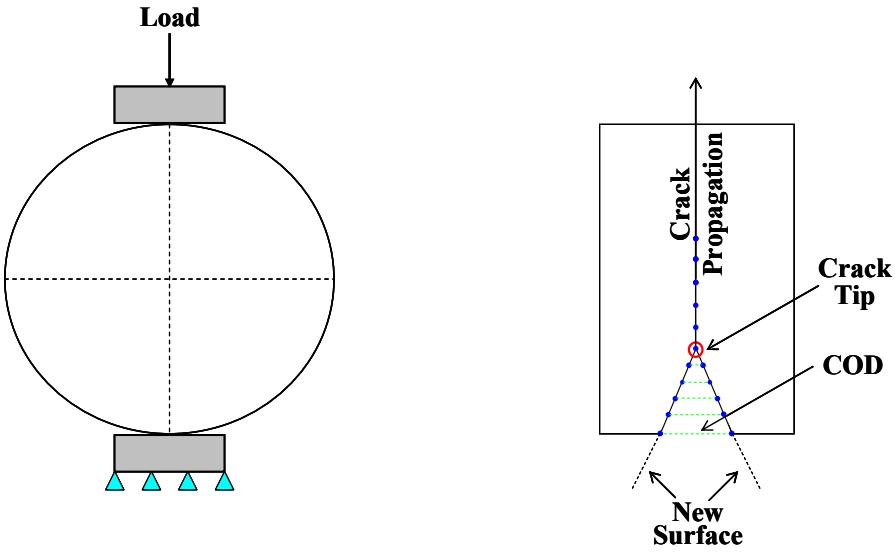

(a) Creep test **(b) Strength test**

Figure 45. Finite element simulation

Stress Analysis

Knowing the location of the maximum tensile stress along the horizontal axis (Figure 46a) is vital for modeling the crack initiation. Figures 46b, 46c, and 46d show the distribution of tensile stresses at a 1.9-mm interval along the horizontal axis. Detailed simulation results are listed in Table 9. Clearly, the maximum tensile stresses always occur at the edge of the specimen. This observation agrees with the finding from Roque and Buttlar (1992). The difference between the edge and the center becomes more significant at lower temperatures. It can be concluded that the crack starts from the edge of the specimen during the IDT test. The maximum tensile stress does not vary among mixtures, which means this tensile stress is independent of material properties.

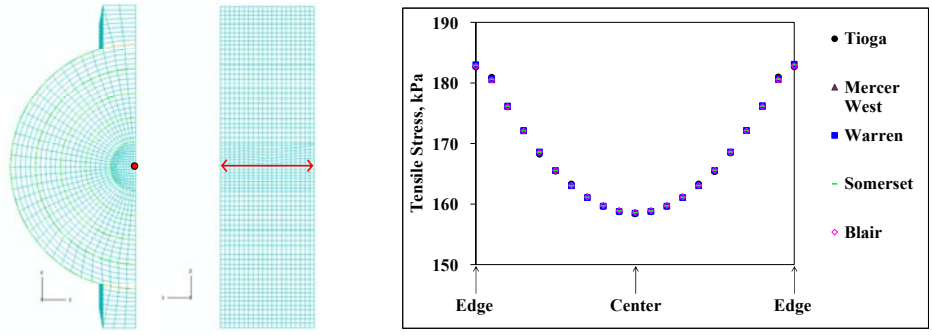

(a) Analysis location **(b) 0°C**

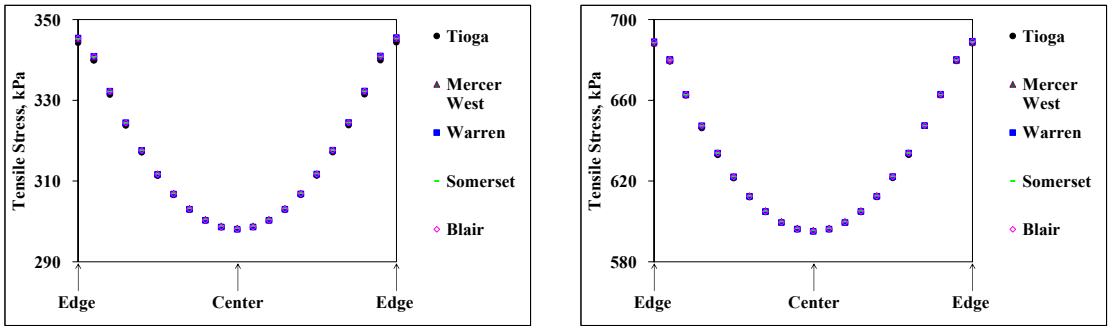

(c) -10°C **(d) -20°C**

Figure 46. Tensile stresses along the horizontal axis

Table 9. Summary of tensile stresses during the creep test, KPa

Mixture	Locations along the thickness	Temperature, °C		
		0	-10	-20
Tioga	Edge*	182.64	344.36	688.22
	Center	158.35	298.07	595.10
Mercer West	Edge	182.85	345.23	688.61
	Center	158.63	298.35	595.66
Warren	Edge	183.05	345.47	689.14
	Center	158.50	298.06	595.08
Somerset	Edge	182.96	345.24	688.73
	Center	158.56	298.34	595.56
Blair	Edge	182.83	345.44	689.11
	Center	158.65	298.09	595.13

* Average of two sides of the specimen

Crack Initiation

By placing the initial crack on the edge of the IDT specimen, the energy release rate (*J*-integral) during the strength test can be calculated. Before presenting analysis results, a new term, fracture life, is introduced here. Since SISSI mixtures failed at different times during the strength test, for comparison purposes, these times were first normalized to a unit time, called fracture life, and then evenly divided into 10 time regimes (e.g., 10, 20, and 30 percentage).

The average quantities reported in this section exclude the first contour, as shown in Figure 47a. Results from two sets of simulations are presented in this section. The first

set was conducted using linear viscoelastic material properties, shown in Figure 47b, while the second one was conducted with linear elastic (LE) material properties, seen in Figure 47c. A detailed summary is given in Table 10. The *J*-integral from both sets of simulations gradually increases during the fracture life; however, the magnitudes of the *J*-integral from the LVE and LE solutions are very different. Figure 47d plots the ratio of the *J*-integral from LVE over LE solution. As seen from Table 10, the *J*-integral from the LVE solution is always larger than that from the LE solution during the fracture life, except for Tioga and Blair mixtures at shorter time regimes (i.e., 10 and 20 percent). This observation suggests that the use of linear elastic material properties would result in considerable deviations in the calculation of *J*-integral. Therefore, if an elastic solution is available, satisfying an appropriate traction and displacement boundary conditions, the application of the elastic material properties to a viscoelastic material cannot be used to approximate the solution for a quasi-static problem as in the strength test. Second, this ratio exhibits a much stronger dependency on the mixture during the first 50 percent of the fracture life, seen in Figure 47d. After that, the ratio slowly converges to a value around 1.4 at the end of the fracture life. Mixtures that have the same binder PG grade follow a similar pattern. The ratio of Mercer West and Warren mixtures (PG 76) decreases with time, while the ratio of Tioga, Somerset, and Blair mixtures (PG 64) increases with time. It is expected that the Warren mixture will have a superior cracking resistance than others because of its higher value of the energy release rate.

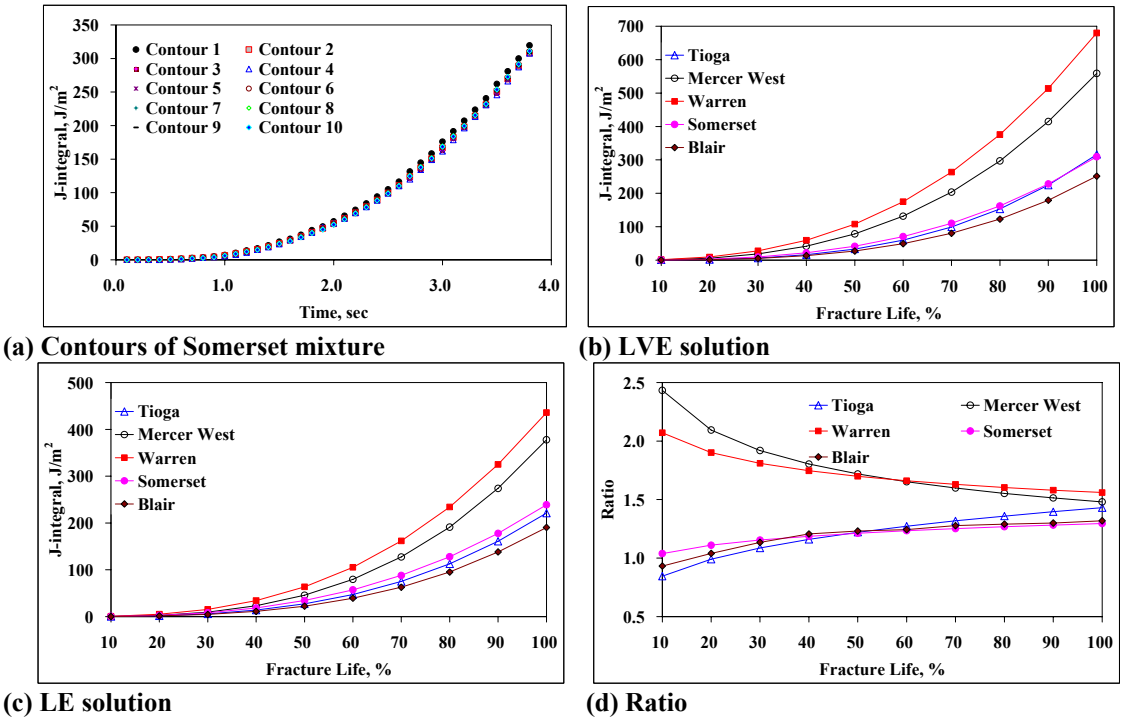

(a) Contours of Somerset mixture **(b) LVE solution**

(c) LE solution **(d) Ratio**

Figure 47. Energy release rate

Table 10. Summary of calculated energy release rate

Fracture Life, %	Energy Release Rate, J/m^2														
	Tioga			Mercer West			Warren			Somerset			Blair		
	LVE	LE	Ratio	LVE	LE	Ratio	LVE	LE	Ratio	LVE	LE	Ratio	LVE	LE	Ratio
10	0	0	0.85	1	0	2.43	1	1	2.07	0	0	1.04	0	0	0.93
20	2	2	0.99	6	3	2.09	9	5	1.90	3	3	1.11	1	1	1.04
30	6	6	1.09	18	10	1.92	28	15	1.81	9	8	1.15	5	5	1.13
40	16	14	1.16	42	23	1.80	60	34	1.75	22	18	1.19	13	11	1.21
50	33	27	1.22	78	46	1.72	108	63	1.70	42	34	1.21	27	22	1.23
60	60	47	1.27	131	80	1.65	175	105	1.66	70	57	1.23	49	39	1.24
70	99	75	1.32	203	127	1.60	263	162	1.63	110	88	1.25	80	63	1.28
80	153	113	1.36	297	191	1.55	376	234	1.60	162	128	1.27	123	95	1.29
90	225	161	1.40	415	274	1.51	514	325	1.58	228	178	1.28	179	138	1.30
100	316	221	1.43	559	378	1.48	680	436	1.56	309	239	1.30	251	191	1.32

Crack Propagation

Figure 48 illustrates the final deformed shape and crack path from the experiment and FE simulations. Figure 48a shows that some portion of the propagated crack is deviated from the center line of specimen. This deviation was not observed in the FE-simulated crack propagation (Figures 48b through 48d) because, in the developed FE model, AC was assumed to be homogeneous, and the existence of particles (i.e., aggregates) was not considered.

Accumulated crack opening displacement (COD) from FE simulations are given in Table 11. A graphic illustration is also provided in Figure 49a. Mixture 3 has the smallest value of COD at failure, 2.10 mm. Together with the observation on the energy release rate from the preceding section, it can be concluded that mixture 3 exhibits the best low temperature performance among the five mixtures included in this study.

Monitoring crack propagation during the strength test requires sophisticated instrumentations, such as the COD gauge. However, the measurement of COD at failure is rather simple. Through such measurement, it would become possible to correlate the energy release rate and COD. Once such correlation is established, the crack propagation at any time (time regime) can be predicted from the energy release rate. Of course, such prediction is only valid for the material and testing conditions (e.g., load and temperature) used in the FE model development.

A nonlinear regression model in a Pure Power Law form was proposed to model the relationship between normalized crack opening displacement (*NCOD*) and normalized fracture energy (*NFE*):

$$NFE = a * (NCOD)^b + e \tag{29}$$

where a and b are nonlinear model coefficients, and e is random normal error with mean 0 and variance σ^2. Two constraints were applied to Equation 29:

- $NFE = 0$ when $NCOD = 0$
- $NFE = 1$ when $NCOD = 1$

Through the nonlinear optimization, values of 0.9859 and 2.1719 were obtained for coefficients a and b, respectively. A R^2 value of 0.95 indicates the appropriateness of the selected model form for the AC mixtures and the strength test conditions (load and temperature) considered in this study, as shown in Figure 49b.

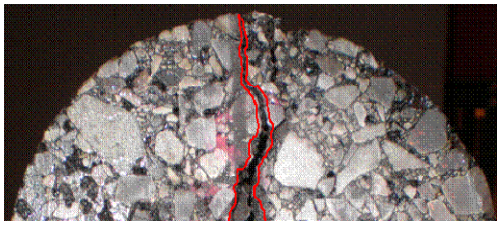

(a) Final stage during experiment

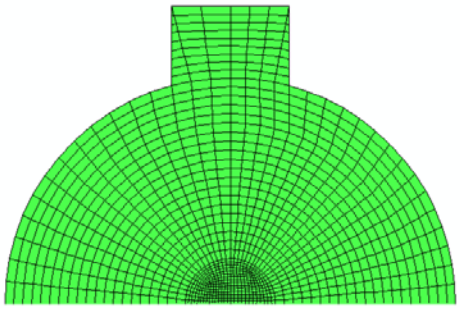

(b) Initial stage during simulation

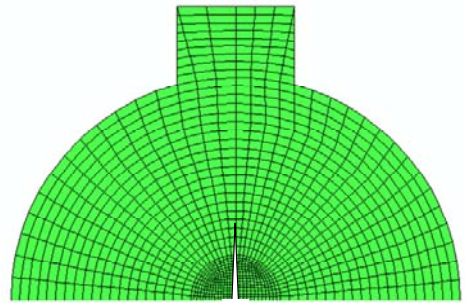

(c) Intermediate stage during simulation

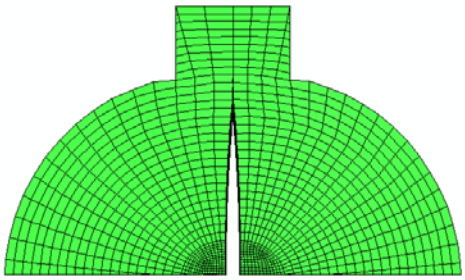

(d) Final stage during simulation

Figure 48. Crack propagation

Table 11. Cumulated crack opening displacement, mm

Fracture Life, %	Crack Opening Displacement, mm				
	Tioga	Mercer West	Warren	Somerset	Blair
10	0.07	0.10	0.08	0.12	0.13
20	0.22	0.33	0.24	0.33	0.46
30	0.41	0.71	0.46	0.56	1.17
40	0.70	0.97	0.66	0.95	1.80
50	1.11	1.30	0.86	1.33	2.42
60	1.45	1.65	1.06	1.76	3.02
70	1.82	2.01	1.34	2.22	3.74
80	2.21	2.43	1.56	2.59	4.65
90	2.76	2.79	1.88	3.07	5.41
100	3.17	3.12	2.10	3.56	6.11

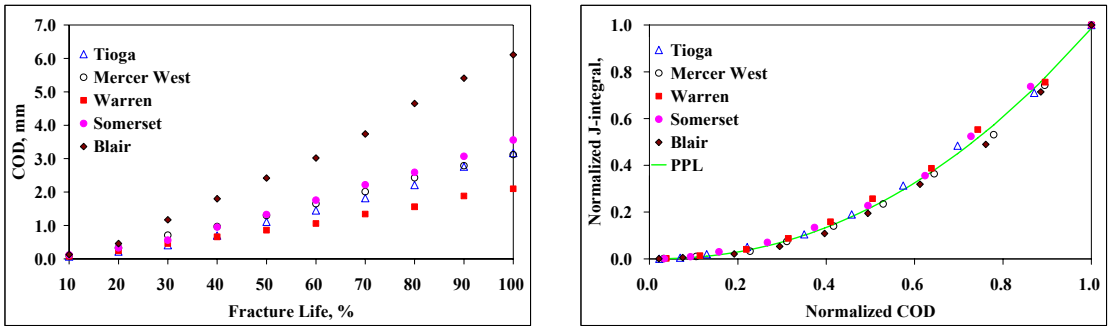

(a) COD **(b) *NCOD* vs. *NFE***

Figure 49. Crack propagation analysis

Flexural Creep Stiffness and M-Values of SISSI Binders

BBR tests were conducted on PAV-aged asphalt binders for seven of the eight SISSI sites. Tests were not conducted for the Tioga site, for which sufficient binder was not available. Two replicates from each site were tested for S(t) at 240-second and 2-hour durations. The detailed test procedure was presented in Chapter 2. Figures 50 through 52 and Table 12 represent the S(t) vs. time, creep stiffness master curves, shift factor curves, and hyperbolic coefficients for the 240-second BBR test for both replicates from Somerset. Data for the other SISSI sites are shown in Appendix B.

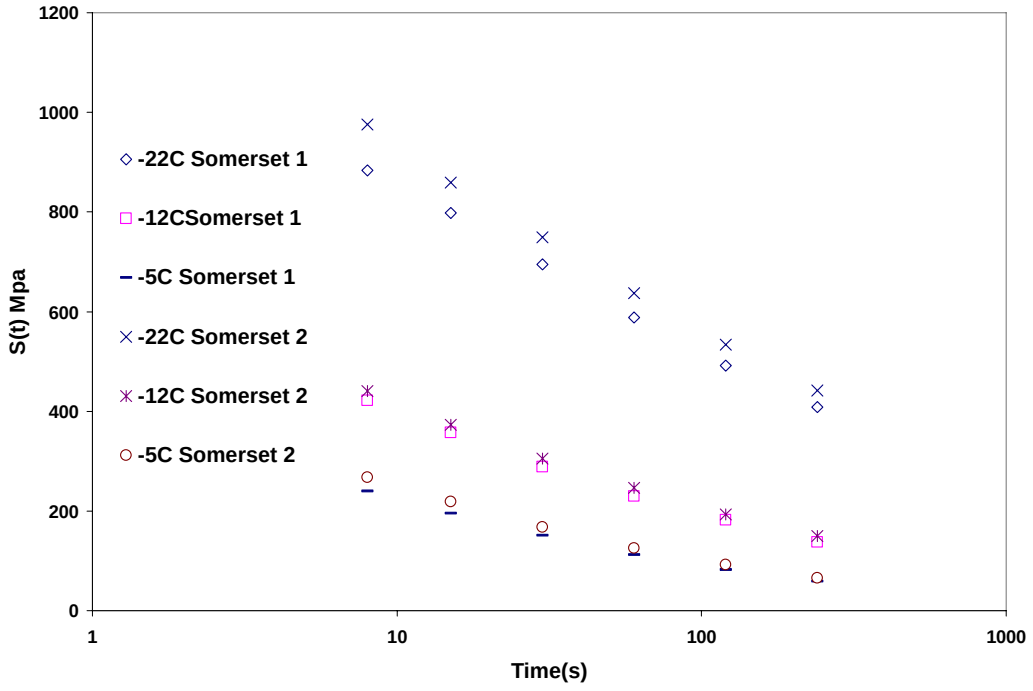

Figure 50. Flexural creep stiffness vs. time for Somerset on a semi-log scale

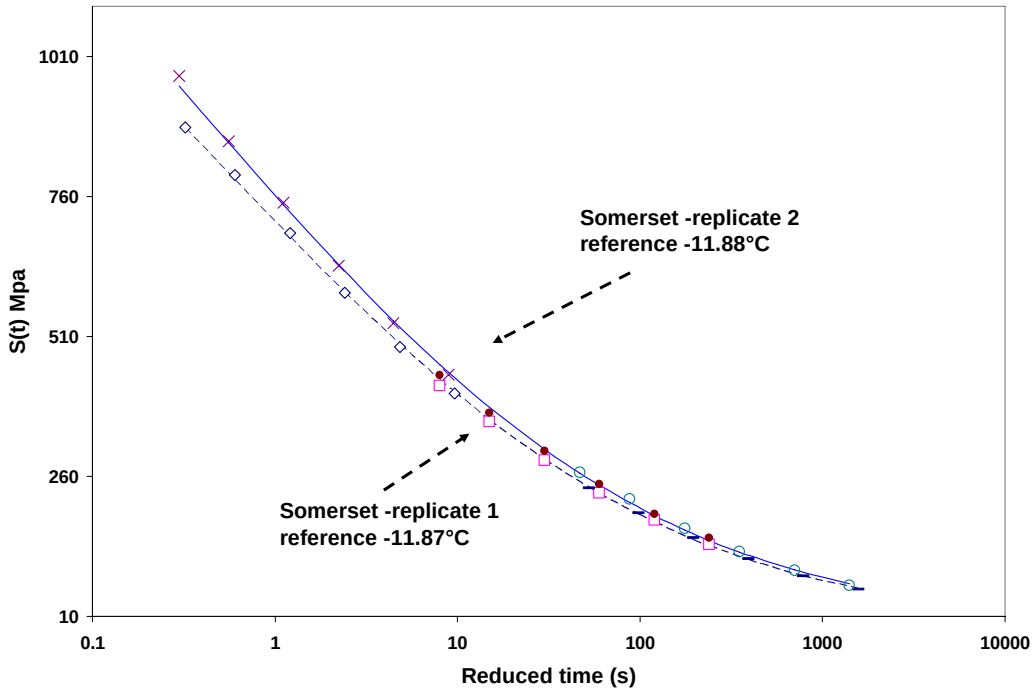

Figure 51. Flexural creep stiffness vs. reduced time for Somerset on a semi-log scale

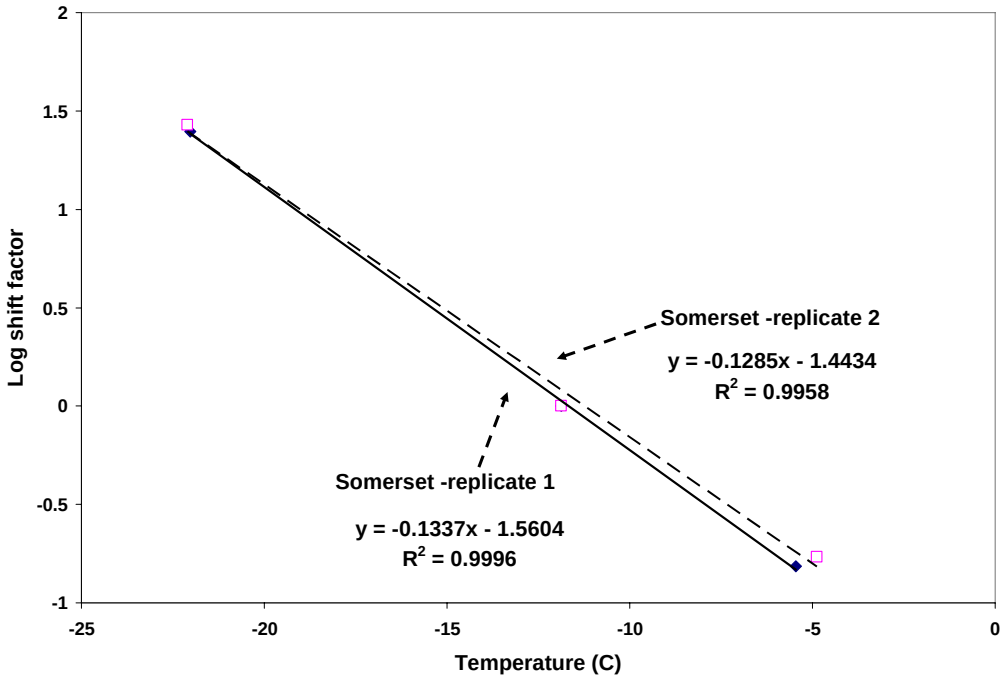

Figure 52. Shift factor curves for Somerset on a semi-log scale

Table 12. Hyperbolic fit coefficients

	Somerset 1	Somerset 2
β2	1.61	1.59
β3	3.22	3.27
To	3.55	3.65

The comparison of average D(t) and m-values at 60 seconds at T_1+10 for two replicates from the SISSI sites is shown in Figure 53 and 54, respectively. The ranking of the SISSI sites with respect to S(t) and m-value is discussed later in this chapter. Both the S(t) and m-value criteria are not satisfied for both Perry and Delaware. Modified asphalt binders are normally more flexible than unmodified binders to satisfy the specification criteria over a broader temperature range and typically tend to have lower stiffness values (SHRP-A-631). However, from this study, the modified asphalt binders, with the exception of Perry, have higher S(t) values at low temperatures compared to the unmodified asphalt binder.

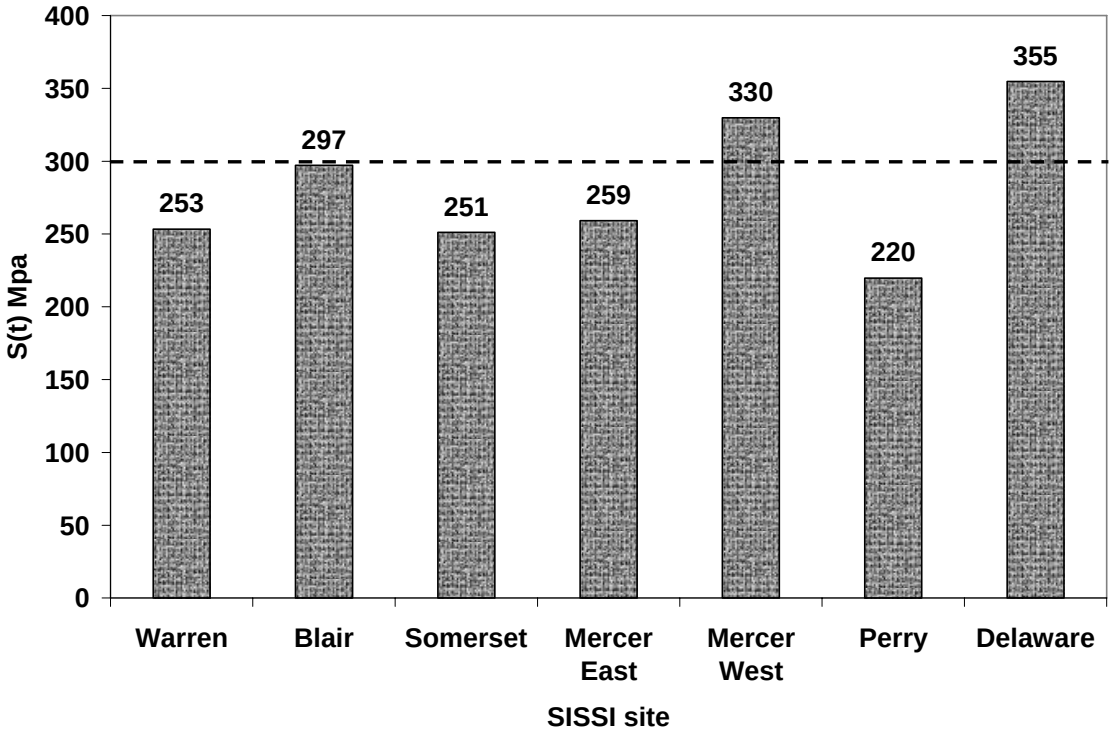

Figure 53. Comparison of average S(60) at T_1+10 for SISSI sites

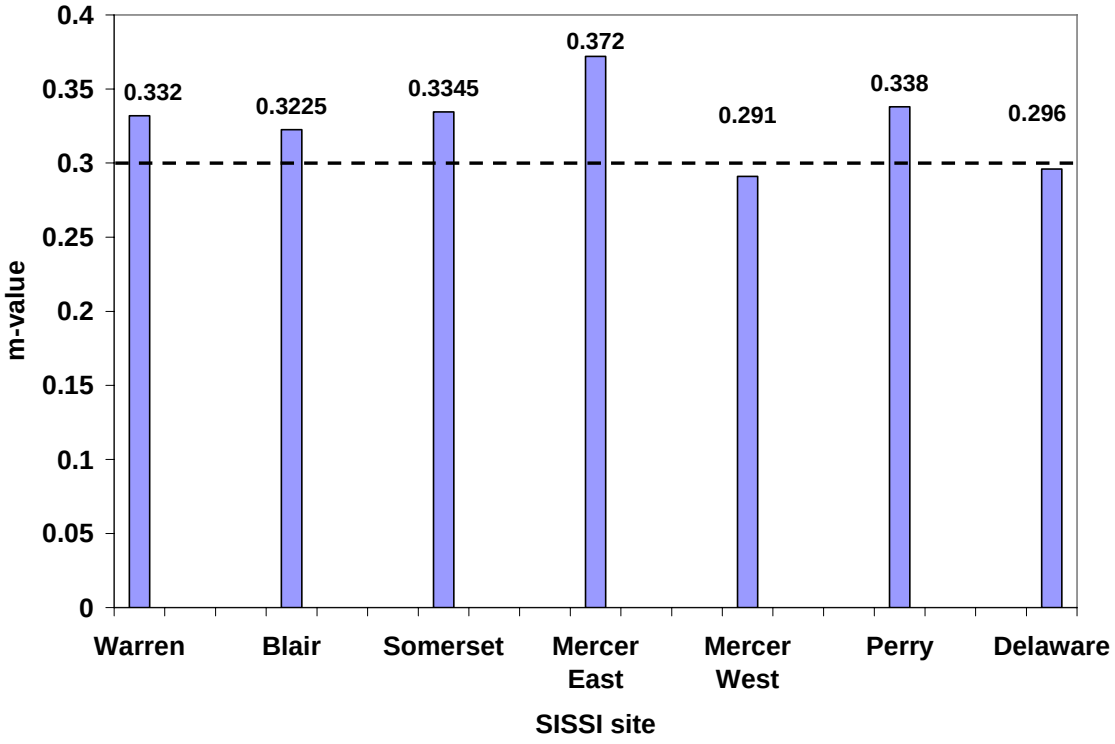

Figure 54. Comparison of m(60) at T_1+10 for SISSI sites

The change in m-value with increase in temperature and duration of the test is shown in Figure 55. It is observed that the m-value generally increases with temperature, as was expected because of the increase in viscoelastic behavior of asphalt binders. Detailed results for all the sites are shown in Table C1 in Appendix C. The m-value for all the sites follows a similar pattern; however, no definite correlation is observed between the m-values obtained from the 240-second and 2-hour tests.

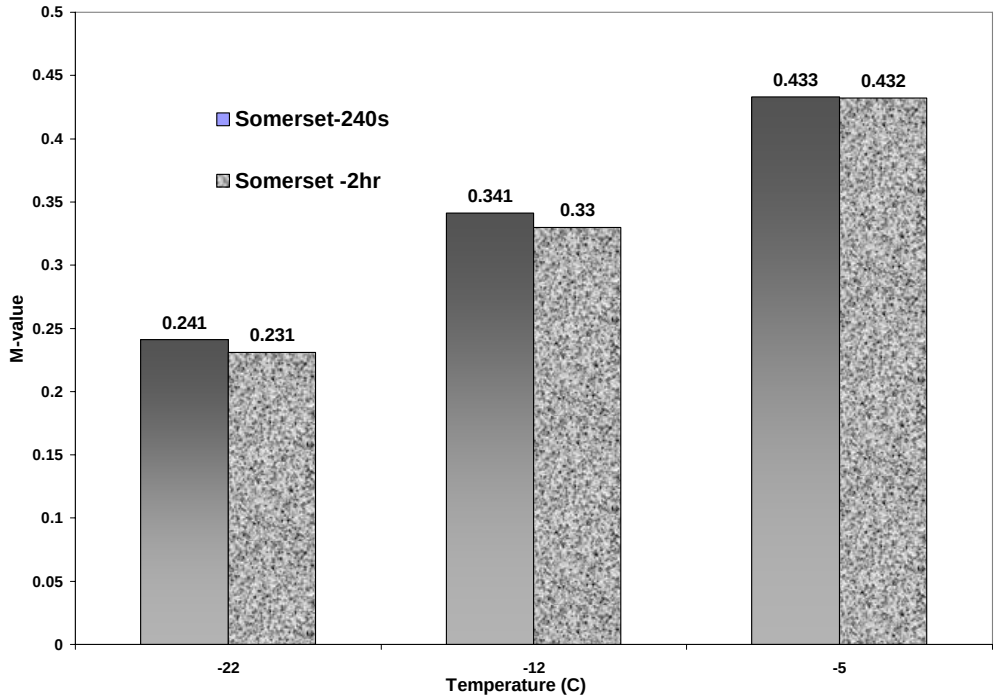

Figure 55. Comparison of m(60) at T_1+10 for 240-s and 2-hr BBR tests for Somerset

Table 13 presents the S(t) values obtained from the BBR software and predicted from the hyperbolic equation. For example, the S(60) obtained directly from the 240-second BBR test at actual testing temperature is shown in Column One. The S(60) at T_1+10 (i.e. -12C) predicted using the hyperbolic equation for the 240-second test is shown in column two. Similarly, columns three and four represent the actual and predicted S(60) at -12C under 2-hour testing. Finally, columns seven and eight represent the actual and predicted S(7200) at temperature T_1 under 2-hour testing. From columns 4 and 6 of Table 13, it is observed that for all the SISSI asphalt binders tested, the equivalence principle is not satisfied. S(60) at T_1+10 is significantly higher than S(7200) at T_1. The percent difference is shown in Figure 56. This difference ranges from 41 percent to 52 percent. It should be noted that the equivalence principle for all the SISSI asphalt binders is evaluated based only on data obtained from the 2-hour testing.

Hence, to satisfy the equivalence principle, it is necessary to adopt alternate testing times or temperatures for the SISSI asphalt binders, as shown in Figure 57 and Figure 58, respectively. Figure 57 represents the predicted time to test for the SISSI binders at T_1+10 to satisfy the equivalence principle and ranges from 240 seconds to 450 seconds. However, the current BBR software (BBR 1.23) is only capable of collecting data up to 240 seconds. To avoid complications in collecting test data, alternate testing temperatures are also predicted, as shown in Figure 58. The alternate testing temperatures predicted range from -5°C to -8°C, indicating that the SISSI binders must be tested on an average at 15°C higher than the lower temperature grade to satisfy the equivalence

principle. The percent difference, actual time, and temperature values predicted for the SISSI binders are shown in Table 14.

Table 13. Actual and predicted flexural creep stiffness values (MPa) for SISSI binders

Column number	1	2		3	4		5	6
	Test duration:240s			Test Duration:2-hr				
	S(t) @ 60s			S(t) @ 60s			S(t) @ 7200s	
SISSI Site								
	Test Temp	-12C		Test Temp	-12C		Test Temp	-22C
	Actual S	Predicted S		Actual S	Predicted S		Actual S	Predicted S
Warren–replicate 1	241.5 (-12.05)	249.6		242.1 (-12.08)	249.7		152.0 (-22.29)	147.0
Warren–replicate 2	238.2 (-11.99)	256.9		248.2 (-11.98)	264.5		149.1 (-22.17)	144.6
Blair-replicate 1	274.2 (-11.88)	279.9		282.8 (-11.89)	297.1		177.5 (-23.05)	155.7
Blair-replicate 2	315.9 (-11.92)	314.4		320.6 (-11.91)	338.2		195.6 (-22.2)	189.2
Somerset-replicate 1	230.3 (-11.88)	238.1		235.2 (-11.85)	242.1		140.8 (-22.17)	137.1
Somerset-replicate 2	246.3 (-11.88)	264.0		256.2 (-11.86)	272.6		149.0 (-22.08)	146.8
Mercer East-replicate 1	234.4 (-11.71)	261.3		239.8 (-11.71)	253.0		144.1 (-21.96)	144.8
Mercer East-replicate 2	228.5 (-11.6)	257.0		232.2 (-11.60)	258.3		143.1 (-21.9)	143.5
Mercer West-replicate 1	297.7 (-11.94)	332.0		312.8 (-11.93)	329.5		185.2 (-22.06)	182.1
Mercer West-replicate 2	300.0 (-11.88)	327.6		313.2 (-11.88)	333.5		181.2 (-22.05)	178.2
Perry-replicate 1	208.4 (-11.99)	221.9		213.0 (-11.99)	222.8		123.7 (-22.43)	120.3
Perry-replicate 2	214.5 (-11.96)	217.5		219.3 (-11.95)	227.0		118.5 (-22.43)	110.7
Delaware-replicate 1	356.5 (-12.09)	352.0		354.0 (-12.07)	364.5		219.2 (-22.49)	210.2
Delaware-replicate 2	352.5 (-12.06)	357.4		370.8 (-12.05)	375.4		219.5 (-22.49)	206.5

*** values in brackets represent the actual test temperature**

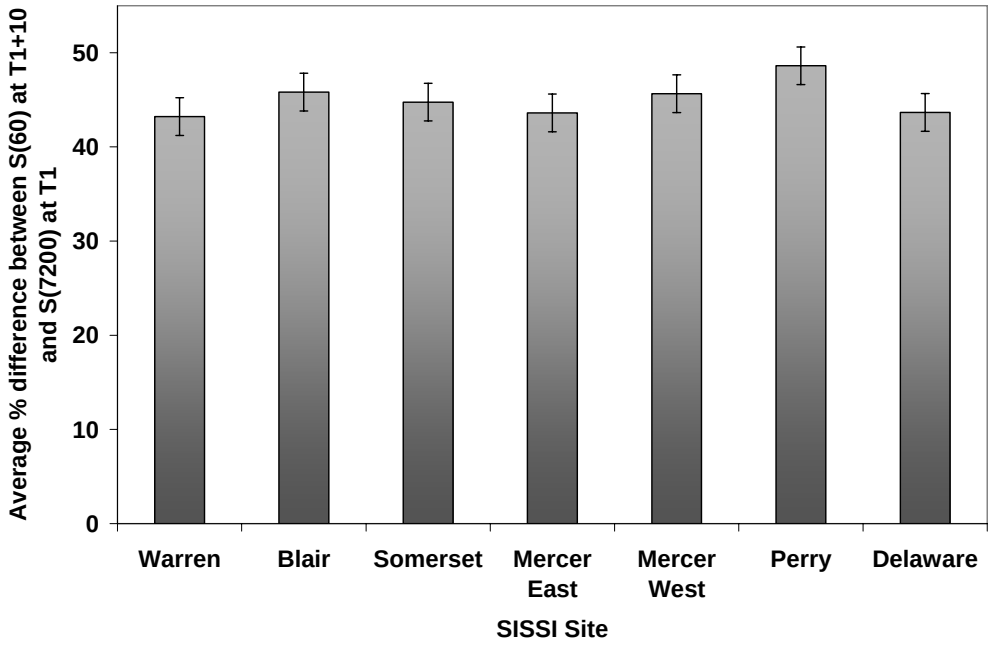

Figure 56. Average % differences between S(60) @ T_1 +10 and S(7200) @ T_2

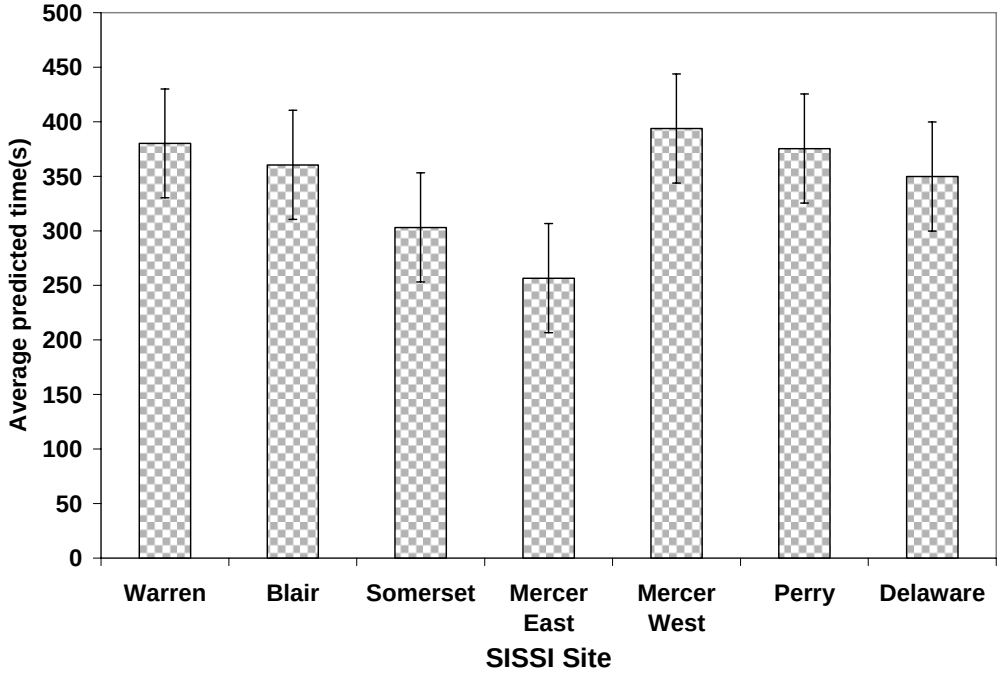

Figure 57. Average predicted time for S(60) @ T_1 +10 and S(7200) @ T_2 to be equivalent

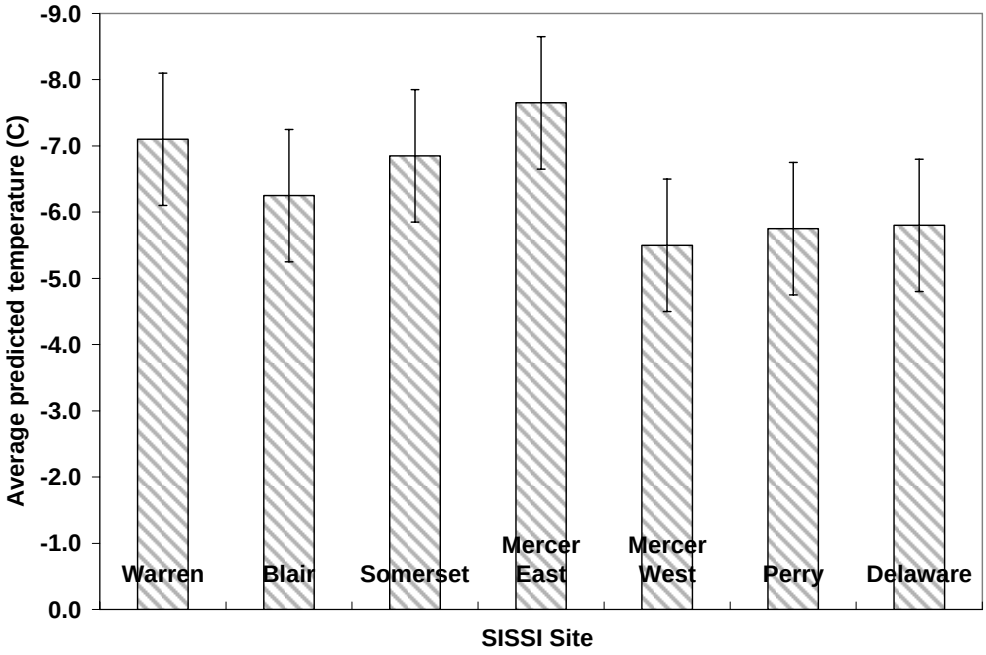

Figure 58. Predicted temperatures for S(60) @ T_1 +10 and S(7200) @ T_2 to be equivalent

Table 14. % difference, actual time, and temperature predicted for SISSI sites

Column number	1	2	3
SISSI Site	Difference	Actual Time	Temp for 60s
	(%)	(seconds)	(°C)
Warren-replicate 1	41	443	-7.5
Warren-replicate 2	45	317	-6.7
Blair-replicate 1	48	395	-6.0
Blair-replicate 2	44	326	-6.5
Somerset-replicate 1	43	284	-7.1
Somerset-replicate 2	46	323	-6.6
Mercer East-replicate 1	43	247	-7.8
Mercer East-replicate 2	44	266	-7.5
Mercer West-replicate 1	45	381	-5.7
Mercer West-replicate 2	47	407	-5.3
Perry-replicate 1	46	340	-6.2
Perry-replicate 2	51	411	-5.3
Delaware-replicate 1	42	340	-5.9
Delaware-replicate 2	45	360	-5.7
Average	**45**	**346**	**-6.4**

Figure 59 shows average shift factors for both the SHRP asphalt binders (Bahia, 1991) and SISSI binders. As discussed in Chapter 2, the shift factor functions for all asphalt binders are considered to be similar, and the slope of the shift factor curve is found to have a common slope between 0.173 log(s)/°C and 0.199 log(s)/°C. From Figure 59 and Table 15, it is observed that all the SISSI binders have similar shift factors. However, the slope of the shift factor curve varies between 0.111 log(s)/°C and 0.142 log(s)/°C and thus contradicts the fact that all asphalt binders have similar shift factors. The SHRP asphalt binders' shift factors are calculated at a reference temperature of -15°C. For comparison, all the SISSI asphalt binders' and the SHRP asphalt binders' shift factors are reported for the reference temperature of -12°C (i.e., the log shift factor values is zero at -12°C).

Table 15. Slope and R^2 for shift factor curves for binders from the SISSI sites

SISSI	Slope (%)	R^2
Warren 1	-0.1395	0.9986
Warren 2	-0.1269	0.9919
Blair 1	-0.1244	0.9994
Blair 2	-0.131	0.9994
Somerset 1	-0.1337	0.9996
Somerset 2	-0.1285	0.9958
Mercer East 1	-0.1344	0.9962
Mercer East 2	-0.1346	0.9961
Mercer West 1	-0.1418	0.9863
Mercer West 2	-0.1183	0.9914
Perry 1	-0.1227	0.9939
Perry 2	-0.1204	0.9998
Delaware 1	-0.1114	0.9999
Delaware 2	-0.1338	0.9996
Average SISSI	-0.1287	0.9963
Average SHRP	-0.1831	0.9991

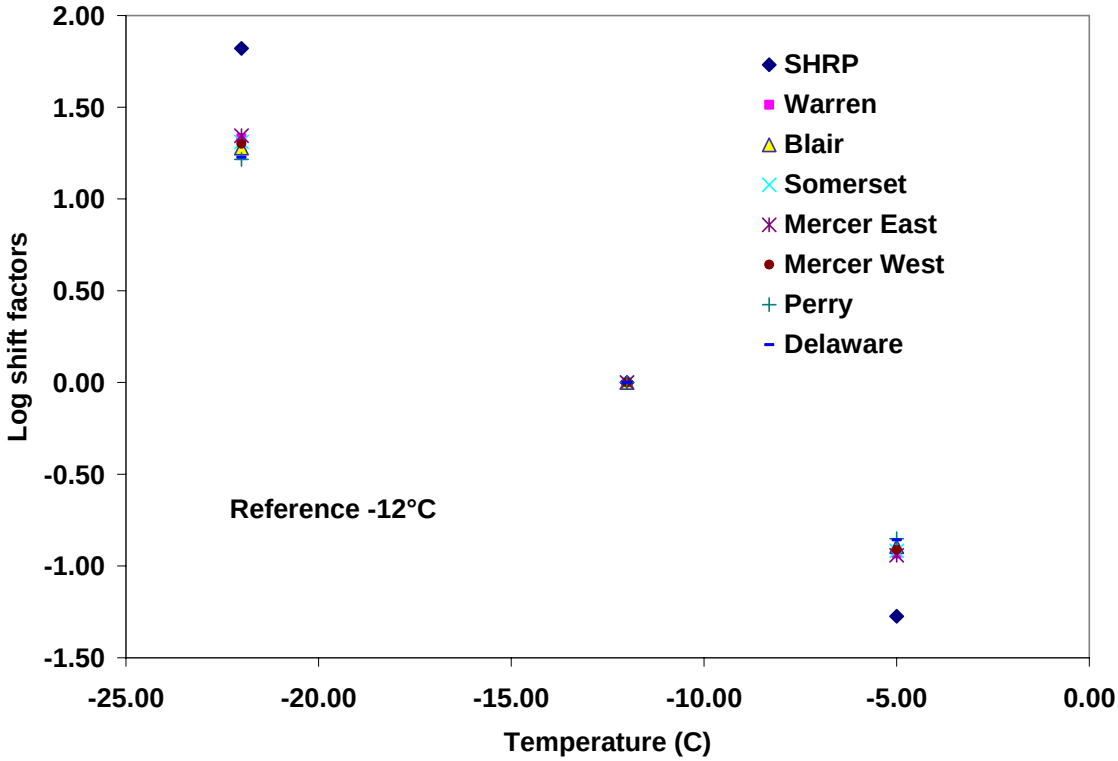

Figure 59. Comparison of shift factors for SHRP core asphalts and SISSI binders

The significance of the need for accurate shift factors is explained by means of an example. Table 16 shows the average log shift factor values at -22°C and -5°C for the SISSI and SHRP asphalt binders. The flexural creep stiffness for any desired temperature can be predicted by Equation 17 (Chapter 3) given the time, log shift factor at the desired temperature, and the hyperbolic fit coefficients. The S(60) predicted at -22°C and -5°C are shown in Table 16 and Figure 60.

Table 16. Predicted S(60) for SHRP and SISSI asphalt binders

	Log shift factors @		Predicted S(60) @ (MPa)	
	-22°C	-5°C	-22°C	-5°C
SHRP	1.82	-1.27	510	52
SISSI	1.29	-0.9	396	76

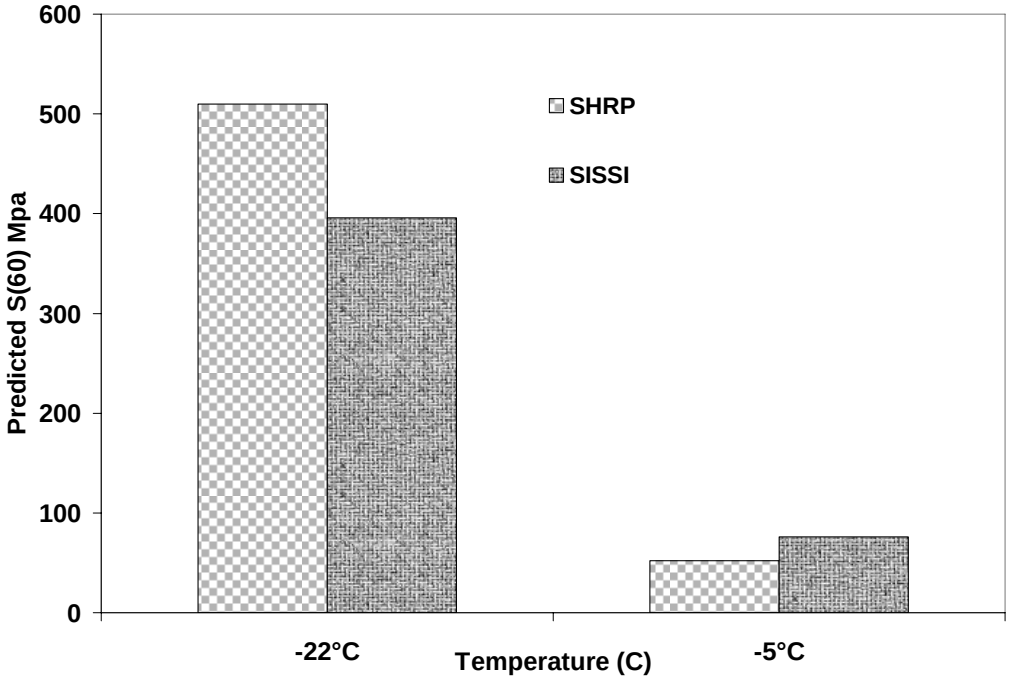

Figure 60. Predicted S(60) at -22°C and -5°C for SHRP and SISSI asphalt binders

From Figure 60, it is observed that the S(60) at -22°C and -5°C are different for the SISSI and SHRP asphalt binders. The observed difference between S(60) at -22°C and -5°C, respectively, for the SHRP and SISSI asphalt binders is 22 percent and 46 percent. The coefficients used to predict the flexural stiffness values are shown in Table 17. The coefficients are usually determined by regression analysis when performing time-temperature superposition. In this case, the coefficients are average values of all SISSI asphalts binders. It is understood that using different coefficients could possibly show varied results in terms of percent difference of the flexural stiffness values. In a broader perspective, however, the need for accurate shift factor values is critical.

Table 17. Hyperbolic fit coefficients

B2	1.5
B3	3.0
T_o	3.5

Comparison of D(t) and S(t) Shift Factor Functions

The average shift factor values from the IDT and BBR tests at a reference temperature of -12°C are shown in Figure 61. It is observed that the shift factor functions for the S(t) and D(t) test data are comparable at higher temperatures, with the exception of Delaware. There exists

considerable variation in shift factor values at -22°C, as seen from Figure 62. At very low temperatures, asphalt concrete or asphalt binders tend to be elastic, and the S(t) and D(t) curves are nearly parallel to the time axis. Thus, while shifting S(t) and/or D(t) data to develop the master curves, several shift factor values for very low temperatures can be used to obtain a smooth and continuous master curve, as shown in Figures 62, 63, and 64, respectively. This could be one possible reason for the variation of shift factor values at low temperatures in the IDT and BBR tests of SISSI mixtures and binders.

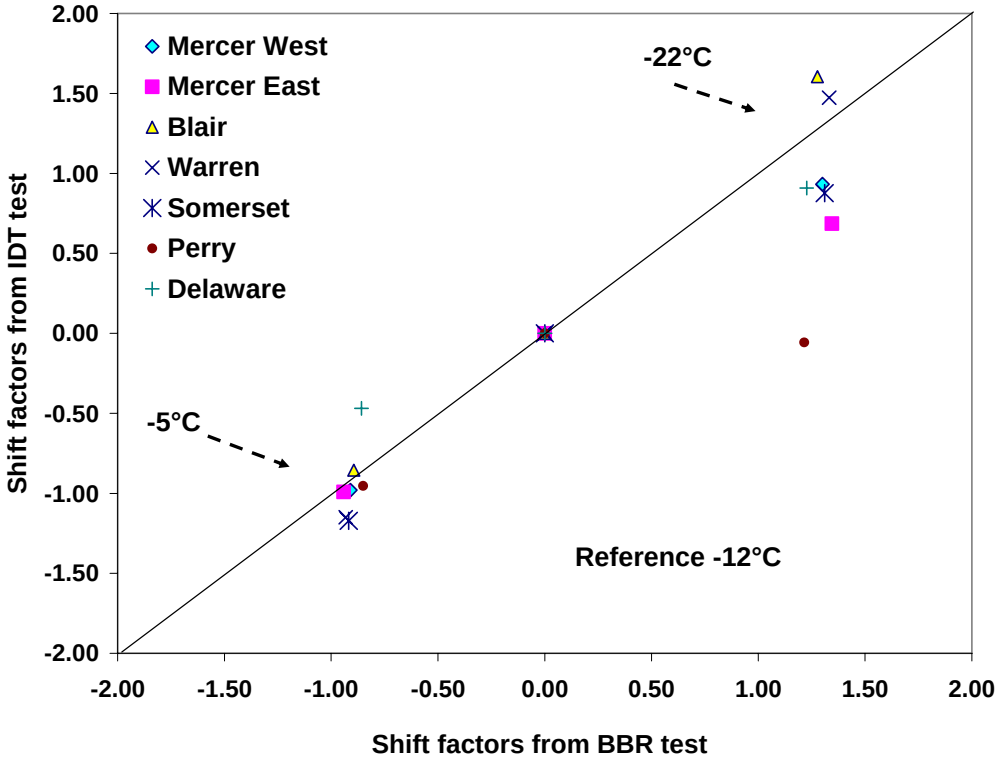

Figure 61. Average shift factors obtained from IDT and BBR tests

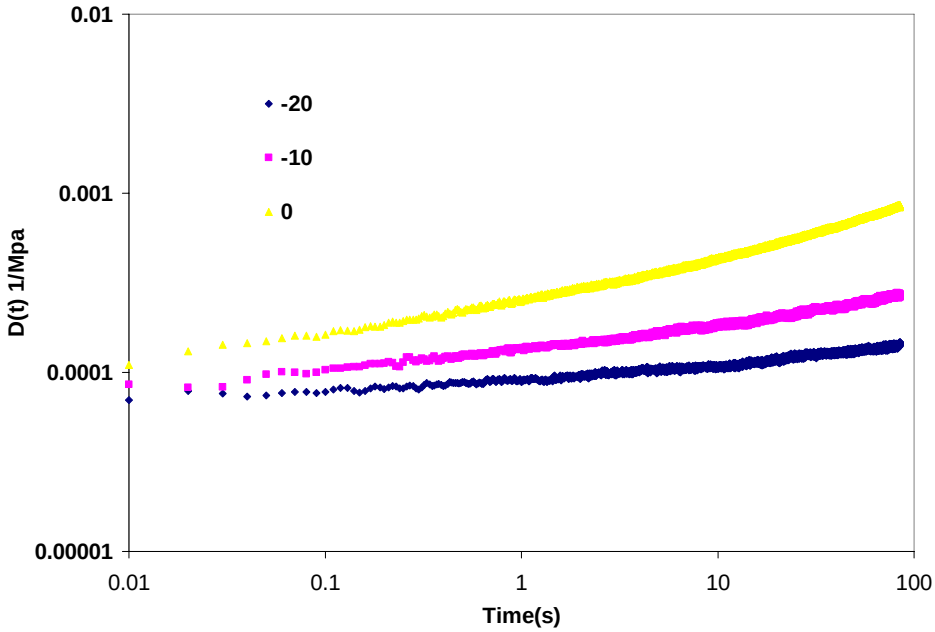

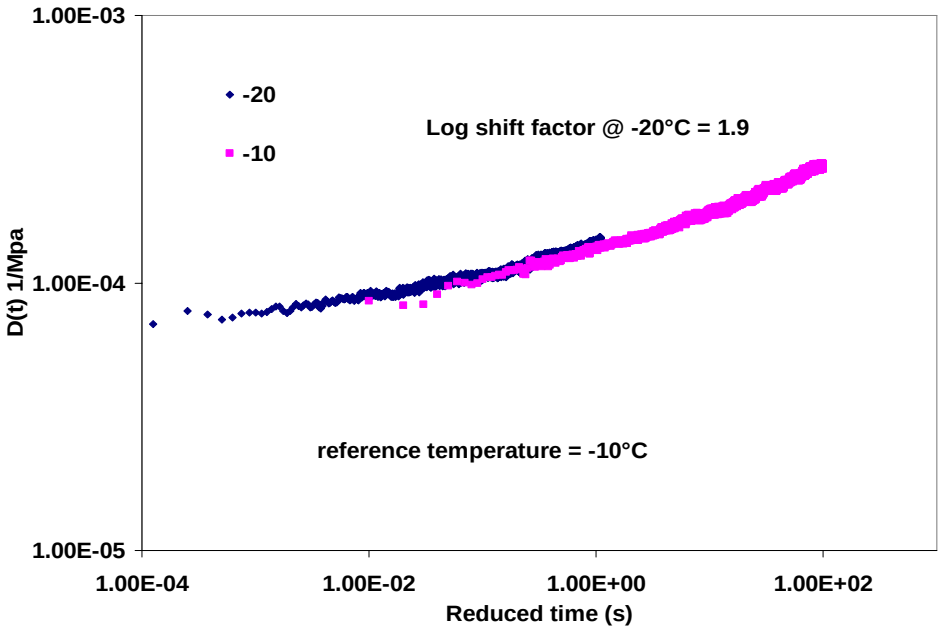

Figure 62. (a) Parallel D(t) curves at low temperatures, (b) D(t) master curve with log shift factor of 1.9 @ -22°C

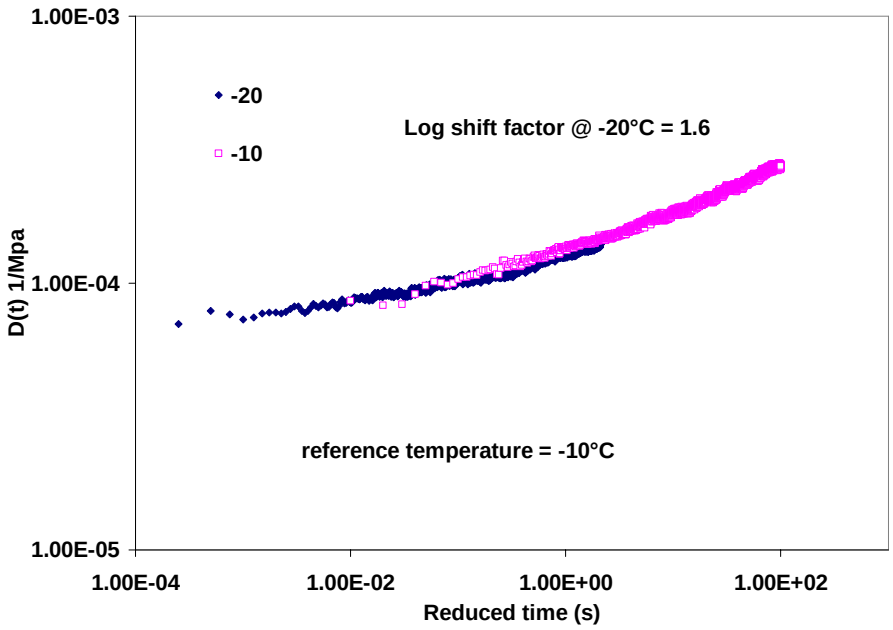

Figure 63. D(t) master curve with log shift factor of 1.6 @ -22°C

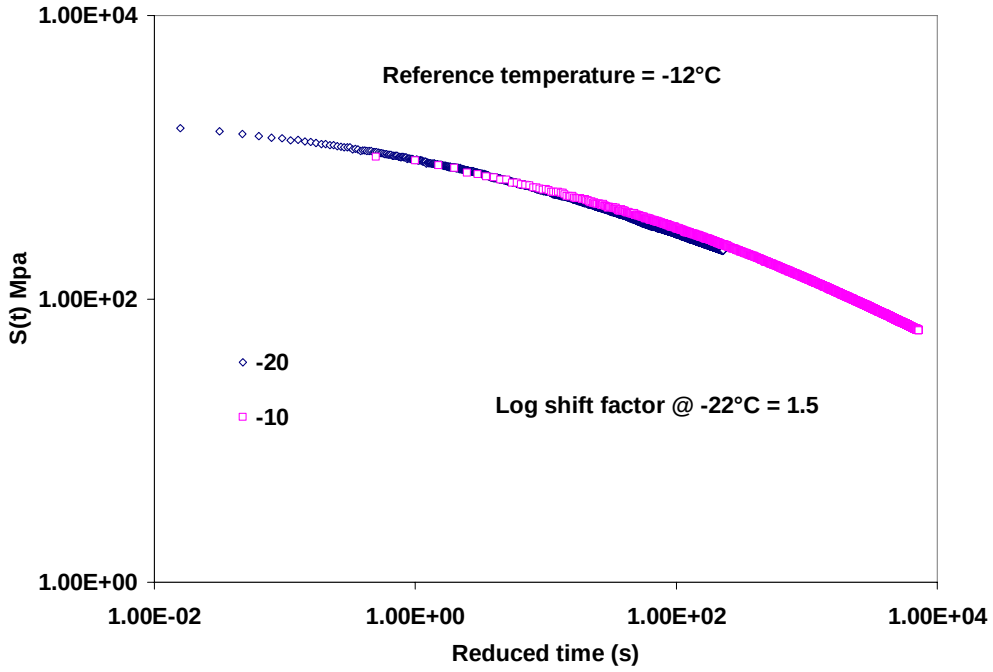

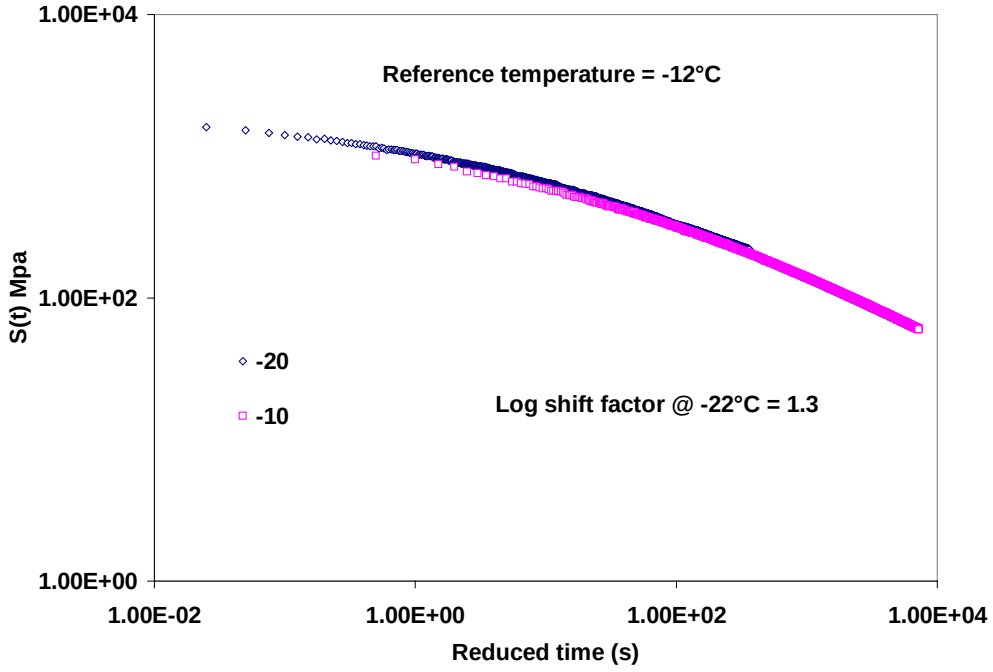

Figure 64. D(t) master curve with log shift factor of 1.5 @ -22°C (b) D(t) master curve with log shift factor of 1.3 @ -22°C

From Figure 62a, it is observed that the D(t) curves of the asphalt mixture at low temperatures tend to be parallel to each other because of their nearly elastic nature. Figure 62b and Figure 63 shows the D(t) master curve developed at a reference temperature of -10°C using different shift factors for -20°C. It can be observed that the curves tend to overlap each other even with differences in shift factor values. Though the difference in log shift factor is relatively small, it is magnified when the shift factor is calculated. A similar example for the S(t) master curve of the asphalt binder is shown in Figure 64. The shift factor values for both D(t) and S(t) curves are shown in Table 18.

Table 18. Shift factor values for D(t) and S(t) master curves for -20°C with reference temperature of -10°C

	Log shift factor	Shift factor
D(t)	1.9	79.4
	1.6	39.8
S(t)	1.5	31.6
	1.3	20.0

While shifting the master curve to a desired reference temperature, the creep compliance [D(t)] of the mixture and/or the flexural creep stiffness of the binder remains constant, causing the reduced frequency to change. In other words, the master curve only shifts along the horizontal time axis. The reduced time is calculated as the product of time and shift factor. From the table above, it is observed that the there could be up to 50 percent variation in the shift factor values, thus producing large differences in the reduced time; however, these shift factors are still capable of producing reasonable master curves, as observed from Figures 62, 63, and 64. Extra care must be exercised when calculating the shift factor values at very low temperatures.

Relationship between Low Temperature Properties of SISSI Mixtures and Binders

Because thermal cracking is dependent on both the properties of the asphalt mixtures and binders, it is important to correlate their D(t) and/or S(t) and m-values. Figure 65 and 66 show the comparison of D(t) and/or S(t) and m-values, respectively, for the all SISSI sites, with the exception of Tioga. No definite correlation exists between the D(t) and S(t) data; however, Blair, Mercer West, Somerset, Tioga, and Warren tend to follow a linear pattern.

The m-values of the mixture are in the range of 0.20 to 0.49 compared to binder m-values with a range of 0.29 to 0.27. With the exception of Delaware, Blair, and Perry, the mixture m-values are lower than that of the asphalt binder. This is expected owing to the elastic nature of the aggregates, with an m-value of zero and a primary component of asphalt concrete mixtures. However, to better correlate the relationships between asphalt mixtures and binders, a detailed analysis incorporating other mixture properties, such as air void content and gradation, must be performed, but that is beyond the scope of this study.

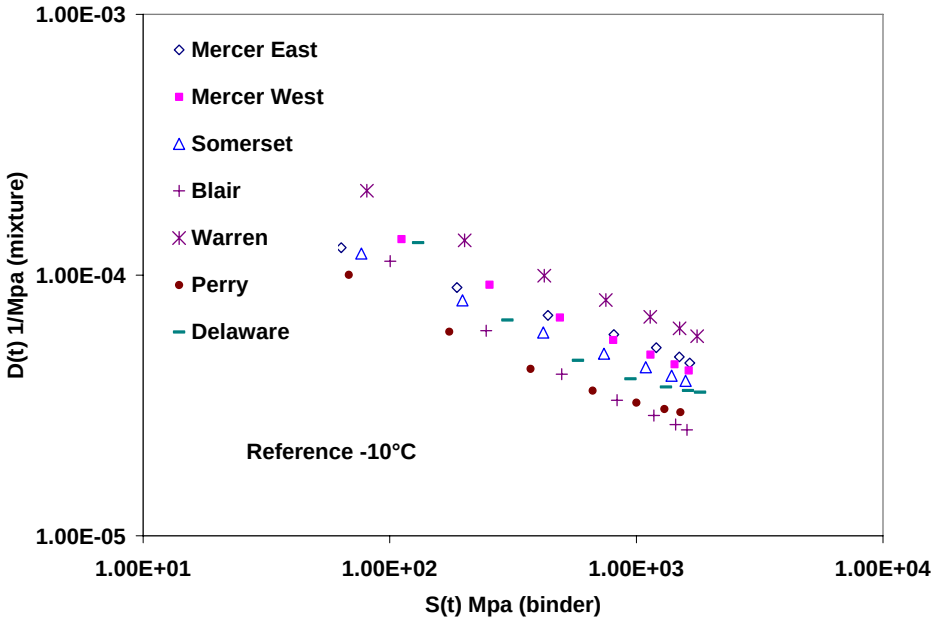

Figure 65. Comparison of average creep compliance/stiffness data for SISSI mixtures and binders

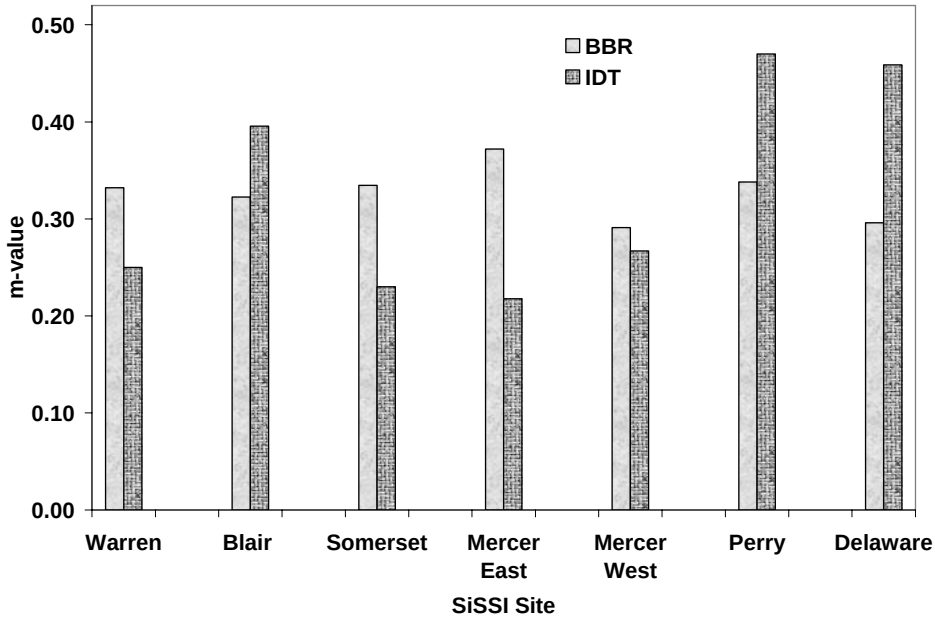

Figure 66. Comparison of average m-value for SISSI mixtures and binders

Ranking of SISSI Sites based on IDT and BBR Material Properties

All the SISSI sites, with exception of the Tioga site, are ranked for susceptibility of thermal cracking based on the IDT and BBR test results, as shown in Table 19. The ranking of all SISSI sites based on mixture data is shown in Table 20. The sites are ranked from 1 to 8 based on their susceptibility to thermal cracking, i.e., 1 is least susceptible, and 8 is the most susceptible. The ranking is based on the following observations and assumptions.

- S (t) (binder stiffness): It is assumed that the lower the binder stiffness, the less susceptible the mixture is to thermal cracking.
- Binder m-value: m-value of the binder represents the rate of stress relaxation and, hence, the ability to absorb more stresses developed in the pavement structure. Thus, binders with higher m-values are assumed to have the least susceptibility to thermal cracking.
- Mixture m-value: The same concept as that of the m-value for asphalt binders is adopted for ranking the SISSI sites.
- Tensile strength: Generally, if the strength of the mixture is high, it is less susceptible to thermal cracking. In this study, the sites were ranked based on tensile strength, i.e., high tensile strength leads to lower susceptibility to thermal cracking. The tensile strength and thermal stresses obtained from a typical BBR and DSR test is shown in Figure 67.
- D(t) [Creep compliance of the mixture]: The higher the creep compliance, the lower the complex modulus of the mixture; therefore, sites with higher creep compliance are assumed to have lower susceptibility to thermal cracking.

The S(t) and m-values of asphalt binder are calculated at -12°C and time of 60 seconds. From Figure 38, it is observed that the m-value of the creep compliance curve varies with respect to time. It should be noted that the m-value of the asphalt mixture is calculated as the maximum slope of the D(t) master curve. The D(t) data at 60 seconds at -10°C and the strength data calculated at -10°C are considered in ranking the SISSI sites. The ranking of the sites with respect to D(t) of the mixture might vary if times greater than 100 seconds are considered due to overlapping of the curves, but for the sake of comparison values at D(t) at 60 seconds is taken into account. The creep compliance master curve at -12°C will shift only along the time axis with the same creep compliance values; hence, the ranking of the sites at -10°C and -12°C will be the same at 60s. The ranking of the sites varies with material property, and an overall ranking could not be derived.

From Table 19, with exception of tensile strength and the m-value of the mixture, the pavement at the Delaware site appears to be the most susceptible to thermal cracking. Field observations indicate transverse cracks at the Delaware site as shown in Figure 68. These cracks could very well be thermally induced even though such conclusion could not be drawn with certainty. Correlating the laboratory test data with field observations could provide an insight to the susceptibility to thermal cracking. Another important observation from Table 19 is that no single low temperature material property can be used for ranking the mixture for thermal

cracking susceptibility, which is evident from the difference in rankings of the SISSI sites. Thus, developing a system by assigning weights for the low temperature material properties will be useful for achieving an overall ranking for the SISSI sites.

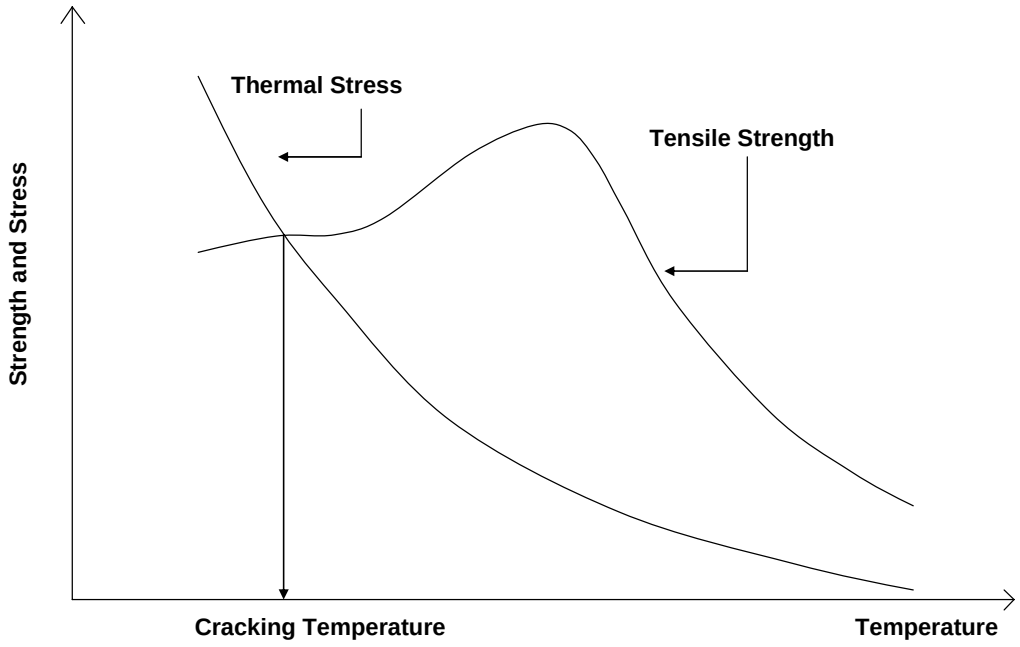

Figure 67. Tensile strength and thermal stress obtained from BBR and DSR testing

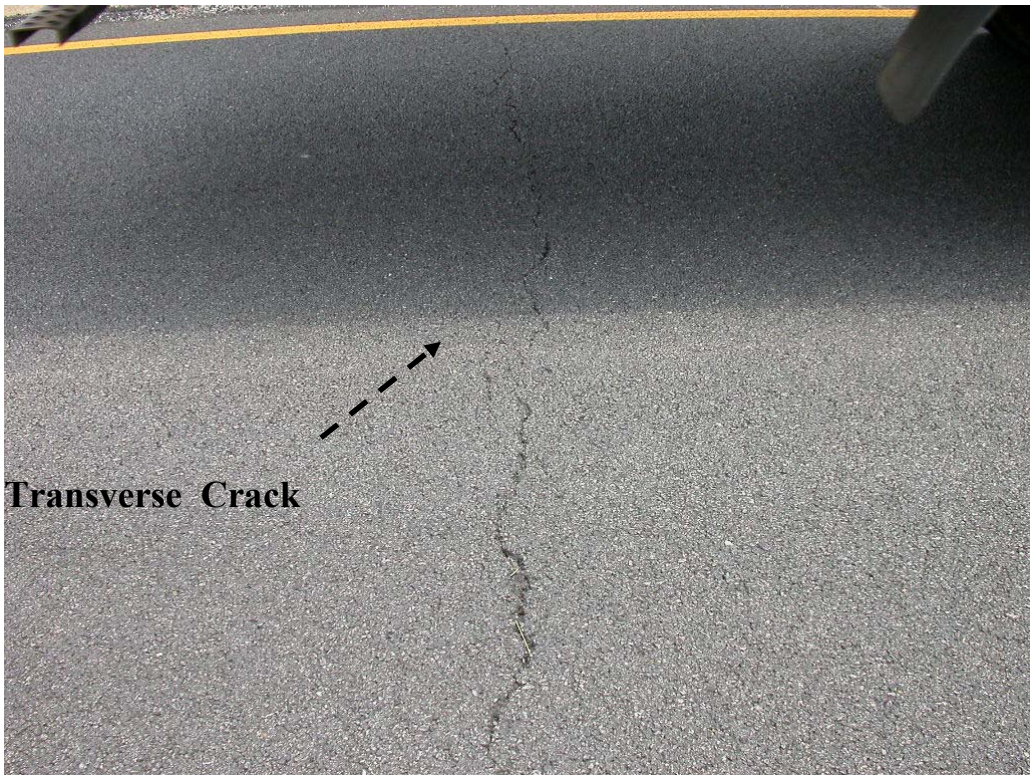

Figure 68. Transverse cracking in Delaware section (Stoffels and Solaimanian, 2006)

Table 19. Ranking of SISSI sites based on IDT and BBR test results

SISSI site		Ranking based on				
		S(t)	Binder m-value	Mixture m-value	Tensile strength	D(t)
Blair		5	5	3	2	7
Delaware		7	6	2	1	5
Mercer East		4	1	7	5	2
Mercer West		6	7	4	4	3
Somerset		2	3	6	6	4
Perry		1	2	1	3	6
Warren		3	4	5	7	1

Table 20. Ranking of all SISSI sites based on IDT test results

SISSI site		Ranking based on	
		Tensile strength	D(t)
Blair		2	8
Delaware		1	6
Mercer East		5	2
Mercer West		4	4
Somerset		6	5
Perry		3	7
Warren		7	1
Tioga		8	3

Shear Test Results and Analysis

Table 21 presents the repeated shear test results for the SISSI mixtures at 52°C, the temperature selected to represent summer pavement temperature in the vicinity of surface temperature for the pavements in Pennsylvania. The average maximum permanent shear strain presented in Table 21 is the result of applying 5,000 cycles of a shear load to the specimen. The peak shear stress during each cycle of loading was 70 kPa. Figure 69 and Figure 70 represent the average shear deformation for wearing and binder layers of the SISSI sites, respectively. These results indicate performance of SISSI mixtures in the range of good to excellent. For the wearing layer, the permanent shear strain ranged from 0.3 to 1.7 percent, indicating an excellent to good rutting resistance. For the binder layer, the range was between 0.4 and 1.7 percent, indicating good to excellent rutting resistance. The exception was the binder layer of the Perry site, for which a permanent strain of 2.4 percent was obtained, indicating fair rutting resistance even though no excessive rutting was observed in the field for this site. Overall, the field-measured rutting, after 5 to 8 years of service, ranged from 2.5 to 8.5 millimeters, indicating good to excellent rut resistance of SISSI mixtures at all the sites. This is in general consistent with laboratory-measured shear strains as discussed above.

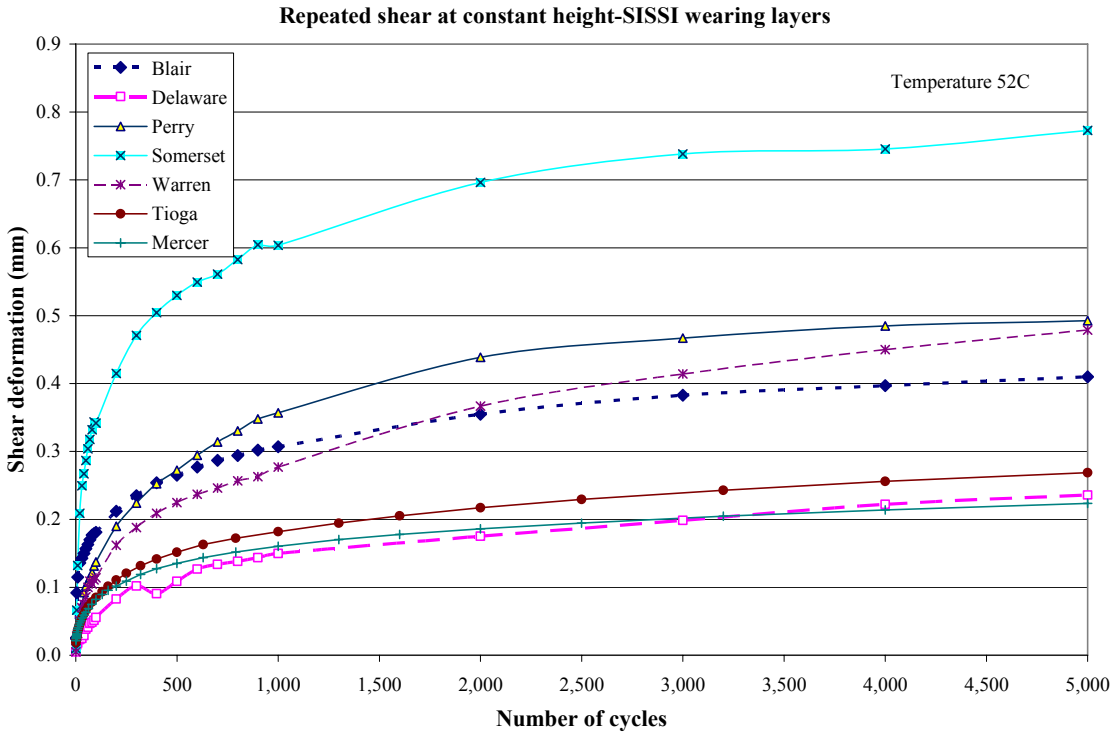

Figure 69. Shear deformation from RSCH test for wearing layers of SISSI sites at 52°C

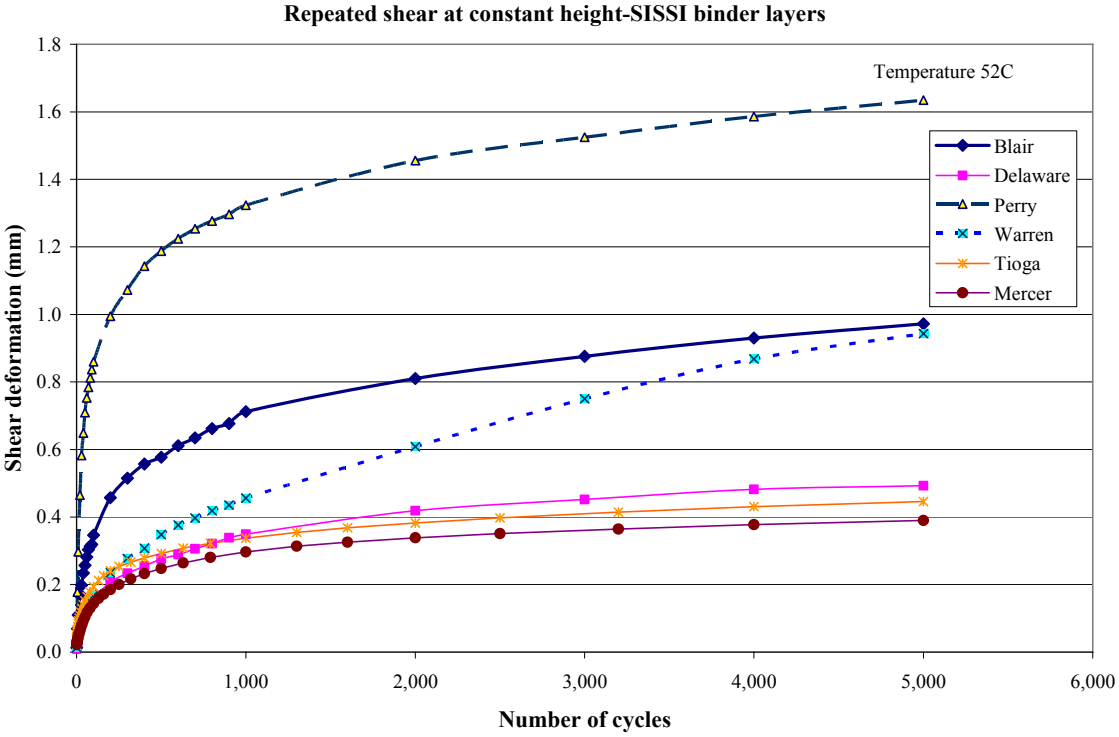

Figure 70. Shear deformation from RSCH test for binder layers of SISSI sites at 52°C

Table 21. Results of stress-controlled repeated shear constant height test at 52ºC

SISSI Site	Pavement Course	Air Voids (%)	Specimen Information		Shear Deformation (mm)		Max. Permanent Shear Strain (%)	
			Replicate #	Thickness (mm)	After 1 cycle	After 5000 cycles	For each specimen	Average
Tioga	Wearing	3.0	1	49.8	0.011	0.147	0.30	0.27
		3.0	2	48.6	0.008	0.118	0.24	
	Binder	3.0	1	50.0	0.012	0.153	0.31	0.45
		3.0	2	50.2	0.027	0.297	0.59	
Mercer	Wearing	3.0	1	49.1	0.011	0.102	0.21	0.23
		3.0	2	51.0	0.010	0.120	0.24	
	Binder	3.0	1	51.5	0.009	0.150	0.29	0.39
		3.0	2	50.3	0.013	0.245	0.49	
Perry	Wearing	3.5	1	49.9	0.008	0.420	0.84	0.98
		4.0	2	51.1	0.013	0.565	1.11	
	Binder	3.0	2	52.1	0.013	1.366	2.62	2.45
		4.6	3	48.1	0.004	0.226	0.47	
		5.2	4	50.9	0.010	1.158	2.28	
Warren	Wearing	3.0	1	52.3	0.005	0.479	0.92	0.92
	Binder	3.0	1	51.5	0.013	0.943	1.83	1.70
		7.0	1	52.7	0.008	0.830	1.57	
	BCBC	3.0	1	77.2	0.012	0.491	0.64	0.54
		3.0	2	77.2	0.003	0.317	0.41	
		3.0	3	77.5	0.005	0.431	0.56	
Delaware	Wearing	3.0	3	51.2	0.006	0.112	0.22	0.29
		3.0	2	52.2	0.007	0.182	0.35	
	Binder	3.0	1	48.0	0.007	0.510	1.06	1.03
		3.0	2	48.0	0.011	0.475	0.99	
Somerset	Wearing	3.2	1	48.2	0.018	0.687	1.43	1.72
		3.4	2	47.5	0.017	1.142	2.40	
		3.8	3	48.4	0.003	0.641	1.32	
		4.4	4	49.3	0.001	0.621	1.26	1.26
Blair	Wearing	3.5	2	52.1	0.025	0.410	0.79	0.79
	Binder	2.4	1	53.5	0.018	0.922	1.72	0.86

CHAPTER 5
SUMMARY AND CONCLUSIONS

Characterization of materials is an integral part of the overall effort to validate the Superpave system and to calibrate the performance prediction models for the environmental conditions observed in the Commonwealth of Pennsylvania. Material properties are among the most important input parameters to the models of the Mechanistic Empirical Pavement Design Guide for flexible pavements. These models encompass a large number of other input parameters, such as pavement structure, traffic data, and climatic factors.

An extensive laboratory testing program was followed during Phase I of the Superpave In-situ Stress Strain Investigation (SISSI) project to determine binder properties, mix volumetric properties, and mix dynamic modulus for all SISSI mixtures. To compliment this material characterization, further laboratory testing was conducted during Phase II of the project. The second phase of this work concentrated on determination of SISSI mixtures' resistance to low temperature cracking and permanent deformation. The tests were performed on mixes procured from the sites at the time of construction.

Of the eight SISSI sites, six were constructed using BCBC, binder, and wearing courses. Only a binder course and a wearing course were used for the remaining two. All surface mixes had a nominal maximum aggregate size (NMAS) of 12.5 mm, except one that was prepared as a 9.5-mm mix. The binder courses were either 19 or 25 mm, and the BCBC courses were 37.5 mm, except one that was a 25-mm mix. The hot-mix asphalt samples for all of these courses were procured behind the paver and were tested in the laboratories. AASHTO test procedures were followed for conducting relevant tests.

Validation of the Superpave Binder Specification for Low Temperature Cracking

Characteristics of asphalt binder provide the opportunity to relate the results to the performance of the SISSI test sections and determine the role of the binder grade in observed performance. This statement is made knowing that many other factors, such as aggregates, the base condition, traffic intensity, climatic condition, layer configuration, and drainage condition affect pavement performance. Since such a large number of factors affect pavement performance, it will be very difficult to develop a simple correlation between performance and the binder physical properties.

The binder specification tests have been much more widely used than the mixture tests since implementation of SHRP began about 12 years ago. Therefore, there is more confidence at this time in the binder tests. On the other hand, binder properties cannot fully account for mixture performance. Low temperature cracking resistance, for example, depends to a large extent on binder stiffness and creep properties but also to some extent on mix properties, such as air voids and aggregate structure within the mix.

Therefore, the binder test results would provide further insight in complete understanding of the pavement performance and occurrence of distresses when integrated with other test results and variables.

The testing program for SISSI binders during Phase II included tests with the bending beam rheometer at various temperatures and loading times to validate the specifications. The validity of the Superpave binder specification in regard to the equivalence principle for the binder flexural creep stiffness was evaluated during Phase II. Based on this principle, the binder creep stiffness at a specified temperature under two hours of loading (S(7,200) is approximately equal to its creep stiffness at a temperature 10ºC warmer under 60 seconds of loading (S(60). This principle also assumes that all asphalt binders can be characterized by similar shift factors. A set of seven different asphalt binders from the SISSI sites was tested at three different temperatures and two testing times to obtain the S(t) master curves. Based upon the results of testing and analysis, the conclusions are as follows:

- The comparison of the S(60) at T_1+10 and S(7,200) at T_1 shows significant differences for all the asphalt binders tested. The S(60) values are significantly higher than the S(7,200) values, and the differences range between 40 and 52 percent.
- Alternative testing times and temperatures to satisfy the equivalence principle for the SISSI binders are provided. To satisfy the equivalence principal, the SISSI asphalt binder stiffness values should be obtained on an average at 340 seconds at T_1+10 or at 60 seconds at T_1+16.
- The shift factor curves obtained from the SISSI asphalt binder S(t) master curves had an average slope of 0.129 compared to the value of 0.183 suggested for all asphalt binders, which was based on the study conducted on SHRP asphalt binders (Bahia, 1991).

Characterization of Low Temperature Cracking Resistance Properties of the SISSI Mixtures

During Phase II of the SISSI project, indirect tensile creep and strength tests were conducted on mixtures of wearing layers of all SISSI sites as part of the project. Based on the results, the SISSI sites were ranked based on resistance against low temperature cracking.

- Comparison of the shift factors of the asphalt mixtures and constituent binders showed that at higher temperatures, the shift factors were much closer than at lower temperatures.
- Correlating the D(t), S(t), and m-values of the asphalt mixtures and constituent binders does not yield significant results to derive any conclusion. Detailed analysis involving more material properties should be conducted.

- The SISSI sites were ranked based on their low temperature material properties. For ranking the sites, all material properties must be taken into account, and no single property can be given preference over the other; however, based on measured properties, it seems that the SISSI mixture used at the wearing course of the Delaware site is the most susceptible to thermal cracking. Transverse cracks observed at this site might be thermally induced.

Fracture Analysis of SISSI Mixtures

Fracture properties of AC are crucial for understanding the mechanism of low temperature cracking in flexible pavements. Nevertheless, sophisticated instrumentations are usually needed to characterize such properties during experimental tests. Finite element simulation is one means to overcome this obstacle.

During the first phase of this study, viscoelastic material properties (e.g., creep compliance and Poisson's ratio) of five SISSI mixtures were obtained from the IDT test at -20°C, -10°C, and 0°C. The focus of the second phase was the development of a 3-D finite element model implemented with fracture mechanics. This FE model was further validated with the horizontal strains calculated using an analytical solution. Key fracture properties of AC, including energy release rate and crack opening displacement (COD), were simulated through FEA in the last phase.

From the study, the following can be concluded:

- Under the IDT mode, a crack always initiated from the edge of the specimen regardless of testing temperatures. The maximum tensile stress, which stimulates the cracking initiation, is independent of types of AC mixtures.
- Considerable deviations were observed between the calculated fracture energy from linear elastic and linear viscoelastic solutions. This deviation varies from one mixture to another and can be up to 56 percent at the end of the fracture life.
- A developed prediction model for the COD during the crack propagation has a great benefit for an experiment situation where instrumentations are not available. However, further experimental investigations are necessary to validate this prediction model.

Characterization of Rutting Resistance Properties of the SISSI Mixtures

Results of repeated shear testing at maximum pavement temperature indicates performance of SISSI mixtures in the range of good to excellent because no excessive permanent deformation was observed from these laboratory tests. For the wearing layer, the permanent shear strain ranged from 0.3 to 1.7 percent, indicating a good to excellent rutting resistance. For the binder layer, the range was between 0.4 and 1.7 percent, indicating good rutting resistance. The exception was the binder layer of the Perry site, for which a permanent strain of 2.4 percent was obtained, indicating fair rutting resistance even though no excessive rutting was observed in the field for this site.

Overall, the field-measured rutting ranged between 2.5 and 8.5 millimeters, indicating excellent rut resistance of SISSI mixtures at all the sites. In general, this is consistent with laboratory-measured shear strains, as discussed above.

REFERENCES

AASHTO T 313 (2002). "Standard Method of Test for Determining the Flexural Creep Stiffness of Asphalt Binder Using the Bending Beam Rheometer (BBR)," *Standard Specifications for Transportation Materials and Methods of Sampling and Testing*, American Association of State Highway and Transportation Officials, Washington D.C., Twenty-second edition.

AASHTO T 322 (2005). "Standard Method of Test for Determining the Creep Compliance and Strength of Hot-Mix Asphalt (HMA) Using the Indirect Tensile Test Device," *Standards Specifications for Transportation Materials and Methods of Sampling and Testing*, American Association of State Highway and Transportation Officials, Washington D.C., Twenty-fifth edition.

ABAQUS/Standard Version 6.6. (2006). *Finite Element Computer Program*, Hibbitt, Karlsson and Sorenson, Inc., Pawtucket, RI, USA.

Allen, D. H. and Searcy, C. R. (2006). "A model for predicting the evolution of multiple cracks on multiple length scales in viscoelastic composites," *Journal of Materials Science*, Vol. 41, No. 20.

Anderson, D. A., Christensen, D.W., Bahia, H.U. (1991). "Physical Properties of Asphalt Cement and the Development of Performance-Related Specifications," *Proceedings of the Association of Asphalt Paving Technologists,* Vol. 60, pp. 437–475.

Anderson, D.A., Christensen, D.W., Bahia, H.U., Dongré, R.N., Sharma, M.G., Antle, C.E., and Button, J. (1994). "Binder Characterization and Evaluation," Report SHRP A-369, Vol. 3, Strategic Highway Research Program, National Research Council, Washington, D.C.

Anderson, D.A., Christensen, D.W., Dongre, R., Sharma, M.G. and Jorhal, P. (1990). "Asphalt Behavior at Low Service Temperatures," Report FHWA A-RD-88-078, U.S. Department of Transportation, FHWA, March.

Anderson, D.A., and Kennedy, T.W. (1993). "Development of SHRP Binder Specification," *Journal of the Association of Asphalt Paving Technologists,* AAPT, Vol. 62, pp. 481-507.

Applied Research Associates (2003). "Guide for Mechanistic-Empirical Design of New and Rehabilitated Pavement Structures. Appendix HH: Field Calibration of the Thermal Cracking Model," Transportation Research Board, National Research Council.

Asphalt Institute (1996). *Superpave™ Mix Design*, Asphalt Institute Superpave™ Series No. 2 (SP-2).

Bahia, H.U. (1991). "Low-Temperature Isothermal Physical Hardening of Asphalt cements," Ph.D. Dissertation, The Pennsylvania State University.

Bahia, H.U., and Anderson, D.A. (1993). "The Development of the Bending Beam Rheometer: Basic and Critical Evaluation," *Physical properties of Asphalt Cement Binders,* STP 1241, pp.28-50.

Bahia, H. U., Anderson, D.A. and Christensen, D.W. (1992). "The Bending Beam Rheometer: A Simple Device for Measuring Low-Temperature Rheology of Asphalt Binders," *Journal of the Association of Asphalt Paving Technologists,* Vol. 61, pp. 117–148.

Bakuckas, J.G. (1999). "Comparison of Boundary Correction Factor Solutions for Two Symmetric Cracks in A Straight-Shank Hol," Final Report, DOT/FAA/AR-98/36. Federal Aviation Administration, NJ.

Baney, J.M. and Hui, C.Y. (1999). "Viscoelastic Crack Healing and Adhesion," *Journal of Applied Physics,* Vol. 86, No 8.

Barenblatt, G.I. (1962). "The mathematical theory of equilibrium cracks in brittle fracture," *Advances in Applied Mechanics,* Vol. 7.

Basu. A., Marasteanu, M.O. and Hesp, S.A.M. (2004). "Time Temperature Superposition and Physical Hardening Effects in Low-Temperature Asphalt Binder Grade," *Transportation Research Record* 1829, TRB, National Research Council, Washington, D.C., pp. 22-57.

Birgisson, B., Soranakom1, C., Napier, J.A.L., and Roque, R. (2003). "Simulation of Fracture Initiation in Hot-Mix Asphalt Mixtures," *Transportation Research Record,* 1849, Washington, D.C.

Bradford, L.G., Dong, S.B., Nicol, D.A., and Westmann, R.A. (1984). "A central crack element in fracture mechanics," *International Journal of Fracture,* Vol. 24.

Buttlar W.G. (1996). "Relationships Between Asphalt Binder and Mixture Stiff nesses at Low Temperatures for the Control of Thermal Cracking Pavement Performance," Ph.D. Dissertation, The Pennsylvania State University.

Buttlar, W.G. and Roque, R. (1994). "Development and Evaluation of the Strategic Highway Research Program Measurement and Analysis System for Indirect Tensile Testing At Low Temperature," *Transportation Research Record,* 1454, Transportation Research Board, National Research Council, Washington, D.C.

Buttlar, W.G. and You, Z. (2001). "Discrete Element Modeling of Asphalt Concrete: Microfabric Approach," *Transportation Research Record,* 1757, Transportation Research Board, National Research Council, Washington, D.C.

Chang, H. S., Lytton, R. L., and Carpenter, S. H. (1976). "Prediction of Thermal Reflection Cracking in West Texas," Research Report 18-3, Study 2-8-73-18, Texas Transportation Institute, College Station, TX.

Chehab, G., E. O'Quinn, and Y.R. Kim (2000) "Specimen Geometry Study for Direct Tension Test Based on Mechanical Tests and Air Void Variation in Asphalt Concrete Specimens Compacted by Superpave Gyratory Compactor," *Transportation Research Record*, 1723, Transportation Research Board, National Research Council, Washington, D.C., 2000, pp. 125-132.

Christensen, D. and Bonaquist, R. (2005). "Evaluation of Indirect Tensile Test (IDT) Procedures for Low-Temperature Performance of Hot Mix Asphalt," NCHRP Report 530, Phase III of Project 9-29, Washington, D.C.

Dave, E. V., Braham, A. F., Buttlar, W. G., Paulino, G. H., and Zofka, A. (2008). "Integration of laboratory testing, field performance data and numerical simulations for the study of low-temperature cracking," *Proceedings*, *the 6th International RILEM Conference,* Chicago, Illinois.

Dave, E. V., Song, S. H., Buttlar, W. G., and Paulino, G. H. (2007). "Reflective and Thermal Cracking Modeling of Asphalt Concrete Overlays," Proceedings, the Advance Characterization of Pavement and Soil Engineering, Athens, Greece, pp. 1241-1252.

Davis, P. (1993). "Levenberg – Marquardt Methods and Nonlinear Estimation," *SIAM News,* Vol. 26, No. 6.

De Souza, F.V., Soares, J.B., Allen, D.H., and Evangelista, J.F. (2004). "Model for Predicting Damage Evolution in Heterogeneous Viscoelastic Asphaltic Mixtures," *Transportation Research Record,* 1891, Transportation Research Board, National Research Council Washington, D.C.

Diamantoudis, A.T. and Labeas, G.N. (2005). "Stress intensity factors of semi-elliptical surface cracks in pressure vessels by global-local finite element methodology," *Engineering Fracture Mechanics,* Vol. 72.

Dugdale, D.S. (1960). "Yielding of steel sheets containing slits," *Journal of the Mechanics and Physics of Solids,* Vol. 8.

Griffith, A.A. (1921). "The phenomena of rupture and flow in solids," *Philosophical Transactions of the Royal Society of London Series A, Containing Papers of a Mathematical or Physical Character,* Vol. 221, pp. 163-198.

Hiltunen, D. And Roque, R. (1994). "A Mechanistic-based Prediction Model for Thermal Cracking of Asphalt Concrete Pavements," *Journal of the Association of Asphalt Paving Technologists,* Vol. 63.

Hoyt, D.M., Lytton, R.L., and Roberts, F.L. (1987). "Criteria for Asphalt- Rubber Concrete in Civil Airport Pavements, Vol. 2 - Evaluation of Asphalt-Rubber Concrete,", Report DOT/FAA/PM-86/39.11, Federal Aviation Administration, College Station, TX.

Huang, Y.H. (1993). *Pavement Analysis and Design,* Prentice Hall.

John, H.C., Margot, T.Y., and Fred, M.F. (1993). "Review of Relationships between Modified Asphalt Properties and Pavement Performance," (SHRP A-631), Strategic Highway Research Program, National Research Council, Washington, D.C.

Jung, D., and Venison, T.S. (1992). "Low temperature Cracking resistance of Asphalt Concrete Mixtures," *Journal of the Association of Asphalt Paving Technologists,* Vol. 62, pp. 54-92.

Kim, K. W. and El Hussein, H. M. (1995). "Effect of differential thermal contraction on fracture properties of asphalt materials at low temperature," *Journal of Association of Asphalt Paving Technologists,* Vol. 64.

Kim, Y.R. and Wen, H. (2002). "Fracture Energy from Indirect Tension Testing," *Journal of Association of Asphalt Paving Technologists,* Vol. 71.

Kostrov, B.V. and Nikitin, L.V. (1970). *Archiwum Meckaniki Stosowanej,* Vol. 22.

Lakes, R.S. and Wineman, A. (2006). "On Poisson's Ratio in Linearly Viscoelastic Solids," *Journal of Elasticity* 85, pp. 45-63..

Li, X. and Marasteanu, M.O. (2004). "Evaluation of the low temperature fracture resistance of asphalt mixtures using the semi circular bend test," *Journal of the Association of Asphalt Paving Technologists,* Vol. 73.

Li, X. and Marasteanu, M.O. (2005). "Cohesive modeling of fracture in asphalt mixtures at low temperatures," *International Journal of Fracture,* Vol. 136.

Lu, H., Zhang, X., and Knauss, W.G. (1997). "Uniaxial, shear, and Poisson relaxation and their conversion to bulk relaxation," *Journal of Polymer Engineering and Science.* Vol. 37, pp. 1053-1064.

Lytton, R.L. (2000). "Characterizing Asphalt Pavements for Performance." *Transportation Research Record,* Transportation Research Board, National Research Council, 1723, Washington, D.C.

Lytton, R.L., Uzan, J., Fernando, E.G., Roque, R., Hiltunen, D., Stoffels, S.M. (1993). "Development and Validation of Performance Prediction Models and Specifications for Asphalt Binders and Paving Mixes," Report SHRP A-357, Strategic Highway Research Program, National Research Council, Washington, D.C.

Marasteanu, M.O., and Anderson, D.A. (2000). "Establishing Linear Viscoelastic Conditions for Asphalt Binders," *Transportation Research Record,* 1728, Transportation Research Board*,* National Research Council, Washington, D.C., pp. 1–6.

Marasteanu, M.O., Dai, S, Labuz, J.F., and Li, X. (2002). "Determining the Low-Temperature Fracture Toughness of Asphalt Mixtures," *Transportation Research Record,* 1789, Transportation Research Board, National Research Council Washington, D.C.

Marquardt, D.W. (1963). "An Algorithm for Least Squares Estimation of Nonlinear Parameters," *Journal for the Society of Industrial and Applied Mathematics,* Vol. 11.

McLeod, N.W. (1968). "Transverse Pavement Cracking Related to Hardness of Asphalt Cements," *Proceedings*, *13th Conference Canadian Technical Asphalt Association*.

Organization for Economic Co-operation and Development (OECD) (2005). *Economic Evaluation of Long-Life Pavements,* OECD Publishing.

Owusu-Antwi, E.B., Khazanovich, L., and Titus-Glover, L. (1998). A mechanistic-based model for predicting reflective cracking in AC overlaid pavements*, Transportation Research Record 1629*, Transportation Research Board, National Research Council, Washington, D.C., pp. 234-241.

Park, S. and Kim, Y. (2001). "Fitting Prony-series Viscoelastic Models with Power-law Presmoothing," *Journal of Materials in Civil Engineering,* ASCE.

Park, S.W., Kim, Y.R., and Schapery, R.A. (1996). "A Viscoelastic Continuum Damage Model and its Application to Uniaxial Behavior of Asphalt Concrete," *Mechanics of Materials;* Vol. 24(4).

Paulino, G.H., Song, S.H., and Buttlar, W.G. (2004). "Cohesive zone modeling of fracture in asphalt concrete," *Proceedings*, the 5th *International Conference RILEM "Cracking in Pavements",* Limoges, France.

Portillo, O. and Cebon, D. (2008). "An experimental investigation of the fracture mechanics of bitumen and asphalt"*, Proceedings*, *the 6th International RILEM Conference,* Chicago, Illinois.

Readshaw, E.E. (1972). "Asphalt Specifications in British Columbia for Low Temperature Performance," *Proceedings of the Association of Asphalt Paving Technologists*, Vol. 41, pp. 562–581.

Retting, W. and Kolloid, Z.Z. (1966). *Polymere, 210,* Vol. 54.

Roque, R. and Buttlar, W. G. (1992). "The Development of a Measurement and Analysis System to Accurately Determine Asphalt Concrete Properties Using the Indirect Tensile Mode," *Proceedings of The Association of Asphalt Paving Technologist,* pp. 304-333.

Roque, R. and Buttlar, W.G. (1992). "The Development of a Measurement and Analysis System to Accurately Determine Asphalt Concrete Properties Using the Indirect Tensile Mode," *Journal of Association of Asphalt Paving Technologist,* Vol. 65.

Sangpetngam, B., Birgisson, B., and Roque, R. (2003). "Development of Efficient Crack Growth Simulator Based on Hot-Mix Asphalt Fracture Mechanics," *Transportation Research Record,* 1832, Transportation Research Board, National Research Council, Washington, D.C.

Santucci, L., (1998). "The Role of Compaction in the Fatigue Resistance of Asphalt Pavements," Institute of Transportation Studies, Technology Transfer Program, University of California at Berkeley.

Schapery, R.A. (1975). "A theory of crack initiation and growth in viscoelastic media: I. Theoretical development," *International Journal of Fracture,* Vol. 11, No 1.

Schapery, R.A. (1975). "A theory of crack initiation and growth in viscoelastic media: II. Approximate methods of analysis," *International Journal of Fracture,* Vol. 11, No 3.

Schapery, R.A. (1975). "A theory of crack initiation and growth in viscoelastic media: III. Analysis of continuous growth," *International Journal of Fracture,* Vol. 11, No 4.

Schapery, R. A. (1984). "Correspondence Principles and a Generalized J Integral for Large Deformation and Fracture Analysis of Viscoelastic Media," *International Journal of Fracture,* Vol. 25.

Schapery, R.A. (1984). "Correspondence Principles **a**nd a Generalized J Integral for Large Deformation and Fracture Analysis of Viscoelastic Media," *International Journal of Fracture,* Vol. 25, pp. 195-223.

Schapery, R.A. (1988). "On some path independent integrals and their use in fracture of nonlinear viscoelastic media," *International Journal of Fracture,* pp. 189-208.

Schapery, R.ANonl. (2000). "Linear Viscoelastic Solid," *International Journal of Solids and Structures,* Vol. 37, pp. 359-366.

Soares, J. B., Colares de Freitas, F. A., and Allen, D. H. (2003). "Crack modeling of asphaltic mixtures considering heterogeneity of the material," *Transportation Research Record, No. 1832.*, Transportation Research Board, national Research Council, Washington, D.C., pp. 113-120

Solaimanian, M., D.A. Hunter, J. Shah, and S.M. Stoffels (May 2006). "Characterization of Materials for Superpave In-Situ/Stress Strain Investigation," Final Report, PennDOT Project No. 0R-02, Pennsylvania Transportation Institute.

Solaimanian, M., Stoffels, S.M., Hunter, D.A., Morian, D., and Sadasivam, S. (2006). "Final Report: Superpave In-situ Stress/Strain Investigation," The Pennsylvania Transportation Institute.

Song, H.S., Paulino, G.H., and Buttlar, W.G. (2006). "A bilinear cohesive zone model tailored for fracture of asphalt concrete considering viscoelastic bulk material," *Journal of Engr. Fracture,* Mech., Vol. 73.

Stoffels, S.M., Solaimanian, M. (2006). "Pavement Condition Report: Superpave In-situ Stress/Strain Investigation," The Pennsylvania Transportation Institute.

Tschoegl, N.W. (1989). *The Phenomenological Theory of Linear Viscoelastic Behavior,* Springer-Verlag, Berlin.

Tschoegl, N.W., Knauss, W., and Emri, I. (2002). "Poisson's ratio in linear viscoelasticity – A critical review," *Mech. Time-Depend. Mater.,* Vol. 6.

Vincent, P.I. and Gotham, K.V. (1966). *Effect of crack propagation velocity on the fracture surface energy of PMMA,* Nature 210.

Wagoner, M.P., Buttlar, W.G., Paulino, G.H., and Blankenship, P. (2005). "Investigation of the Fracture Resistance of Hot-Mix Asphalt Concrete Using a Disk-Shaped Compact Tension Test," *Transportation Research Record,* 1929, Transportation Research Board, National Research Council, Washington, D.C.

Wen, H. (2001). "Fatigue Performance Evaluation of WesTrack Asphalt Mixtures Based on Viscoelastic Analysis of Indirect Tensile Test," Ph.D. Dissertation, North Carolina State University.

Whitcomb, J.D. and Woo, K. (1993). "Application of iterative global/local finite element analysis, Part 1: Linear analysis," *Communications in Numerical Methods in Engineering,* Vol. 9.

William, N.F. James, S.L. and Onaran, K. (1989). *Creep and Relaxation on Nonlinear Viscoelastic Materials*, Dover Publications, NY.

Williams, J.G. and Marshall, G.P. (1975). “Environmental crack and craze growth phenomena in polymers,” *Proc., the Royal Society, London* A342.

Williams, M.L. (1964). “Structural Analysis of Viscoelastic Materials,” *AIAA Journal,* Vol. 2, No. 5, pp. 785-808.

Williams, M.L. (1965). “Initiation and Growth of Viscoelastic Frac-ture,” *Proceedings, First International Conference on Fracture,”* Sendai, Japan, Vol. 2.

Appendix A

Results of Indirect Tensile Tests on SISSI Mixtures

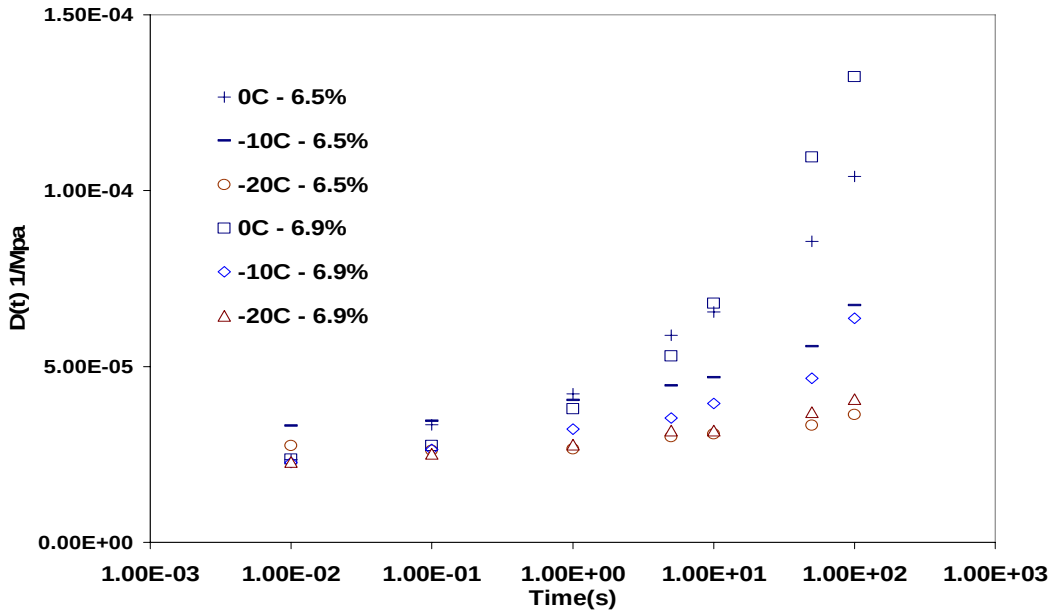

a

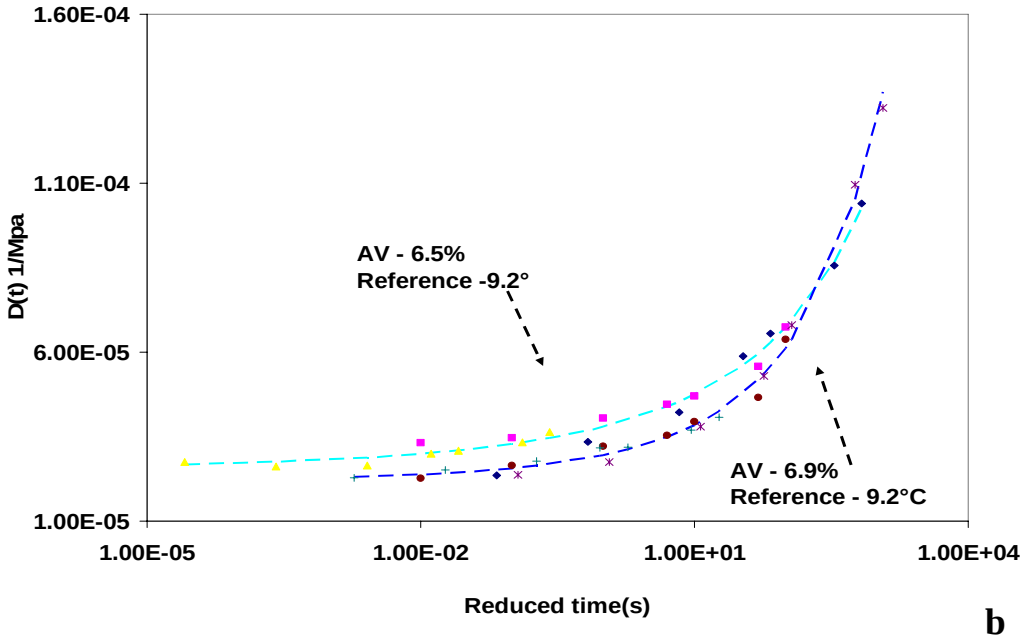

b

Figure A1 Creep compliance vs. time (a) and creep compliance master curve (b) for Blair

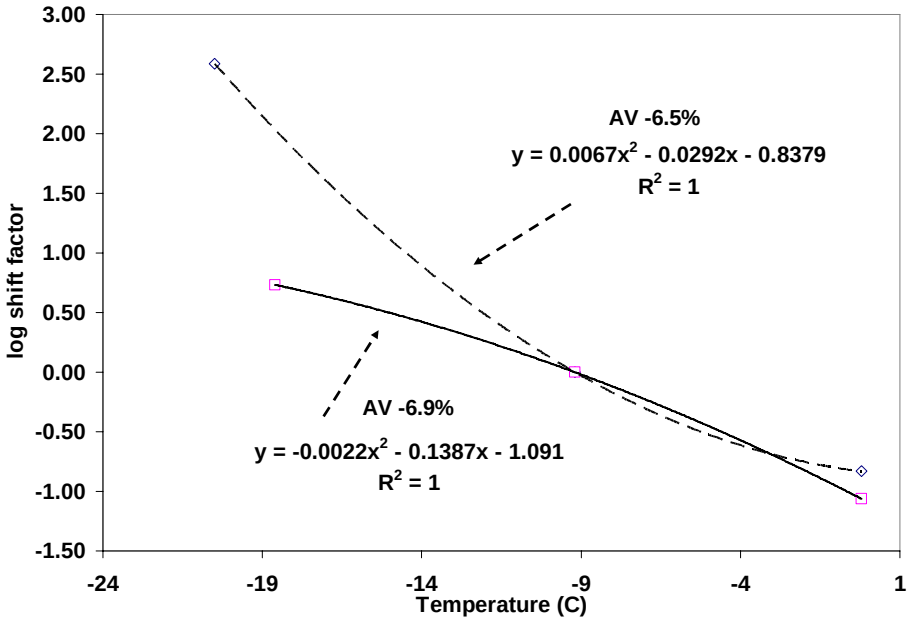

a

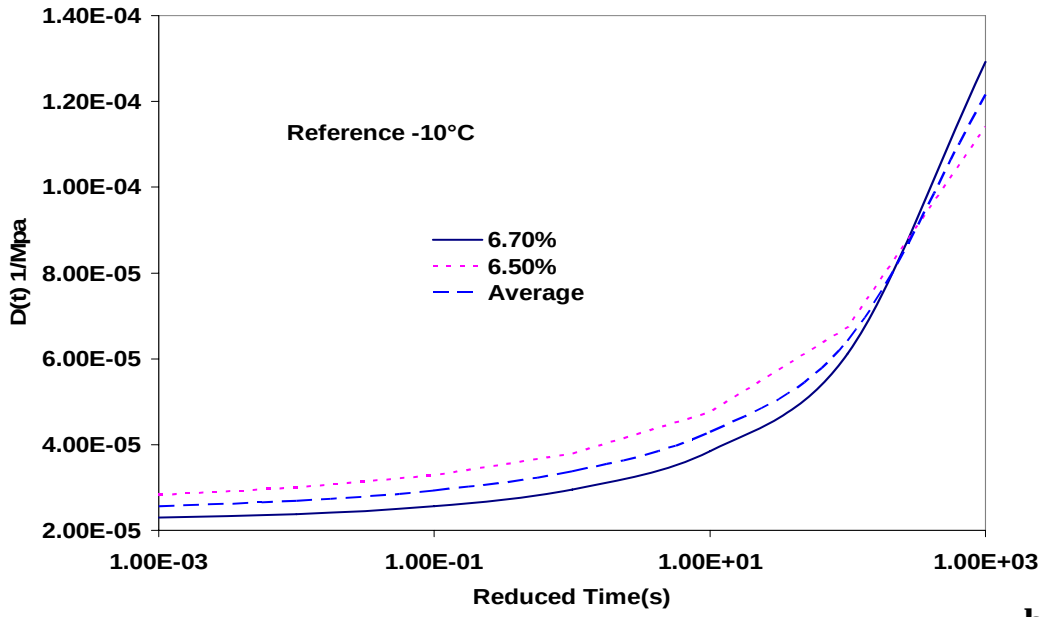

b

Figure A2 Shift factor curve (a) and creep compliance master curve at -10°C (b) for Blair

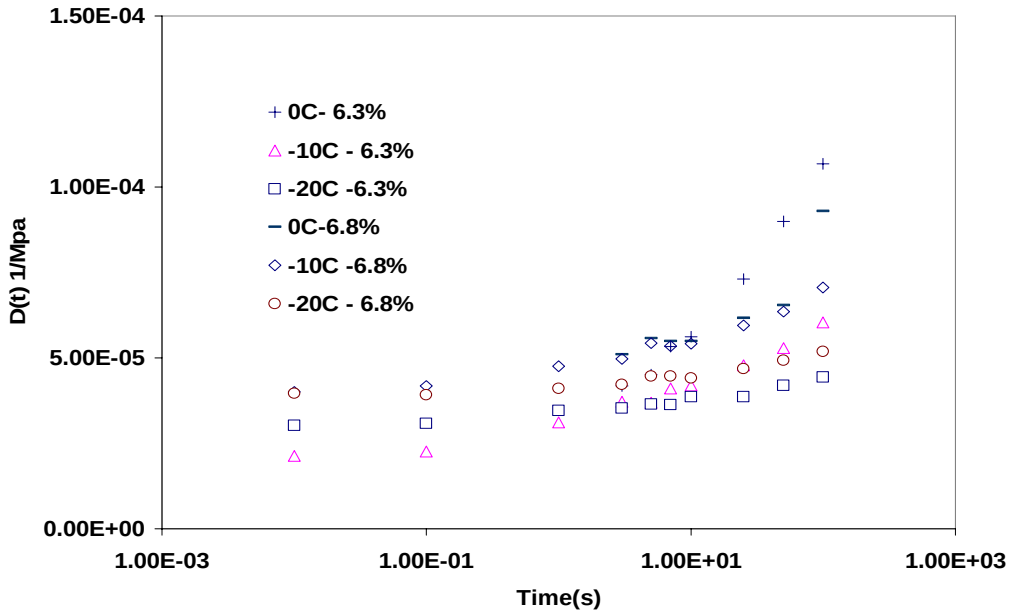

a

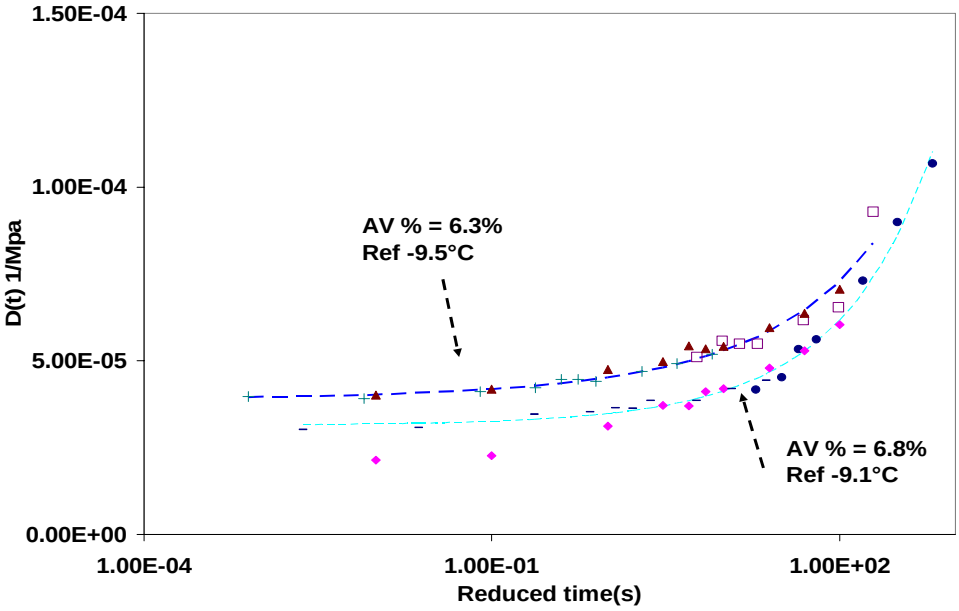

b

Figure A3 Creep compliance vs. time (a) and creep compliance master curve (b) for Delaware

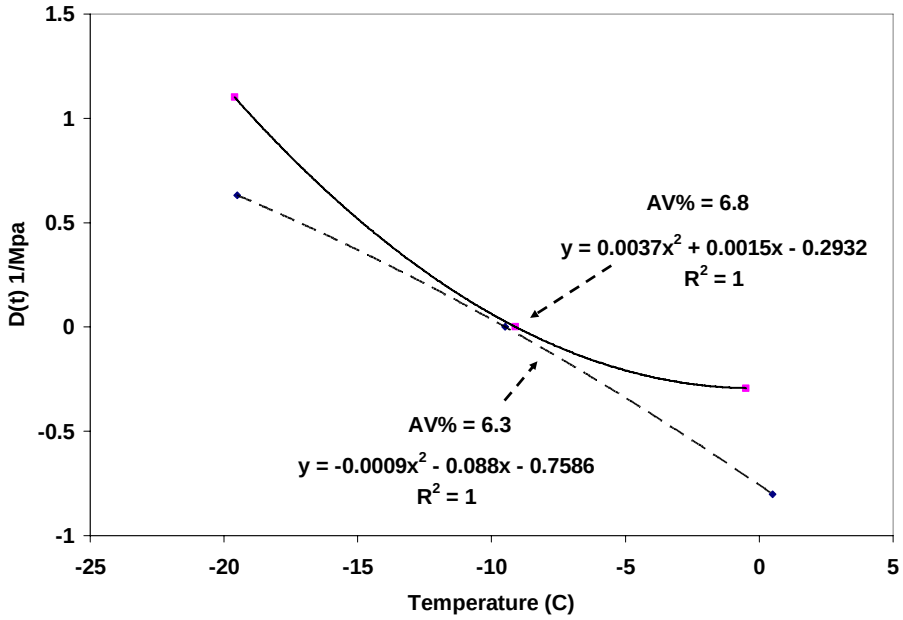

a

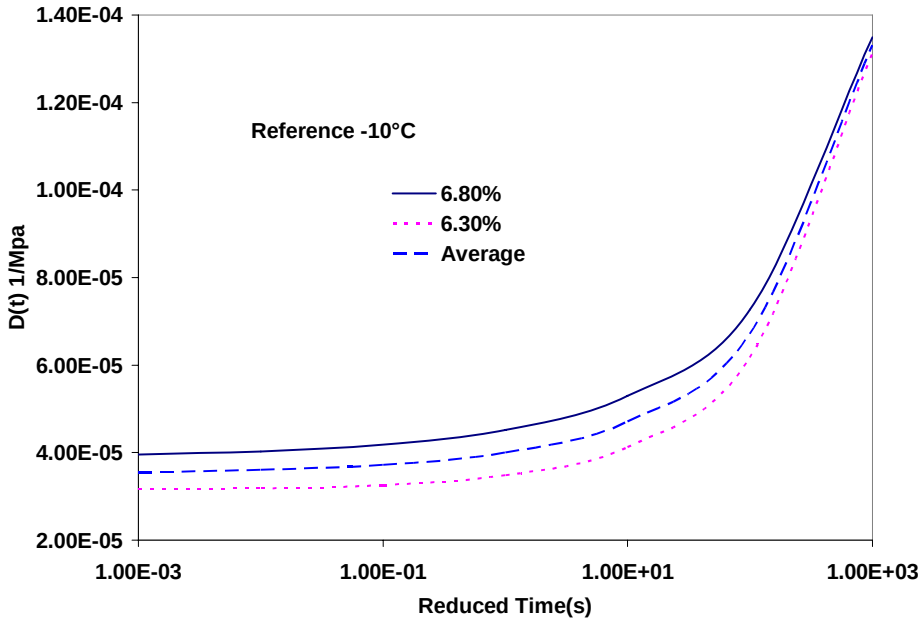

b

Figure A4 Shift factor curve (a) and creep compliance master curve at -10°C (b) for Delaware

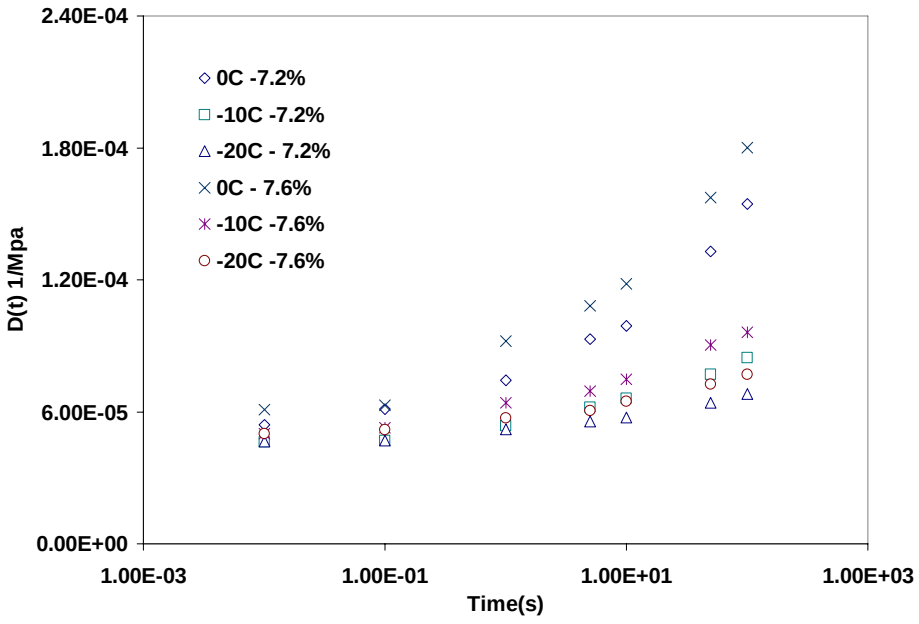

a

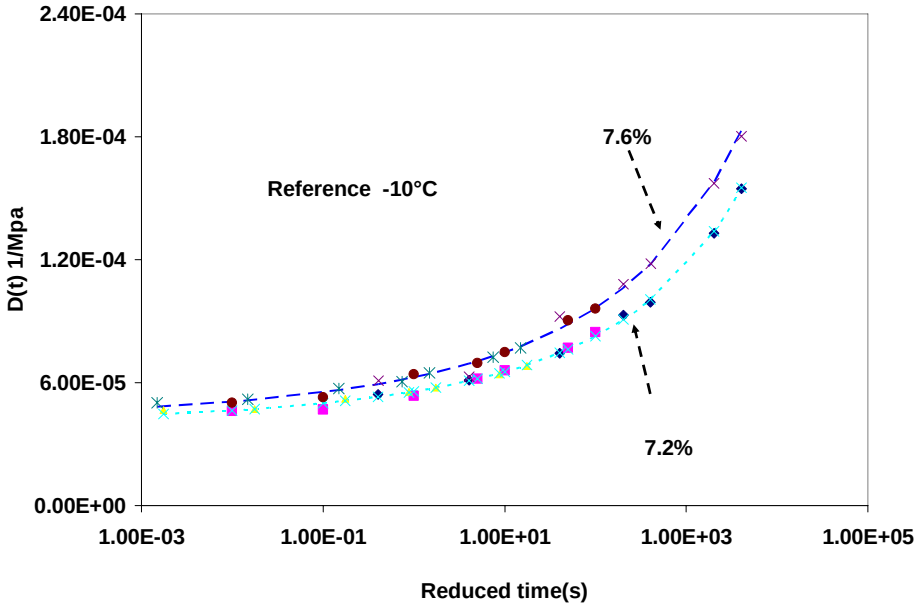

b

Figure A5 Creep compliance vs. time (a) and creep compliance master curve (b) for Mercer East

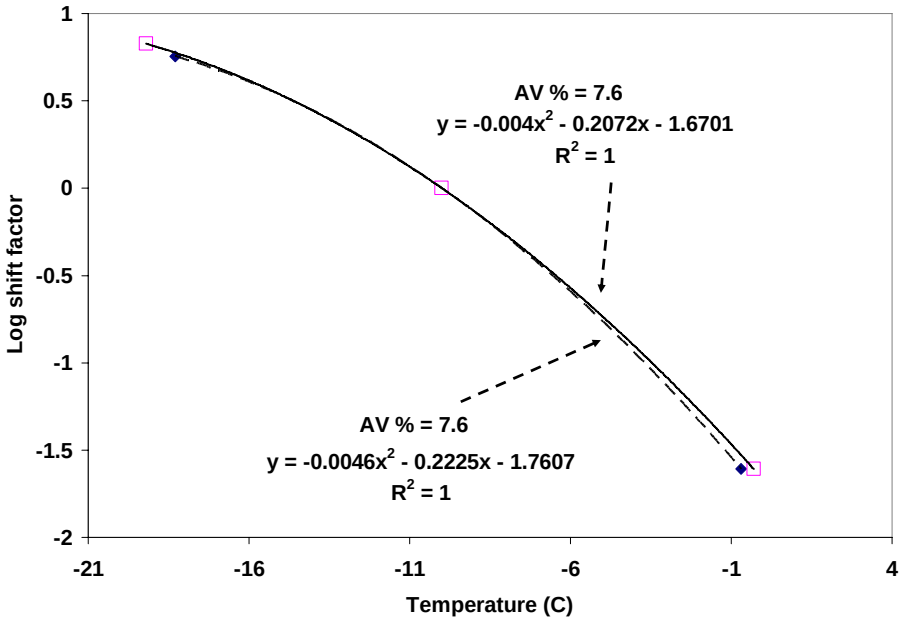

a

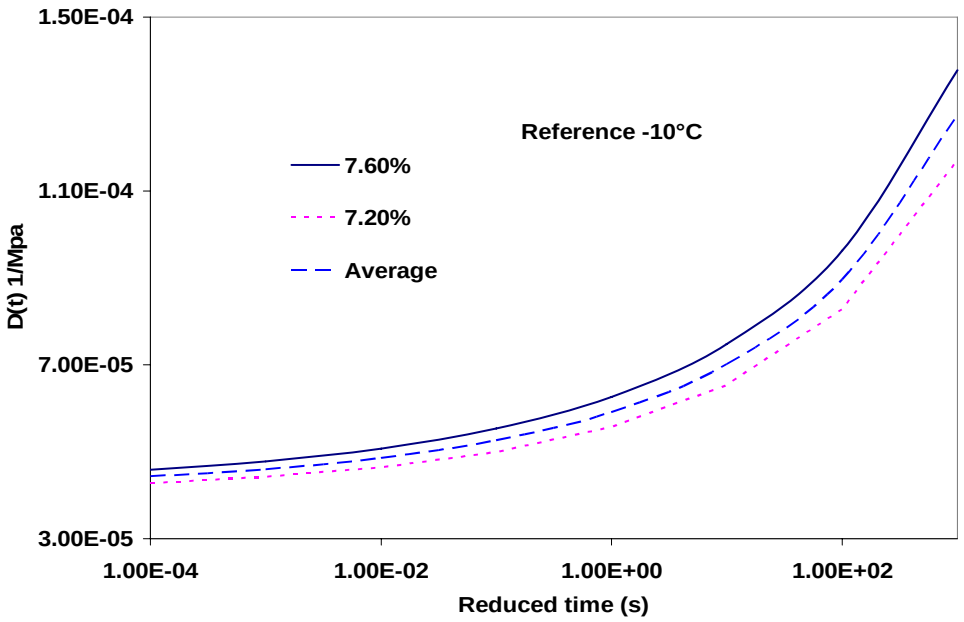

b

Figure A6 Shift factor curve (a) and creep compliance master curve at -10°C (b) for Mercer East

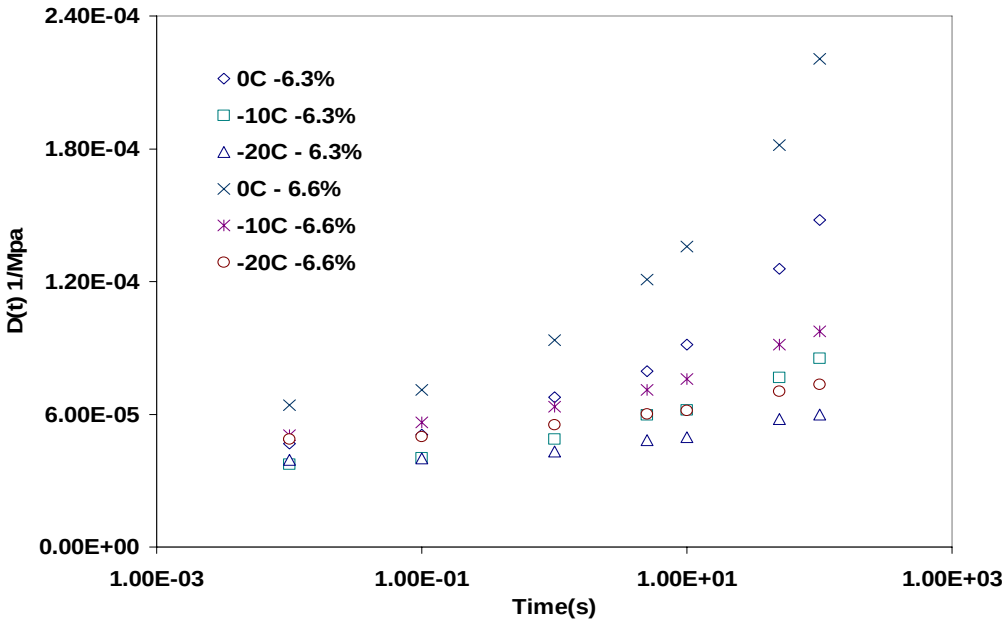

a

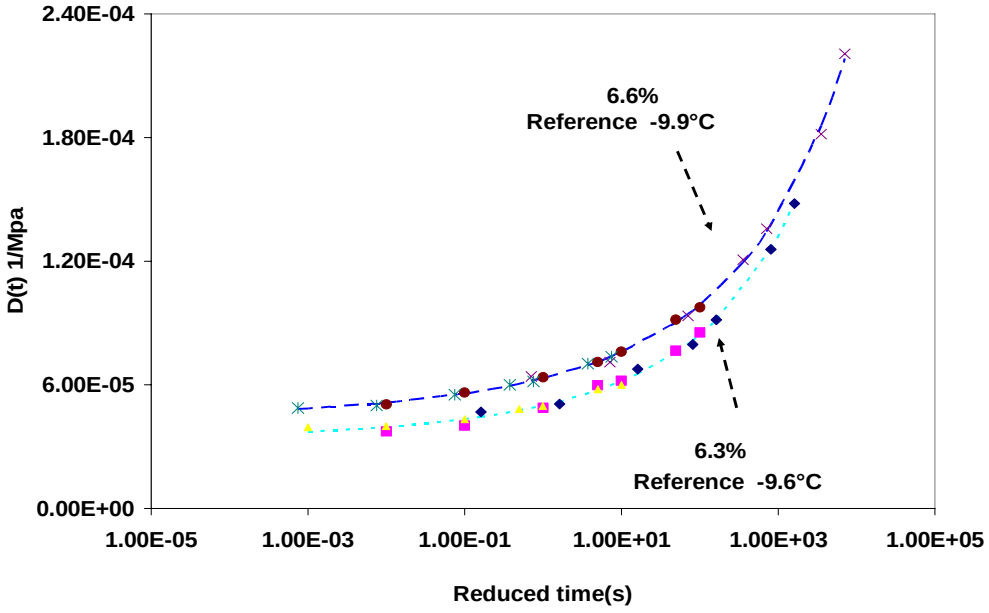

b

Figure A7 Creep compliance vs. time (a) and creep compliance master curve (b) for Mercer West

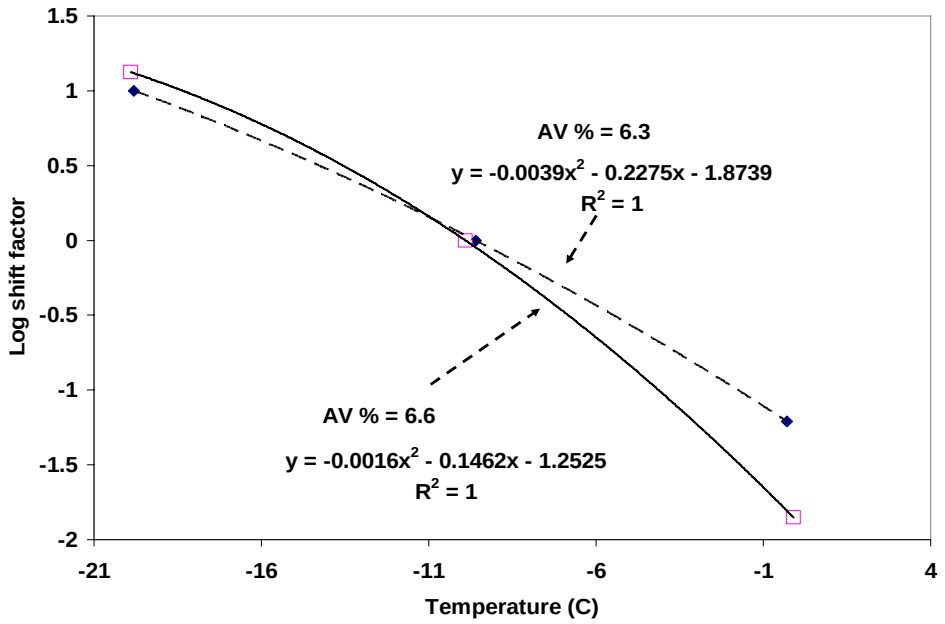

a

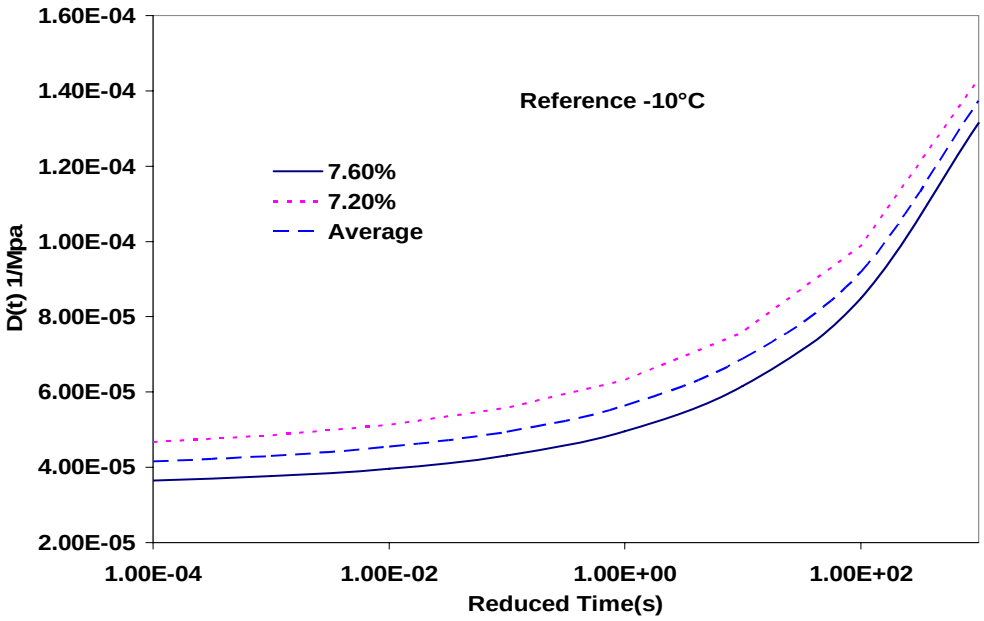

b

Figure A8 Shift factor curve (a) and creep compliance master curve at -10°C (b) for Mercer West

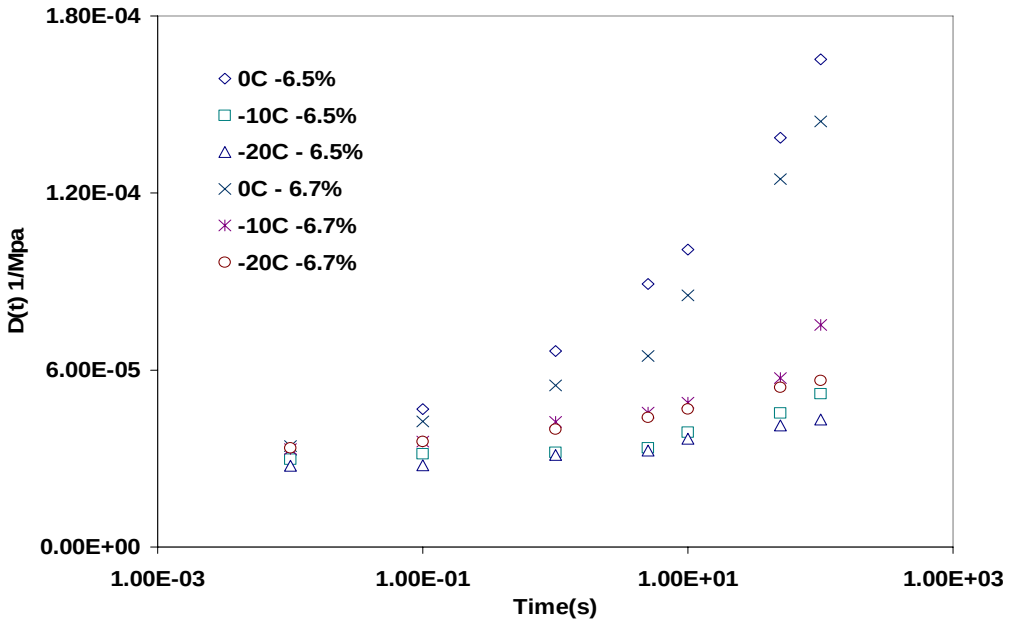

a

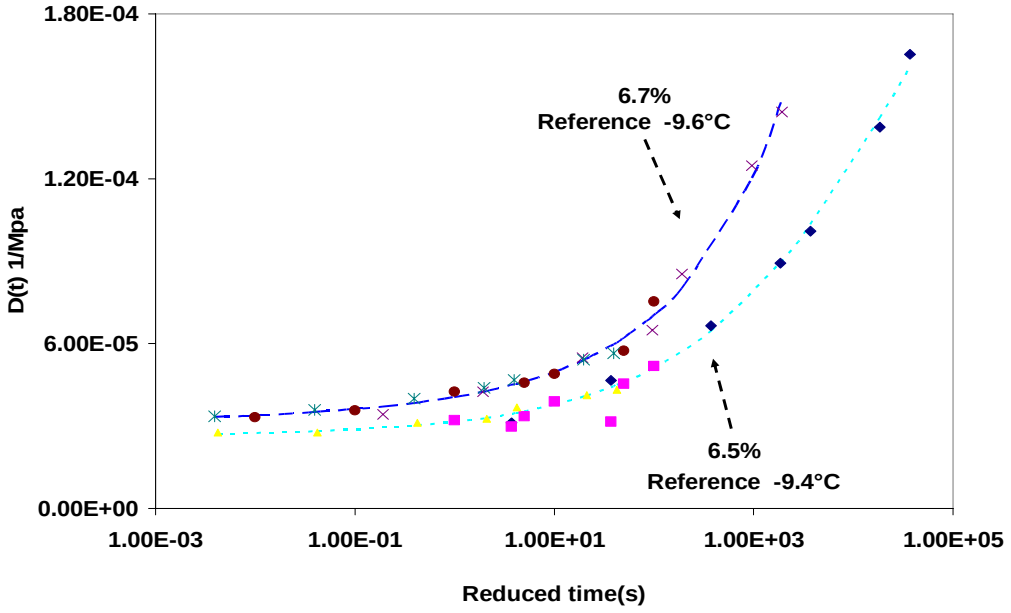

b

Figure A9 Creep compliance vs. time (a) and creep compliance master curve (b) for Perry

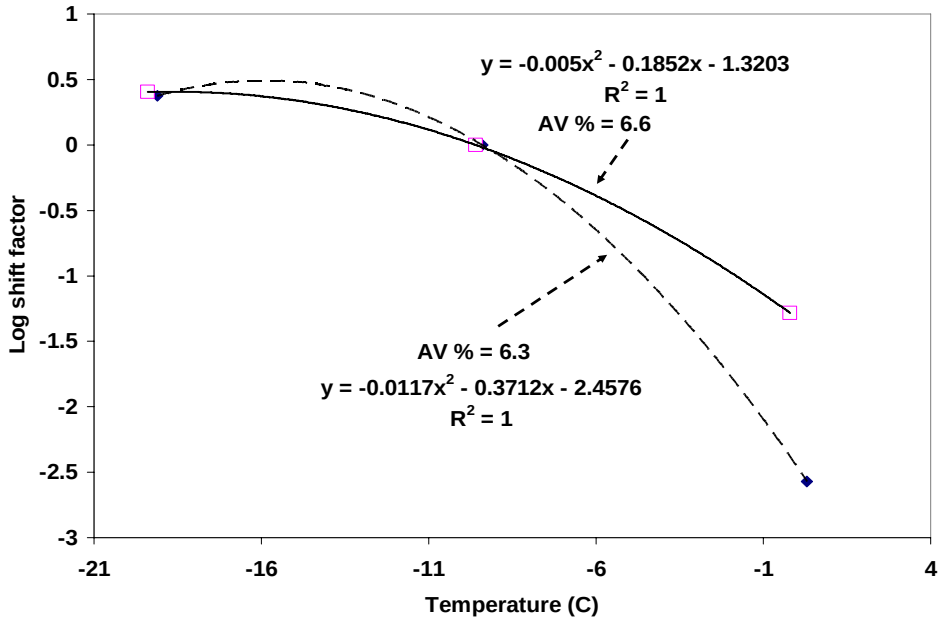

a

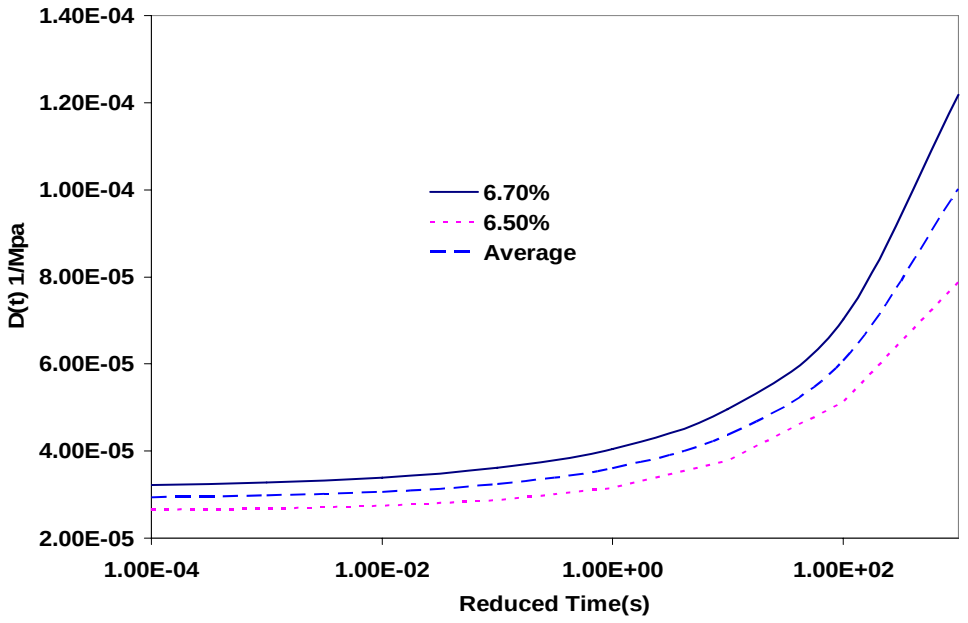

b

Figure A10 Shift factor curve (a) and creep compliance master curve at -10°C (b) for Perry

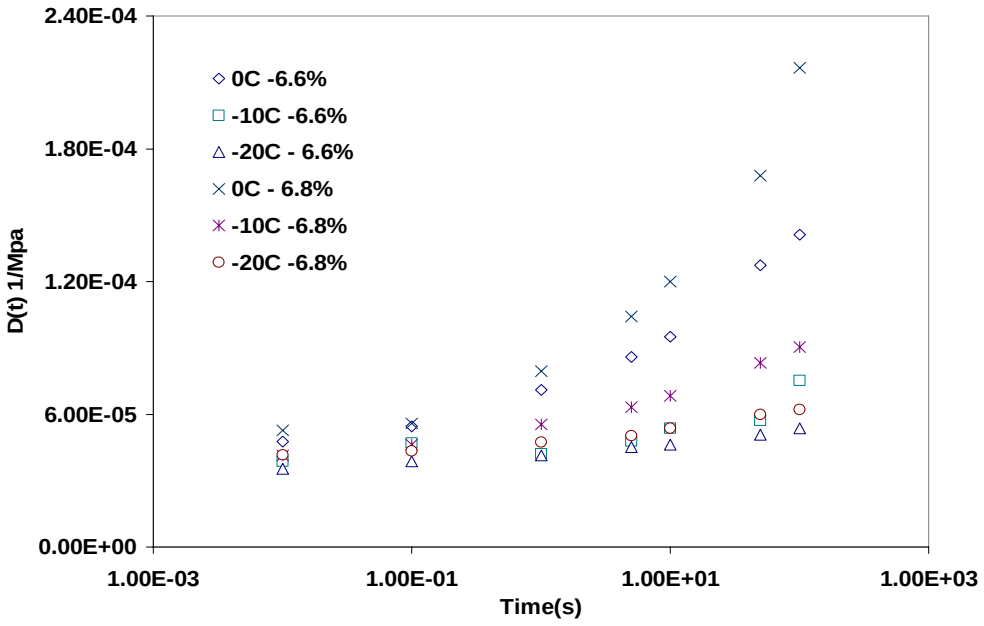

a

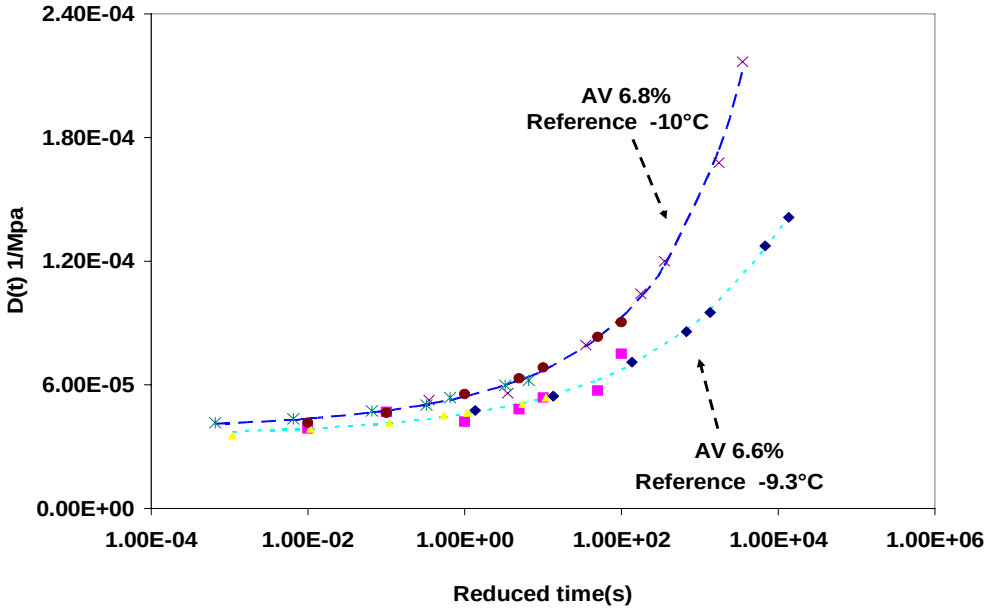

b

Figure A11 Creep compliance vs. time (a) and creep compliance master curve (b) for Somerset

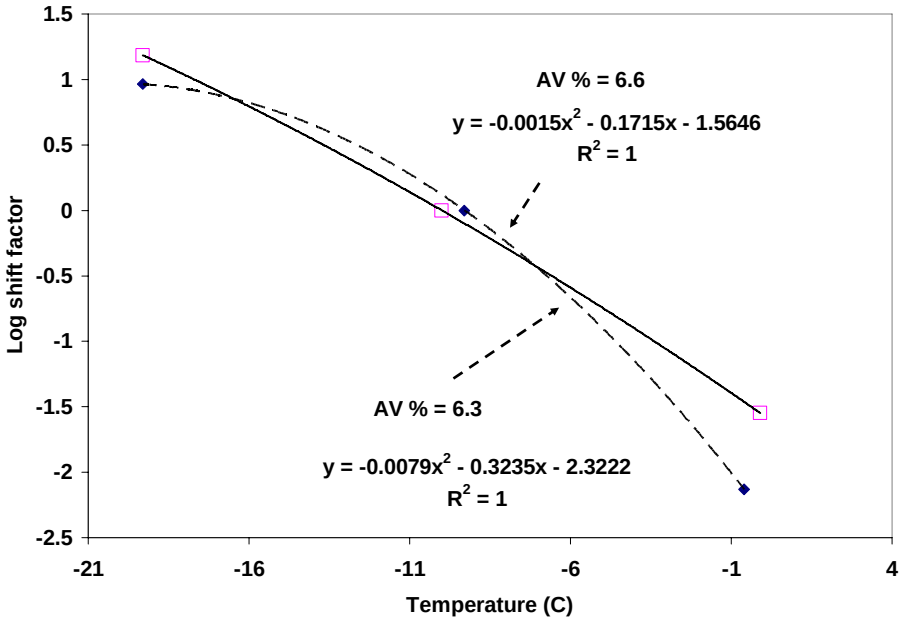

a

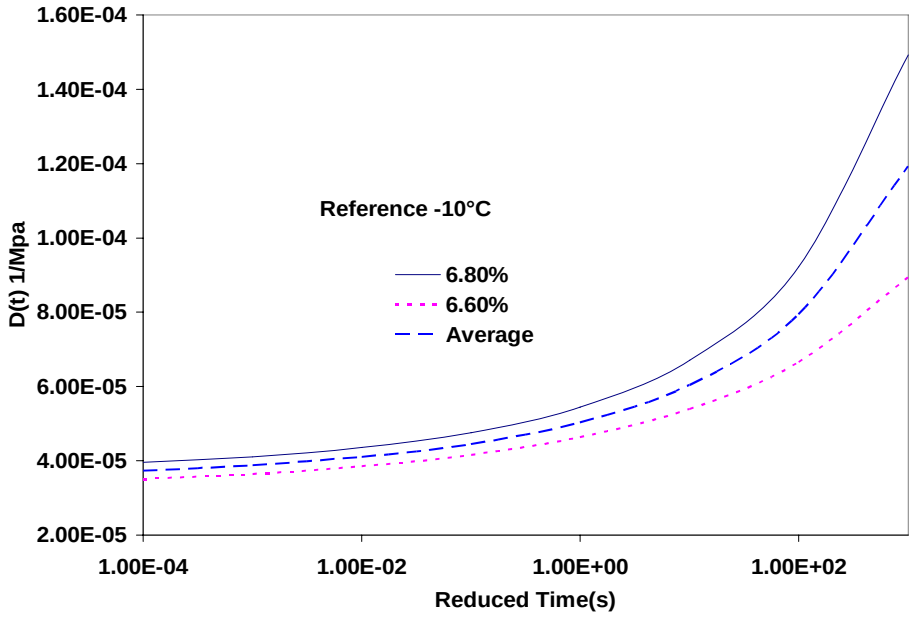

b

Figure A12 Shift factor curve (a) and creep compliance master curve at -10°C (b) for Somerset

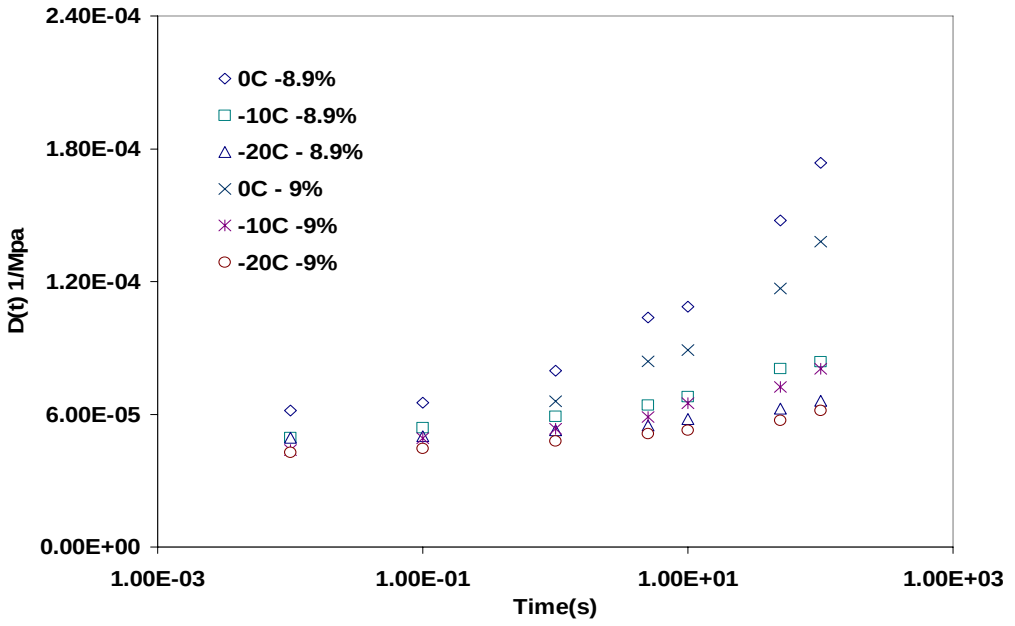

a

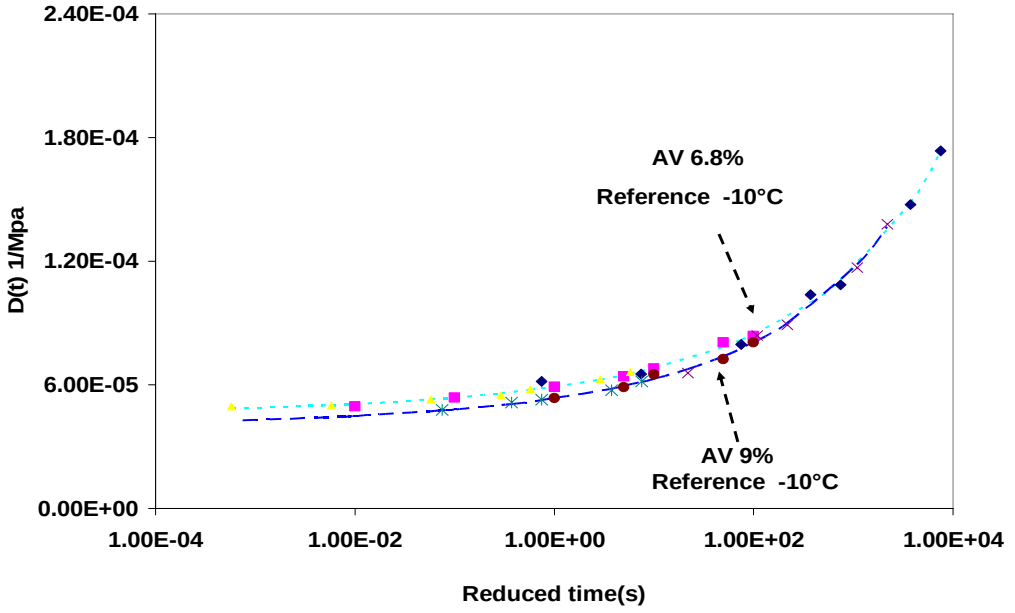

b

Figure A13 Creep compliance vs. time (a) and creep compliance master curve (b) for Tioga

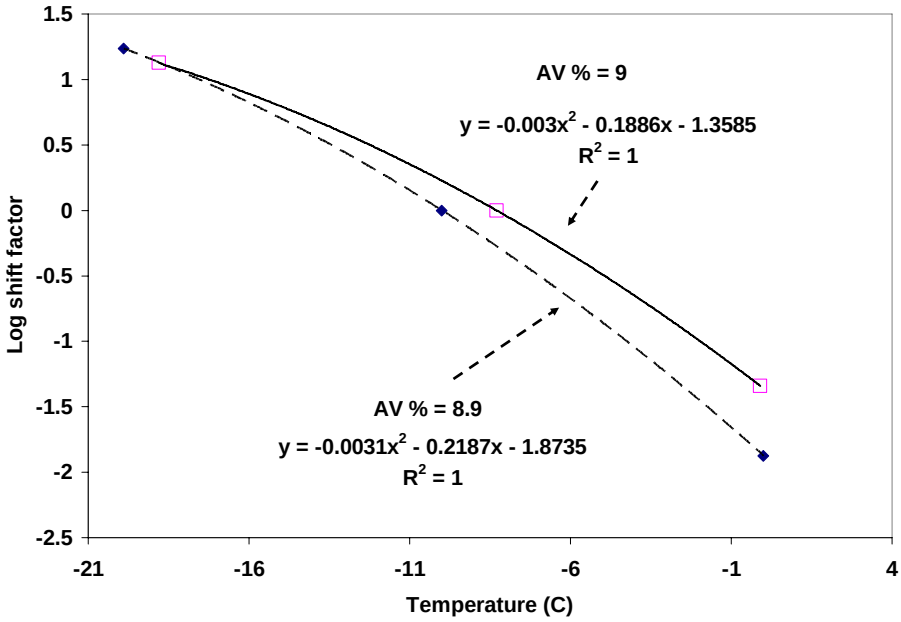

a

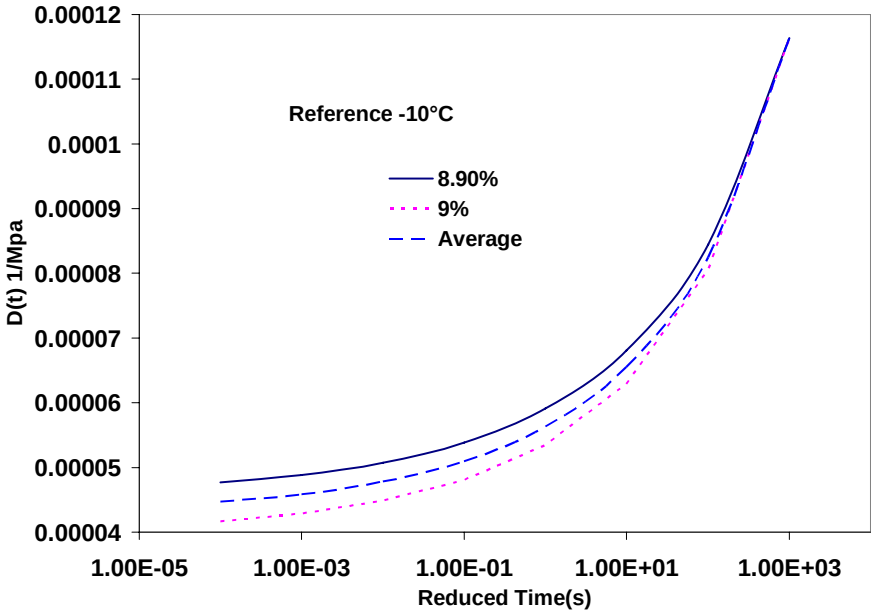

b

Figure A14 Shift factor curve (a) and creep compliance master curve at -10°C (b) for Tioga

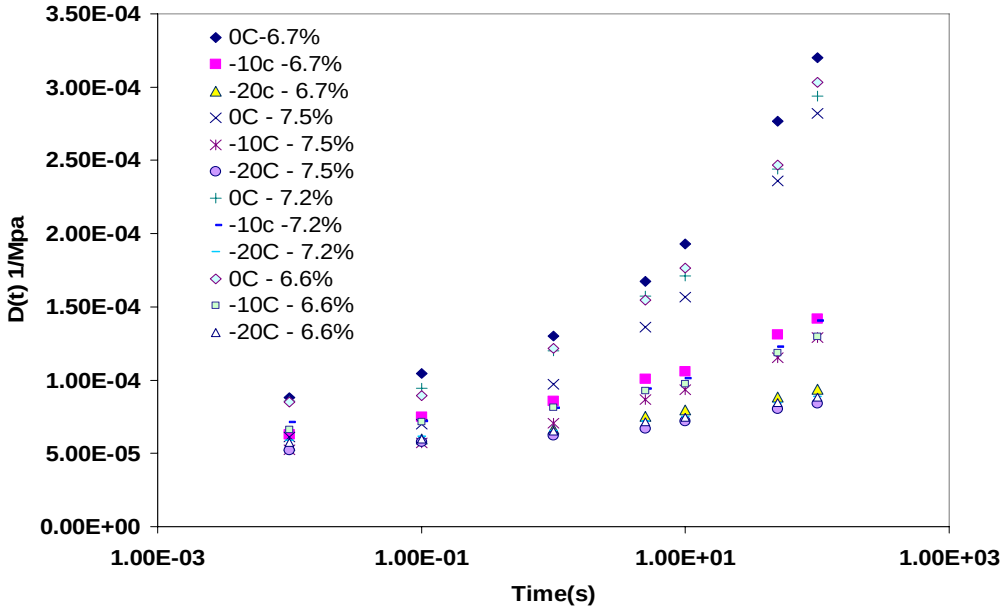

a

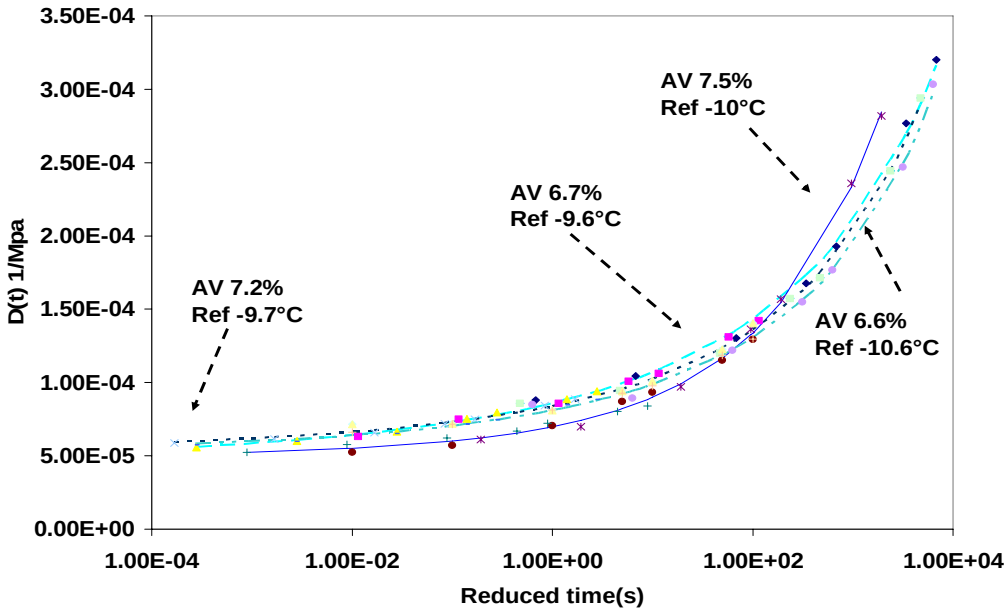

b

Figure A14 Creep compliance vs. time (a) and creep compliance master curve (b) for Warren

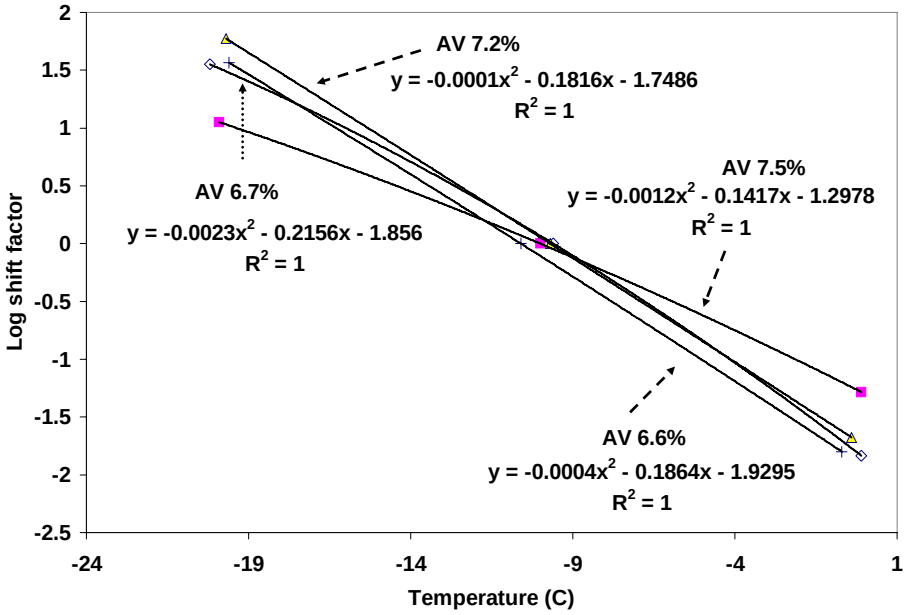

a

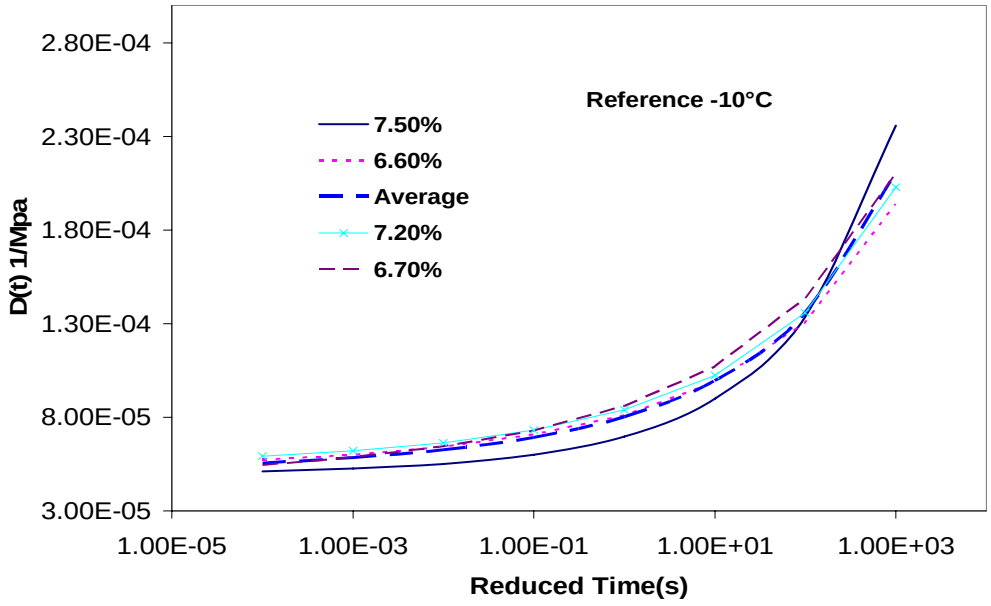

b

Figure A16 Shift factor curve (a) and creep compliance master curve at -10°C (b) for Warren

Table A1 Sigmoidal coefficients for the SISSI sites

			SISSI Site					
	Blair		Delaware		Mercer East		Mercer West	
	6.90%	*6.50%*	*6.30%*	*6.80%*	*7.20%*	*7.60%*	*6.60%*	*6.30%*
a1	-1.62	5.18	-2.85	4.36	7.89	7.92	-0.32	-2.60
a2	-7.94	-25.12	-5.72	-31.96	-29.07	-29.07	-10.43	-5.92
a3	2.61	2.57	3.46	3.64	2.37	2.36	2.58	3.18
a4	0.93	1.93	0.49	2.04	2.87	2.93	0.96	1.15
a5	2.10	3.74	1.64	4.30	4.64	4.45	2.18	1.39
a6	-0.68	-0.46	-1.03	-0.72	-0.40	-0.37	-0.42	-0.54

				SISSI Site						
	Perry		Somerset		Tioga		Warren			
	6.50%	*6.70%*	*6.80%*	*6.60%*	*9%*	*8.90%*	*7.50%*	*6.60%*	*7.20%*	*6.70%*
a1	-3.48	-1.70	-0.22	-3.08	1.70	0.04	-2.18	11.28	10.06	16.09
a2	-4.09	-7.33	-10.78	-4.50	-16.55	-12.81	-5.59	-41.58	-40.18	-50.03
a3	3.73	2.62	2.57	3.28	2.71	2.93	2.63	2.67	2.80	2.45
a4	0.61	0.84	0.99	1.03	1.26	1.05	0.98	2.57	2.38	4.52
a5	0.75	2.06	2.32	1.24	3.06	2.61	1.60	4.32	4.11	4.86
a6	-0.76	-0.63	-0.49	-0.53	-0.45	-0.45	-0.61	-0.36	-0.37	-0.29

Appendix B
Results of 240-Second Tests
with the Bending Beam Rheometer (BBR)
on SISSI Mixtures

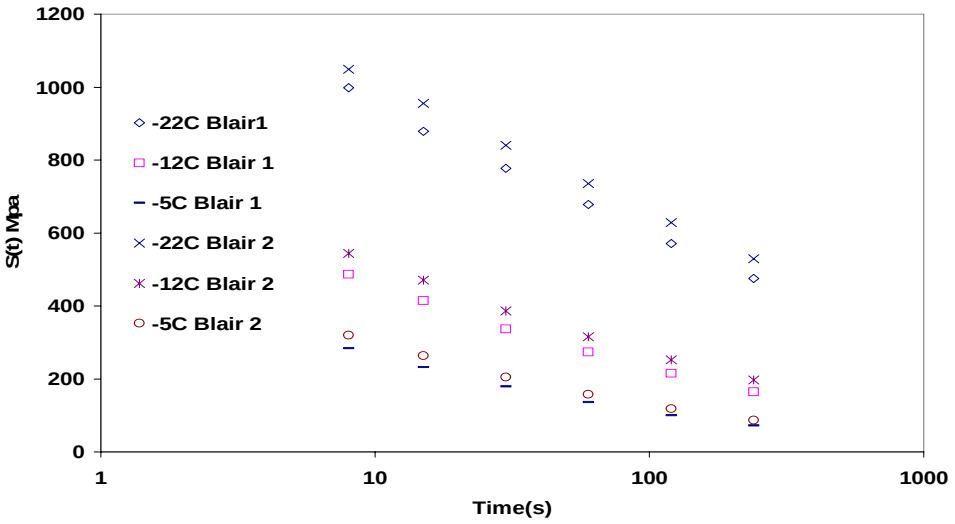

a

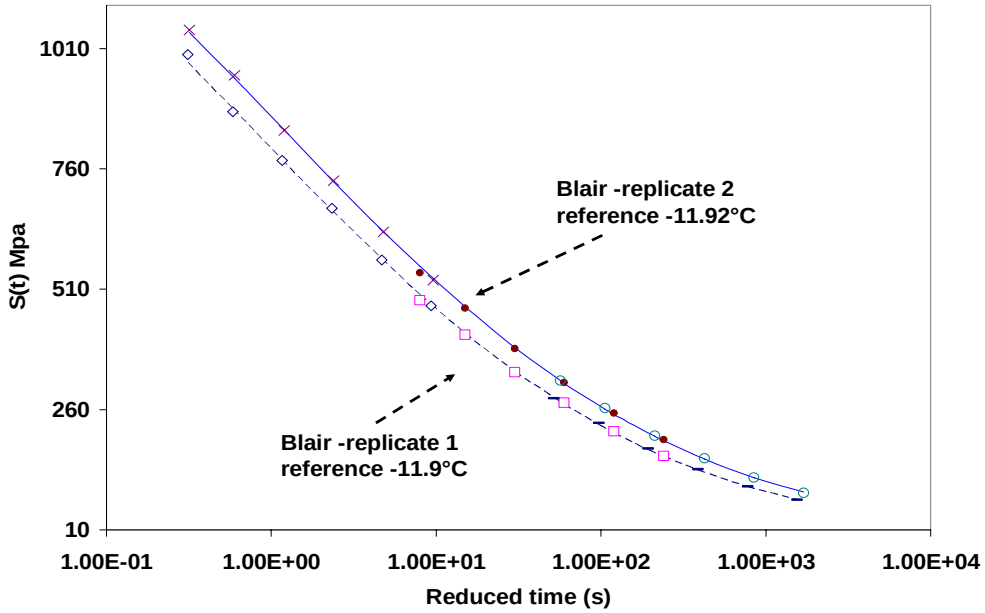

b

Figure B1 Creep stiffness vs. time (a) and creep stiffness master curve (b) for Blair

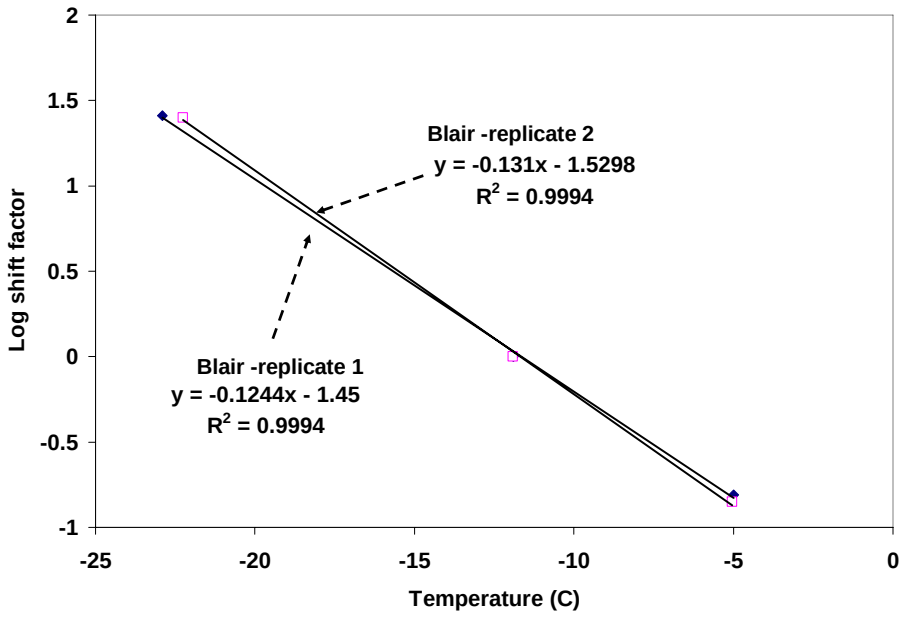

Figure B2 Shift factor curve) for Blair

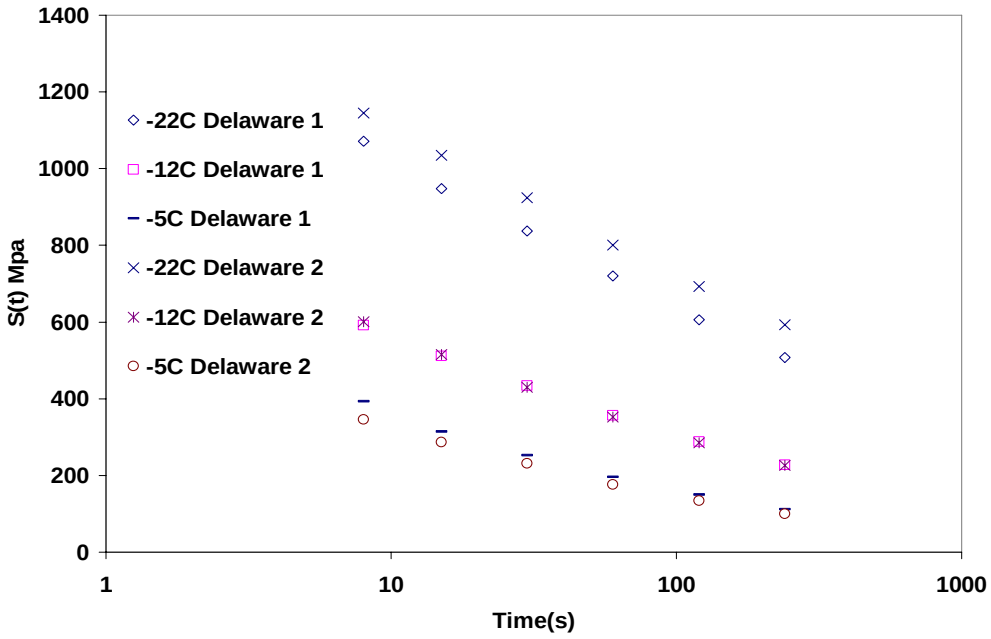

a

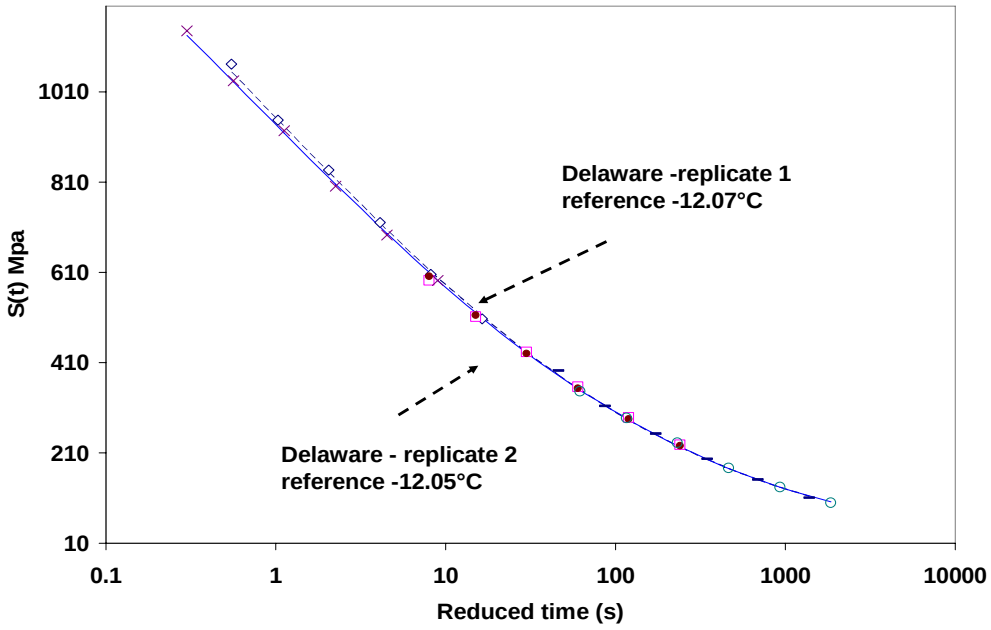

b

Figure B3 Creep stiffness vs. time (a) and creep stiffness master curve (b) for Delaware

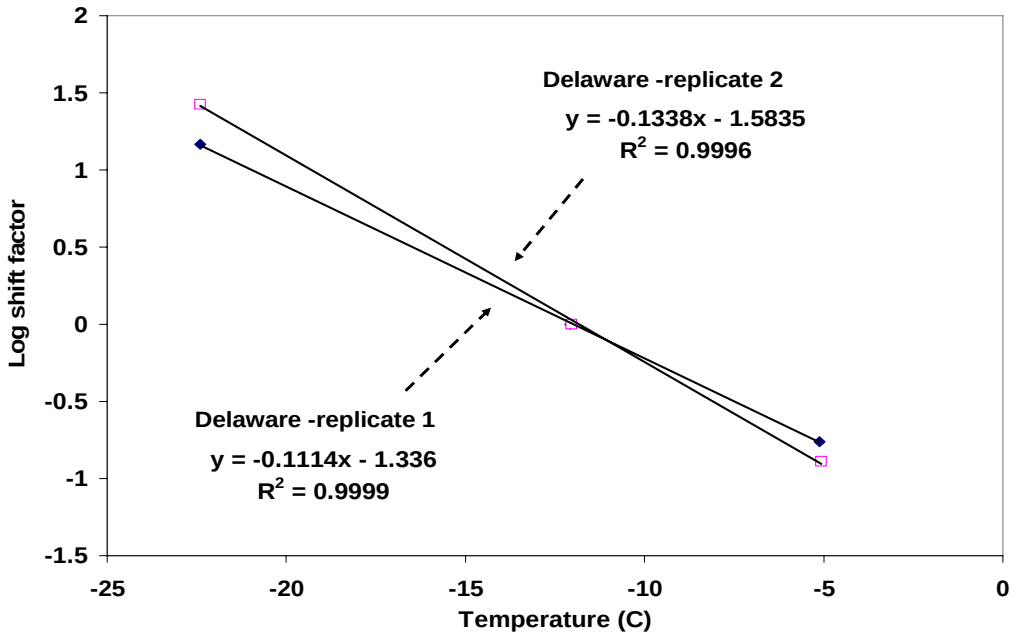

Figure B4 Shift factor curve for Delaware

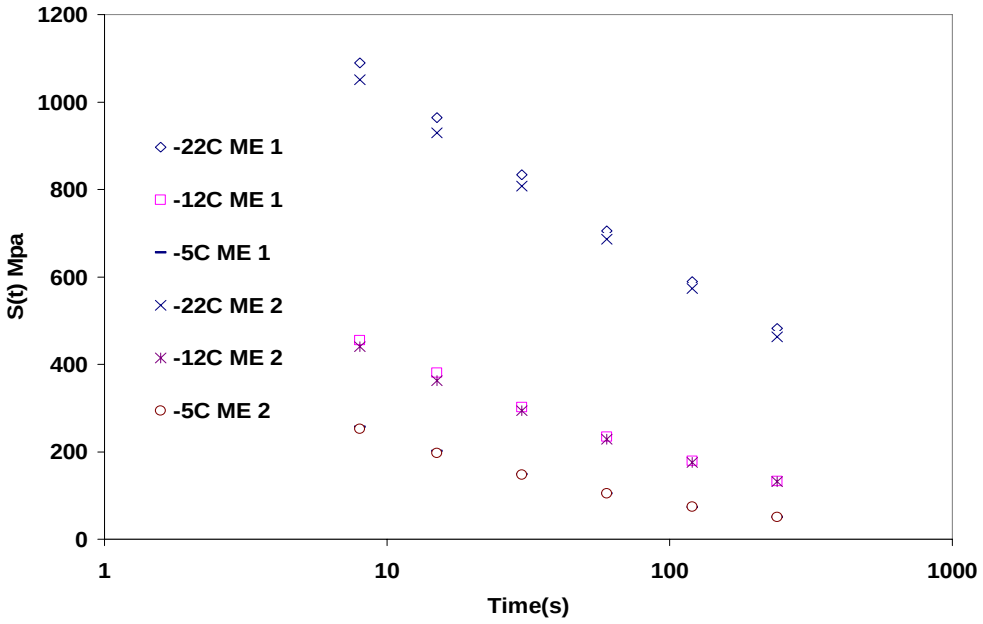

a

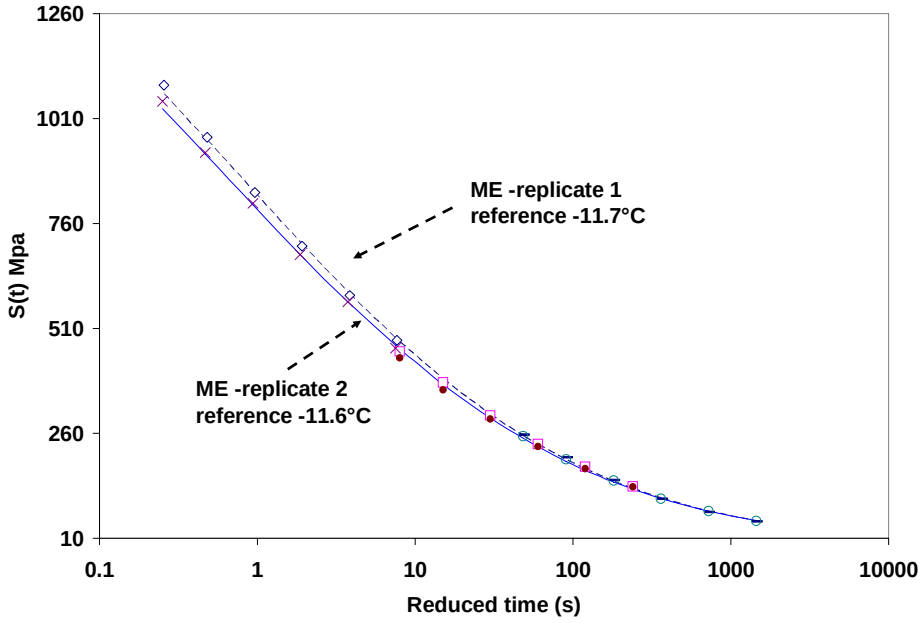

b

Figure B5 Creep stiffness vs. time (a) and creep stiffness master curve (b) for Mercer East (ME)

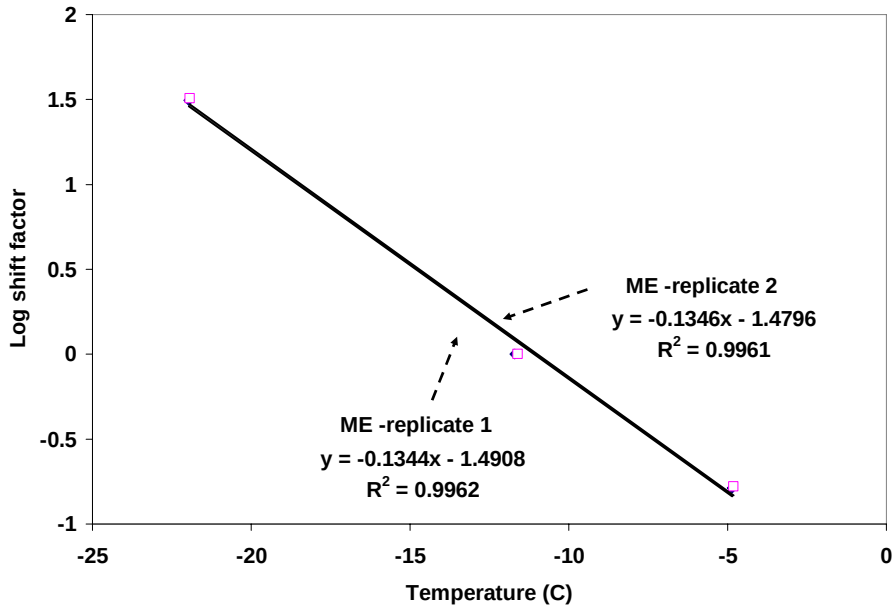

Figure B6 Shift factor curve for Mercer East

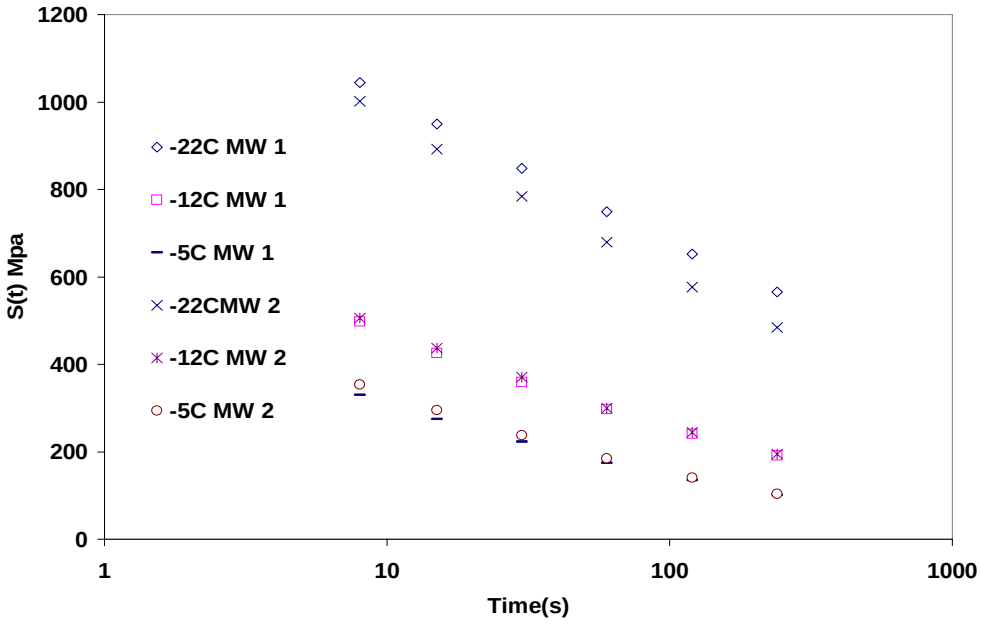

a

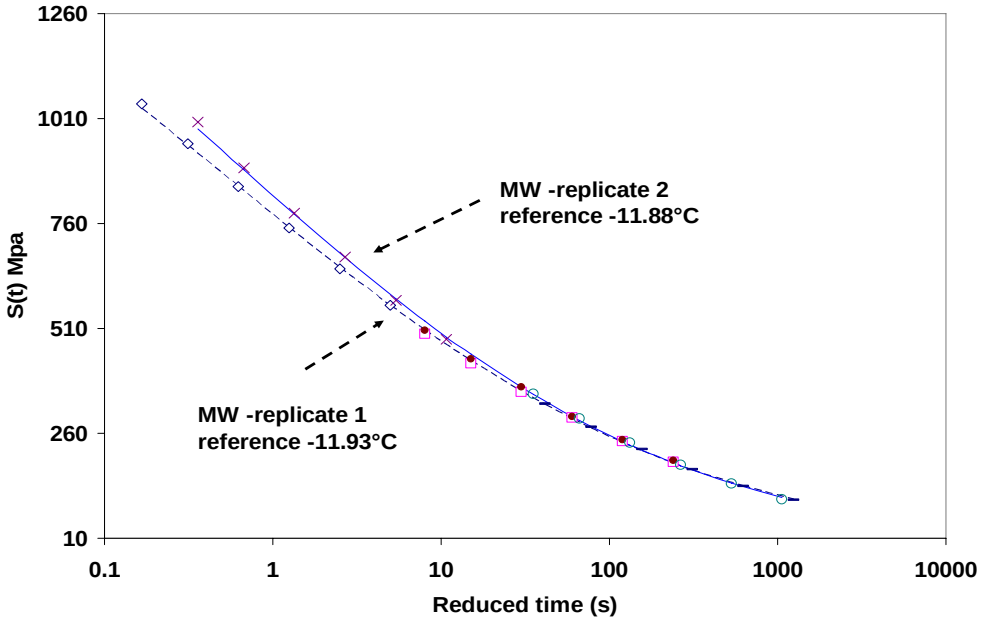

b

Figure B7 Creep stiffness vs. time (a) and creep stiffness master curve (b) for Mercer West (MW)

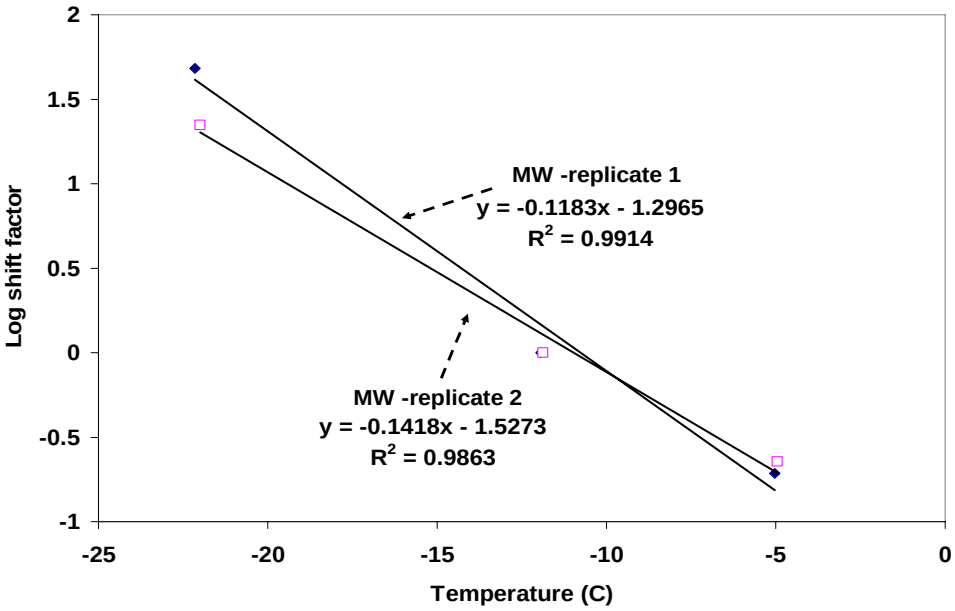

Figure B8 Shift factor curve for Mercer West

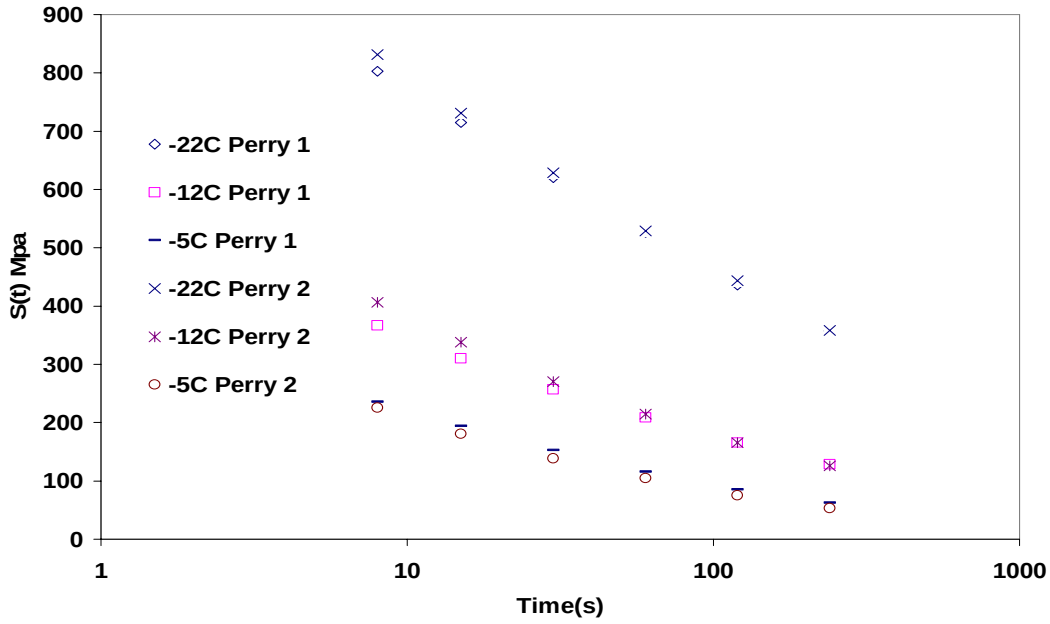

a

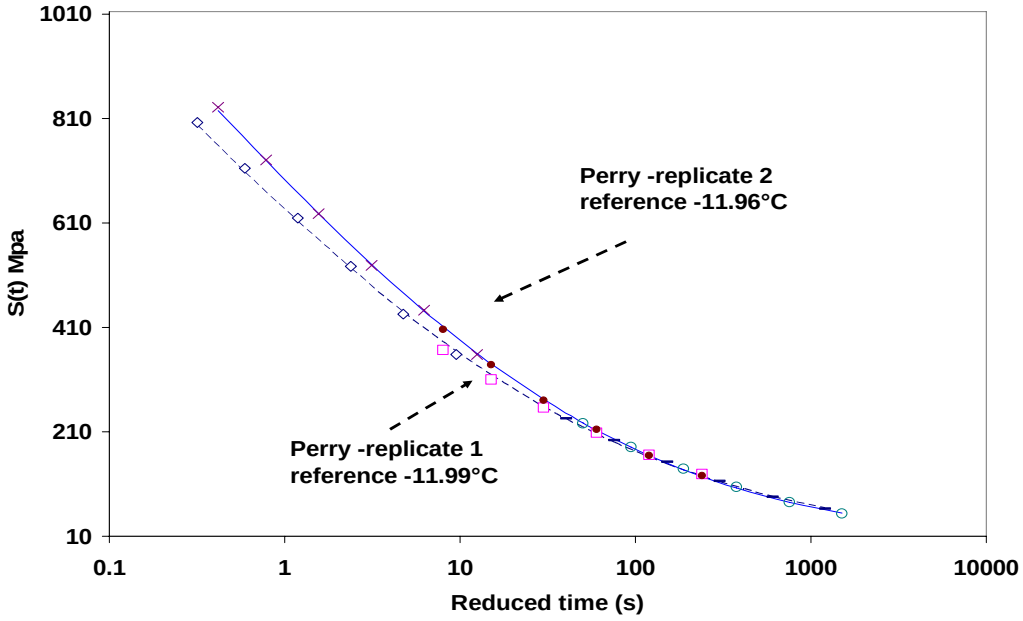

b

Figure B9 Creep stiffness vs. time (a) and creep stiffness master curve (b) for Perry

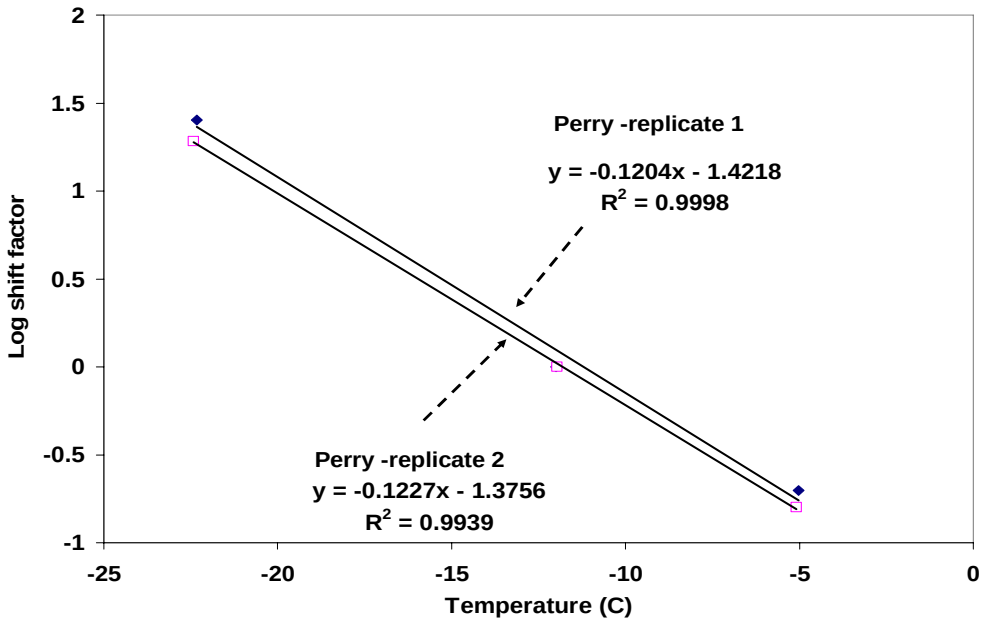

Figure B10 Shift factor curve for Perry

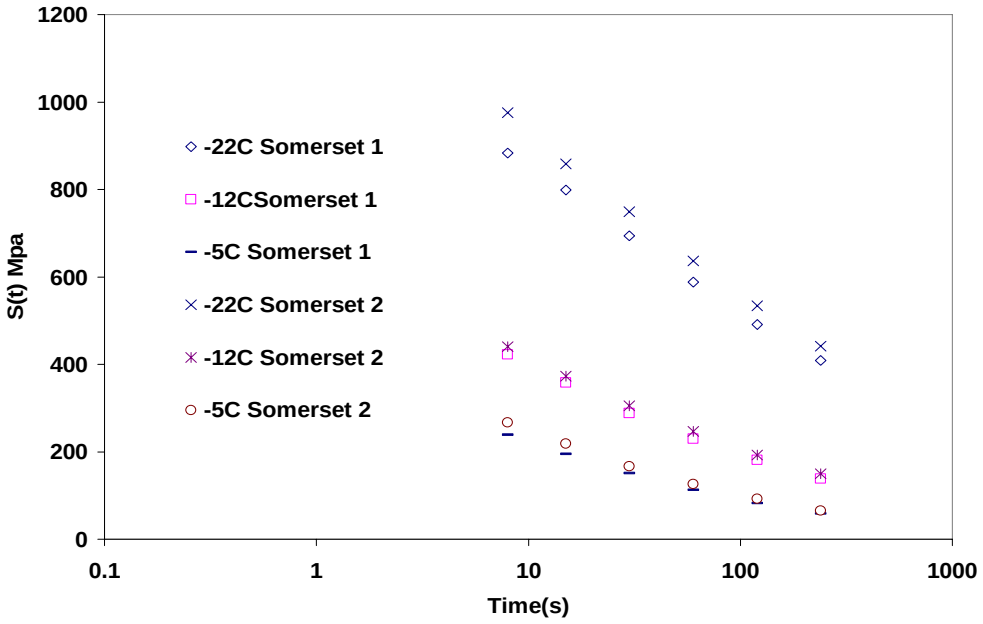

a

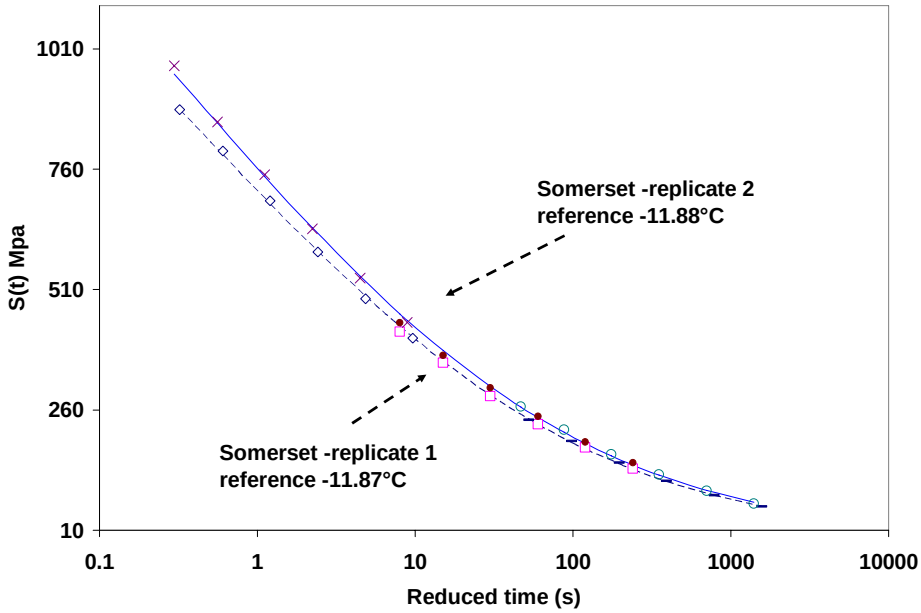

b

Figure B11 Creep stiffness vs. time (a) and creep stiffness master curve (b) for Somerset

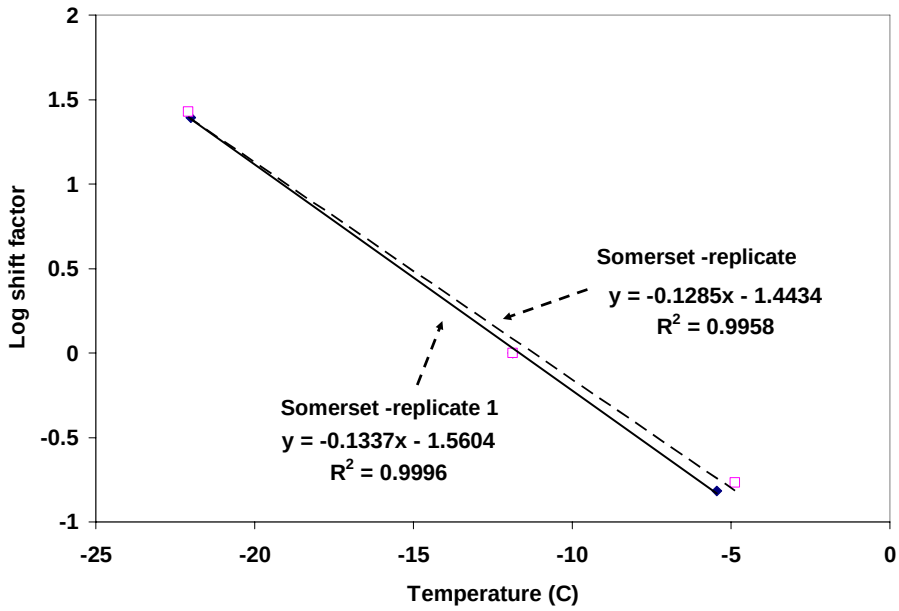

Figure B12 Shift factor curve for Somerset

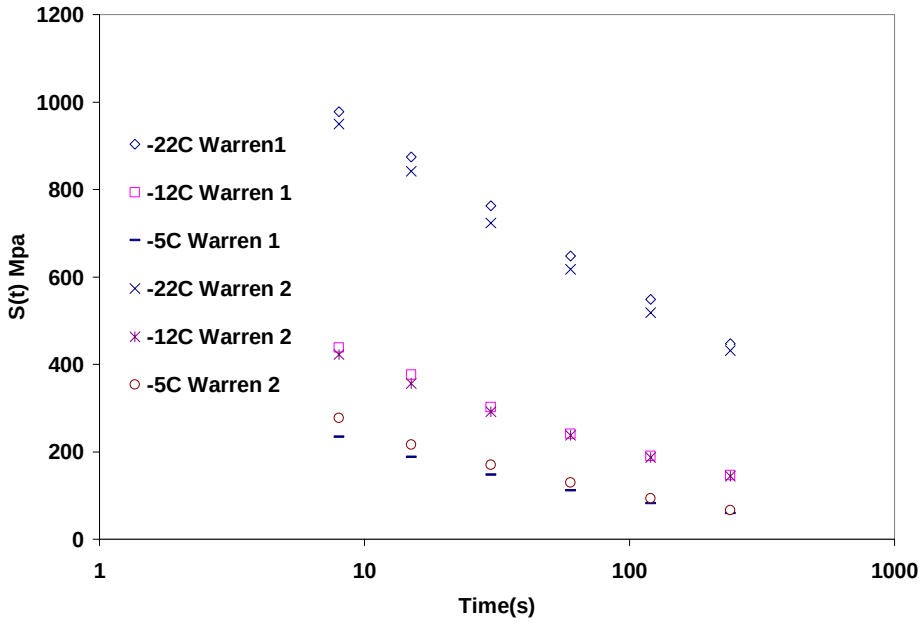

a

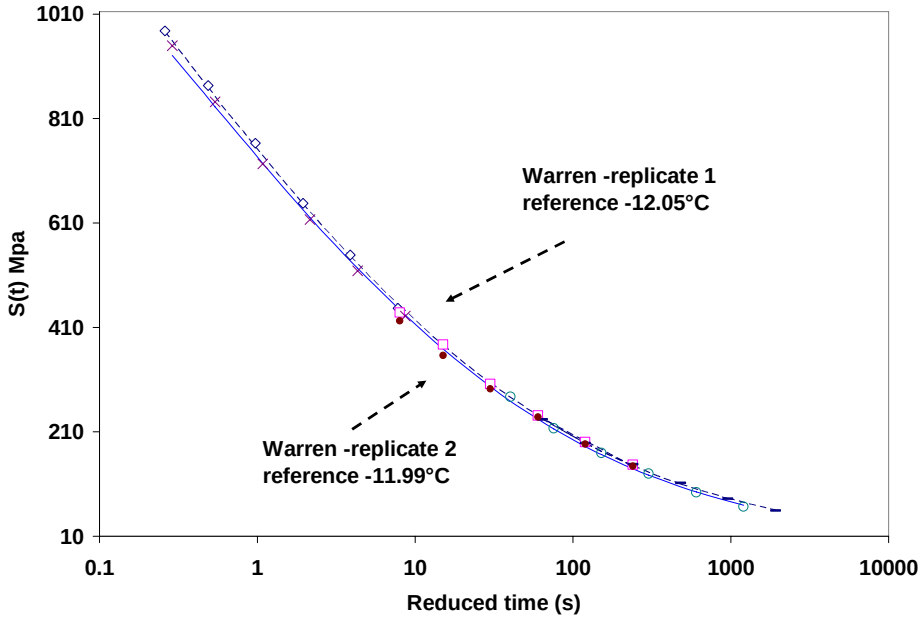

b

Figure B3 Creep stiffness vs. time (a) and creep stiffness master curve (b) for Warren

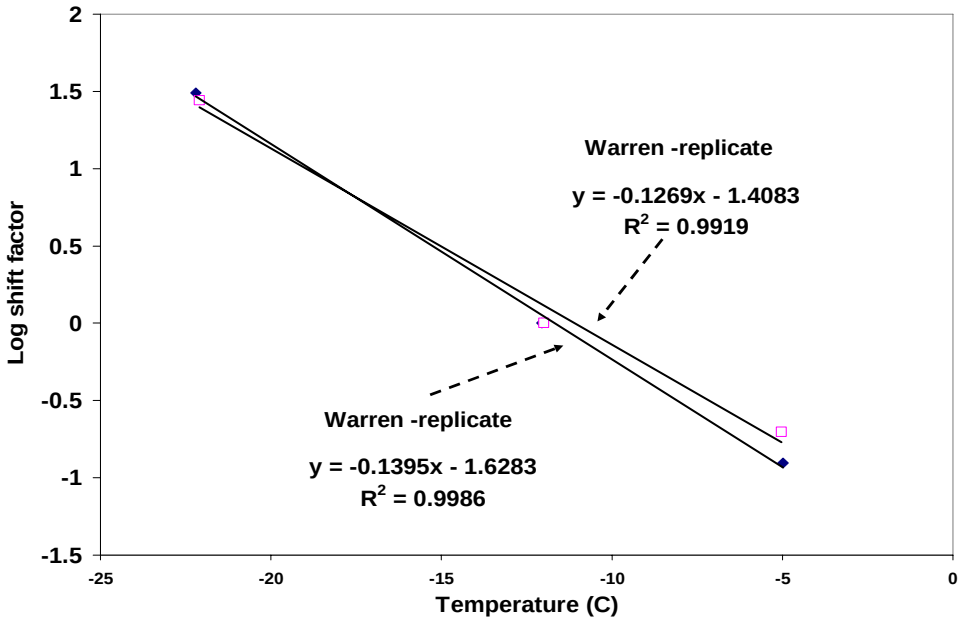

Figure B4 Shift factor curve) for Warren

Appendix C
M-values for 240-second and 2-hr BBR Tests on SISSI Binders

Table C1 M-values for 240s and 2hr BBR tests on SISSI binders

		240s test				2hr test	
SISSI Site		m-value @ 60s				m-value @ 60s	
	Temperature (°C)				Temperature (°C)		
	-22	-12	-5		-22	-12	-5
Warren -replicate 1	0.242	0.337	0.42		0.227	0.32	0.412
Warren -replicate 2	0.24	0.327	0.432		0.227	0.322	0.411
Blair -replicate 1	0.225	0.333	0.42		0.211	0.324	0.422
Blair-replicate 2	0.212	0.312	0.398		0.204	0.299	0.399
Somerset - replicate 1	0.241	0.341	0.433		0.231	0.33	0.432
Somerset -replicate 2	0.242	0.328	0.432		0.231	0.327	0.429
Mercer East -replicate 1	0.251	0.377	0.502		0.255	0.37	0.482
Mercer East-replicate 2	0.252	0.367	0.49		0.242	0.367	0.497
Mercer West- replicate 1	0.187	0.289	0.36		0.214	0.281	0.365
Mercer West - replicate 2	0.222	0.293	0.379		0.217	0.293	0.373
Perry - replicate 1	0.25	0.319	0.41		0.24	0.319	0.419
Perry - replicate 2	0.257	0.357	0.441		0.243	0.35	0.466
Delaware - replicate 1	0.228	0.294	0.378		0.19	0.289	0.389
Delaware - replicate 2	0.202	0.298	0.384		0.201	0.288	0.378